

MECHANICAL AND OPTICAL ANALYSES PROVIDE
A NETWORK MODEL FOR SPIRAL SILK FROM THE ORB WEB
OF THE SPIDER *ARANEUS DIADEMATUS*.

by

Cynthia Catherine Nichols Pollak

BSE, Duke University, 1985

A THESIS SUBMITTED IN PARTIAL FULFILLMENT OF
THE REQUIREMENTS FOR THE DEGREE OF
MASTER OF SCIENCE

in

THE FACULTY OF GRADUATE STUDIES

(Department of Zoology)

We accept this thesis as conforming
to the required standard.

THE UNIVERSITY OF BRITISH COLUMBIA

October 1991

© Cynthia Pollak, 1991

In presenting this thesis in partial fulfilment of the requirements for an advanced degree at the University of British Columbia, I agree that the Library shall make it freely available for reference and study. I further agree that permission for extensive copying of this thesis for scholarly purposes may be granted by the head of my department or by his or her representatives. It is understood that copying or publication of this thesis for financial gain shall not be allowed without my written permission.

Department of ZOOLOGY

The University of British Columbia
Vancouver, Canada

Date 11 Oct 91

ABSTRACT

Glue-coated spiral silk from *Araneus diadematus* orb webs is stretchy compared to the stiff and inextensible frame silk. This thesis examines whether part of the difference between properties may be due to molecular arrangements, not just the glue. Dry and wet spiral samples had average diameters of 2.2 and 3.1 microns and a non-circular cross-section with an average ellipticity of 1.5. The lengthwise contraction of wetted samples is a two-phase process, with an average ratio of wet to dry slack length of 0.6. Stress-extension behavior of samples was analyzed according to theories of rubber elasticity. Dry and wet spiral samples have, on average, network chains with 4.8 and 6.6 random segments between crosslinks; frame silk has two. The average shear moduli of wet and dry spiral samples are 0.67 and 0.32 MN/m² (the modulus of wet frame silk is 0.8 MN/m²). Spiral samples' average volume increase from the dry to the wet state is 1.6 compared to frame's volume change of 2.1, possibly because "dry" spiral silk is already partially plasticized. Samples that are stiffer than average in the dry state require higher than average work of extension in both dry or wet states, but stiffer dry samples have proportionately higher reductions in work of extension when wetted, perhaps because most of the extra stiffness is caused by water-labile structures rather than stable crystals. A solution of guanidine hydrochloride rapidly causes silk to lose its mechanical integrity, supporting hypotheses that the major crosslinking mechanism of *Araneus* silk is non-covalent. Optical analyses yielded a residual birefringence of approximately 1.5×10^{-3} (half that of frame silk, at 3.8×10^{-3}) and a stress-optical coefficient of 2×10^{-9} N/m². Both parameters are significantly higher than expected for wholly amorphous rubbers and provide evidence for crystals or aligned glassy regions. Thus, the hypothesis that the network structure of spiral silk is different than frame silk was supported by the significantly different values for chain densities, segment counts, and birefringences.

TABLE OF CONTENTS

ABSTRACT	ii
TABLE OF CONTENTS	iii
LIST OF TABLES	vi
LIST OF FIGURES	vii
ACKNOWLEDGEMENTS	viii
CHAPTER I: INTRODUCTION	1
CHAPTER II: METHODS	13
A. GENERAL OVERVIEW	13
B. SAMPLE COLLECTION AND STORAGE	13
C. PHYSICAL PARAMETERS	15
1. Diameter measurements.	15
2. Uniformity of diameter.	16
3. Cross-sectional shape analysis.	18
The rotating mount.	18
Analysis of rotation data.	20
4. Volume-extension measurements.	21
D. MECHANICAL STUDIES	21
1. Models for elastomeric materials.	21
Gaussian rubber network theory.	21
Non-Gaussian network theory.	22
2. General setup for extension studies.	24
3. Platter stage mount.	24
4. Glue types and techniques.	27
5. Force calculations.	29
The tapered-beam formula.	30
6. Preparation of wet samples.	31
7. Camera/VDA setup.	32

8. Modifications for dry samples.	33
E. WET CONTRACTION	34
F. OPTICAL STUDIES	34
1. Birefringence theory.	34
2. Rubber photoelasticity theory.	35
3. Microscope and sample setup.	36
4. Modifications for dry samples.	39
CHAPTER III: RESULTS	40
A. DIAMETER AND CROSS-SECTION DATA	40
B. EXTENSION-VOLUME DATA	44
C. WET CONTRACTION DATA	46
D. MECHANICAL RESULTS	49
1. Force-extension data.	49
2. Stress-extension data: Non-Gaussian curve fits.	55
3. Calculation of network chain parameters.	63
4. Test for covalent bonds.	72
E. OPTICAL DATA	74
1. Residual birefringence.	76
2. Stress-optical coefficients.	78
3. Predicted birefringence.	78
CHAPTER IV: DISCUSSION	83
A. PHYSICAL PARAMETERS	83
1. Diameter and cross-section.	83
2. Constant volume.	85
3. Wet contraction.	85
B. MECHANICAL PROPERTIES	86
1. Force-extension behavior.	86
2. Network chain parameters.	88
3. Validity of the network models.	91

C. OPTICAL ANALYSIS	93
D. A MODEL FOR SPIDER SPIRAL SILK	94
E. COMPARISON OF FRAME AND SPIRAL SILK MODELS	94
1. Network parameters and strain amplification.	94
2. Birefringence and crystallites.	98
3. Wet/dry volume ratios.	100
4. Hydrophobic Index.	101
5. Potential for Plasticizers.	104
6. Washed spiral samples.	105
F. WHY IS SPIRAL SILK VARIABLE?	106
CHAPTER V: CONCLUSIONS	108
REFERENCES	111

LIST OF TABLES

3.1	Diameters of dry and wet spiral silk fibers.	41
3.2	Ellipticity data from rotated samples.	42
3.3	Ellipticity data from non-rotated samples.	43
3.4	Wet contraction ratios.	47
3.5	Network parameters of conditioned samples.	57
3.6	Network parameters for successive cycles, successive days, and varying extension rates.	60
3.7	Network chain parameters of a hypothetical network.	64
3.8	Network chain parameters of four samples.	66
3.9	Calculations of birefringence using different assumptions of cross-section shape.	75
3.10	Residual birefringences and stress-optical coefficients of dry and wet samples.	77
4.1	Effects of strain amplification on calculations of network chain parameters.	96
4.2	Some physical parameters of elastin, spiral silk, and frame silk.	99
4.3	Hydrophobic Indices of some silks and elastins.	103

LIST OF FIGURES

1.1	Diagram of an orb web.	2
1.2	Stress-extension curves of four materials.	4
1.3	Stress-extension curves of dry spiral and frame silks.	5
1.4	Stress-extension curves of dry and wetted frame silk.	8
1.5	Three-compartment model of a native spiral silk fiber.	12
2.1	Typical orientations of bave.	17
2.2	Illustration of the principle behind rotation studies.	19
2.3	General instrumentation setup for mechanical studies.	25
2.4	Diagram of the stage-mounted platter.	26
3.1	Extension-volume curves for several samples.	45
3.2	Typical wet contraction time course.	48
3.3	Repeated length-force cycles for dry and wet samples.	50
3.4	Length-force cycles repeated over eleven days.	51
3.5	Changes in forces when samples are wetted.	52
3.6	Plot of initial stiffness of dry samples versus change in force when wetted.	54
3.7	Stress-extension curves for a sample first dry, then wetted.	56
3.8	Regression plot for a viscous dry fiber.	58
3.9	Examples of the range of mechanical properties observed.	61
3.10	Chart record for the guanidine hydrochloride test.	73
3.11	Predicted birefringence for four networks.	79
3.12	Variation in birefringence for 10% deviations in the stress-optical coefficient.	80
3.13	Actual birefringences observed for two samples, with amorphous and crystal components estimated.	81
5.1	Pictorial representations of the network models of spiral and frame silks.	109

ACKNOWLEDGEMENTS

I take this opportunity to thank Dr. John M. Gosline, my research supervisor, for his patient guidance throughout the course of my research; he was ever available during those challenging phases of formulating ideas and devising alternative approaches. I am also grateful to Dr. William Milsom and Dr. Robert Blake for their helpful advice regarding experimental design. Many thanks to the other members of the lab: to Dr. Margo Lillie and Gavin Chalmers, for their insights into the rubbery bits; to Dr. Olaf Ellers, for pointing the way to numerical methods for ellipses; to Dr. Ann Pabst, for her open ears and helpful tips; and to Steve Katz, for his helpful criticism especially regarding statistics.

This research was supported by grants to Dr. Gosline from the Natural Sciences and Engineering Research Council (NSERC) and E.I. du Pont de Nemours and Company (Textile Fibers Department).

CHAPTER I: INTRODUCTION

Many arthropods produce a proteinaceous substance in a fibrous form for use outside their bodies. These materials are called silks (Lucas and Rudall, 1968). Silks are secreted by glands of varying origin; for example, some are modified salivary glands, while others (such as spiders') possibly were originally salt glands. The best-known silk is that of the silkworm, *Bombyx mori*, due to its commercial importance; however, spiders have fascinated researchers interested in learning why silks have such varied properties, because some arachnids produce nine or more distinctive substances (Kovoor and Peters, 1988).

Silks have a wide range of chemical compositions and properties. The gland fluid is primarily proteinaceous, with varying amounts of carbohydrates and smaller molecules (Dreesbach et al, 1983; Sinohara and Tillinghast, 1984). A single gland can even secrete several substances (Shimura, 1983), and fibers from silkworms and spiders also often have a dual nature in themselves, with core and outer layers being secreted from different cell groups in a single gland. This means the number of substances synthesized by an animal may be greater than the number of gland types. Usually the gland material is drawn (that is, pulled out under tension) like many modern polymers in production. Rarely, it is extruded from a gland before being put to use, the way *Chrysopa*, the lacewing, creates egg-stalks (Denny, 1980).

Most spiders secrete only one or two types of silk, but the orb web weavers are capable of secreting several kinds. There are two families which build complex wheel-shaped snares: Araneidae and Uloboridae. This study employed spiders of the superfamily Araneidae because a moderately large-sized species, *Araneus diadematus*, is abundant in the Vancouver area, and therefore laboratory rearing and maintenance were unnecessary. Also, more studies of behavior, gland anatomy, and silk composition have focussed on Araneids. *A. diadematus* has at least seven types of glands (Palmer, 1985). Five of them are used in the orb web alone, producing three silks and at least two glues. The largest pair of glands, called the major ampullate, secrete silk used for the spider's safety dragline and for the construction of the mooring threads, frame, and radial strands in her aerial snare, pictured in Figure 1.1 (Peakall, 1964). A second pair of glands, the minor ampullate, produces fibers which often accompany the frame fibers; these minor, or accessory, fibers are much thinner, appear more crystalline, and do not shorten when

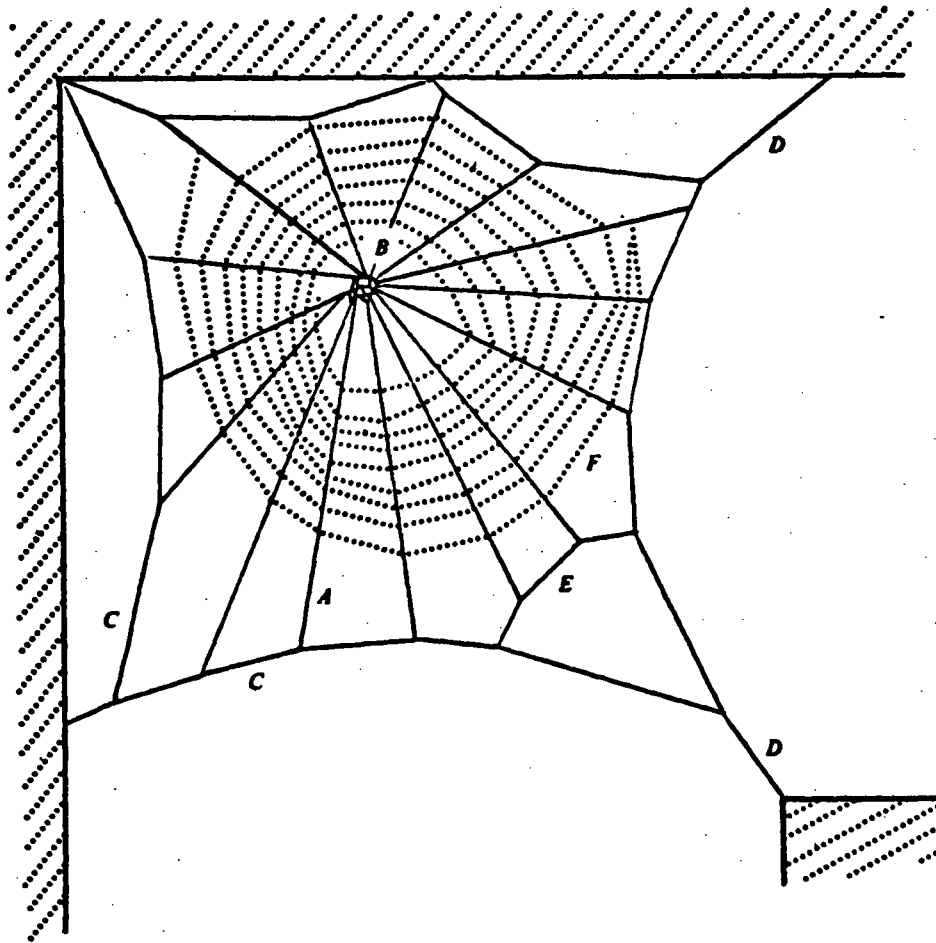


Figure 1.1. A diagram of an orb web showing the various components. Radii (A) diverge from a hub (B) and attach to the frame (C). The frame is anchored by mooring threads (D) to surrounding structures. Extra chords (E) are added to avoid attaching frame threads directly to mooring lines. Lastly, the spiral (F) with its gluey droplets is represented by the dotted line. (Taken from Denny, 1976)

wetted, but their functions are unknown. Their fineness makes them difficult to study using the light microscope, and little is known of their properties. The third pair of glands, the flagelliform, produces the silk used in the web's catching spiral (Andersen, 1970), the focus of this thesis. Spiral silk is often called viscid silk because it is coated with sticky, viscous glue from the many aggregate glands. The fifth set of glands produces the water-insoluble piriform glue which fixes the web to its supports; the source of the glue that attaches spiral to frame silk is unknown, but has staining and digestion characteristics different from the other glues (Kavanagh and Tillinghast, 1979).

These materials must all contribute towards making the orb an effective trapping machine; since the frame and spiral silks are the main structural components, it is especially necessary to understand their roles. In order to describe mechanical properties, a few engineering concepts must be defined. The "extension ratio" of a stretched fiber is the length of the fiber divided by its "slack length", the length in the unstretched state. In this paper, "extension" will mean "extension ratio". "Stress" is here defined as the force or tension on a stretched fiber, divided by the fiber's cross-sectional area at its slack length. "Strength" is the stress at the breaking point of a sample, and "stiffness" is the incremental change in stress per change in extension (the slope of a stress-extension plot). The act of normalizing by slack length and area convert the length and force values, which are specific to a particular object, to a material property.

Figure 1.2 shows the stress-extension curves for a few materials. Frame silk is seen to have a strength of over 10^9 N/m² (Denny 1976); it is stronger by weight than many steels, but not as strong as the synthetic polymer KEVLAR. It has a high stiffness, though its average slope is not quite as high as silkworm silk. It is not very extensible compared to some other silks, stretching only 1.3 times its slack length before breaking, but is more extensible than some of the highly crystalline silks, such as *B. mori* silk which breaks at 1.2 times slack length. In contrast, spiral silk is half as strong as frame silk, but extends as much as three times its slack length before breaking (Denny, 1976).

The manner in which the two silks stiffen as they are stretched is also dramatically different. As Figure 1.3 shows, frame silk is stiff from the start, with a slope of 10 GN/m² at

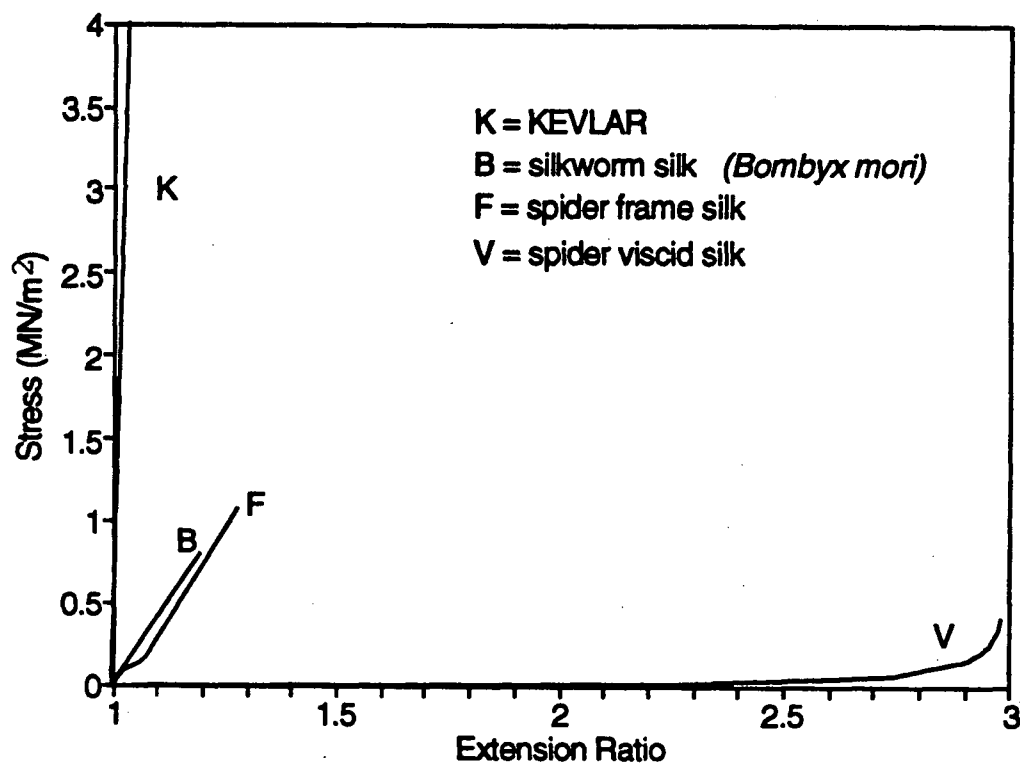


Figure 1.2. Stress-extension curves for four materials. Note that spider frame silk is very similar to silkworm silk, while spider viscid silk is radically different. Also consider that the areas under the curves of the silks are greater than the area under the curve for KEVLAR, meaning the stretchier materials are tougher despite their lower strengths.

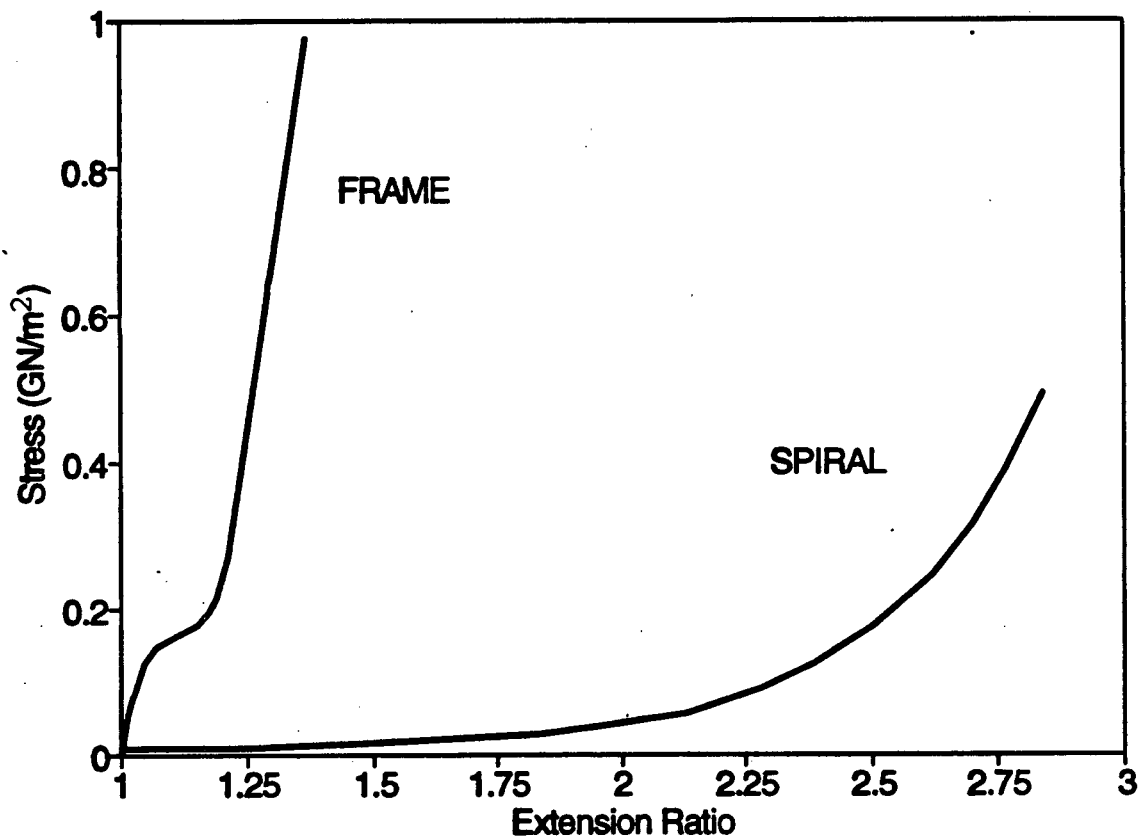


Figure 1.3. Typical stress-extension curves for dry samples of frame and spiral silk.

initial extensions; the slope only drops for a brief portion of the curve called the plateau region and then increases again until rupture, with a stiffness near breaking of 5 GN/m^2 and a strength of 1 GN/m^2 . In contrast, while viscid silk is almost as strong as frame silk (0.5 GN/m^2), it offers almost no resistance to stretching at first. It shows a low initial slope of 0.5 MN/m^2 (10,000 times less than frame silk), only stiffening to 0.5 GN/m^2 after it has been stretched by more than twice its original length, well past the breaking point of frame silk. The latter behavior, called a "J-curve", is characteristic of rubbery polymers.

The energy required to break a material, a form of work, can be expressed as Force times Distance, or Stress times Extension, or the area under a stress-extension curve. Despite the radically different mechanical behavior of frame and spiral silk, the areas under their curves are nearly equal. This means it is as difficult to break a certain quantity of the stretchy spiral silk as it is to break the same quantity of stiff frame silk; thus, the two silks are equally tough.

Interestingly, their toughness is significantly greater than that of the modern polymer, KEVLAR (refer back to Figure 1.2). With such high toughness, frame and spiral silks are admirably suited to catching flying insects. In what other ways are the two silks adapted to their functions?

Denny (1976) has shown that there is an optimal extensibility of about 1.4 for a tensile strand whose function is to sustain a load vector perpendicular to the strand. Frame silk's extensibility of 1.25-1.3 allows it to carry over 90% of the load it would if it could extend all the way to 1.4, so it operates close to the theoretical optimum. Perhaps its lower extensibility is a compromise related to other optima for vibration transmission (Masters, 1984).

If the situation is analyzed further from a dynamic perspective, it is obvious that a web should absorb the energy of an incoming missile, and not bounce dinner back out. Both frame and spiral silk have low resilience, around 33%. Thus, spiral silk fulfills the latter requirement, but it stretches far more than optimization calculations would predict if its function were merely to sustain static loads. Being stretchy, however, allows deceleration of an insect over a greater distance, thus lowering impact forces while still permitting high energy absorption. Realizing that spiral silk's function is also to restrain the victim once it has arrived, the stretchiness can obviously prevent solid purchase against the fibers, since they stretch the distance of an insect's kick with little resistance.

The properties of these silks change when they are wetted. Figure 1.4 shows that frame silk's stress-extension plot changes to a J-curve, while the wet slack length is only two-thirds that of the dry slack length (Work, 1981). Spiral silk retains its J-curve, while also contracting lengthwise. However, if wetted spiral silk is dried and stretched again, its behavior resembles that of dry frame silk, with a high initial stiffness, a plateau region, and increasing stiffness to breaking (Gosline et al, 1991).

As exemplified by frame and spiral silks, silks can be strong and stiff, strong and stretchy, weak and stiff, or weak and stretchy. What chemical or physical characteristics cause these huge differences in behavior? What characteristics are common to silks, and which may be the keys to understanding the control of their properties? Silks from arthropods have been categorized using many methods, both in an effort to determine taxonomically useful characteristics and in an effort to clarify the controlling factors of physical properties. First of all, a single silk can consist of protein units of different sizes. For example, silkworm silk is known to contain both very large chains (350kD) and "light" chains (25kD), which probably are covalently linked (Shimura et al, 1982). Frame silk is comprised of 300kD units (Xu and Lewis, 1990), and possibly smaller units.

Amino acid composition seems to have little effect by itself; silks fairly similar in composition can show remarkably different behavior. The simplest silk seems to be that of an east-African communal caterpillar: it contains little else but glycine and alanine, two crystal-forming residues (Lucas, Shaw and Smith, 1960). Other amino acid compositions range from somewhat hydrophobic to fairly hydrophilic, as will be described later. While silks generally have large amounts of residues with small side chains, proportions do vary, and the amounts of certain key residues, such as proline and cysteine, are widely variable between species. A few animals, like the silkworm, apparently use disulfide bonds for cross-linking (Sasaki and Noda, 1973), but spider silks have been assumed to be non-covalently linked due to lack of cysteine. Sequencing shows greater promise for unravelling the differences between fibroins, but thus far, only *Bombyx mori* (Nakajima, 1981) and *Nephila clavipes* dragline (Xu and Lewis, 1990) have been analyzed (and the latter not yet completely). Sequencing procedures take large amounts of time, expense, and dedicated instrumentation; yet knowing even the exact sequence of a protein

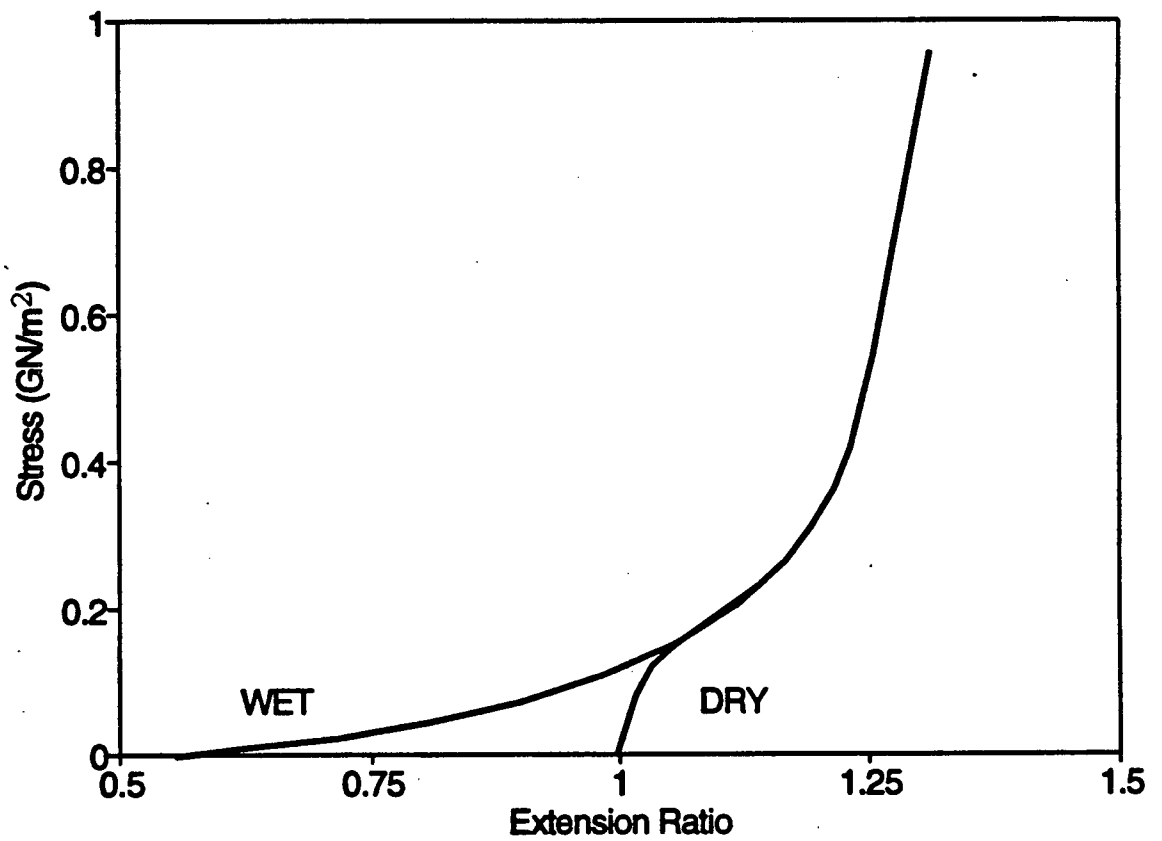


Figure 1.4. Typical mechanical behavior of wetted frame silk.

does not allow its structure and properties to be accurately predicted. Too many factors, like fluid components and processing, combine to determine molecular conformations, fiber structure, and ultimately, mechanical properties. As mentioned earlier, silks contain more than just protein. Amounts of carbohydrate vary, and various small hygroscopic molecules might function as plasticizers in amorphous networks. Thus, amino acid analysis or protein-sequencing alone might miss such critical modulating factors. Additional methods of investigation should therefore be concurrently pursued.

Regarding final conformations, crystal types have been analyzed for a wide range of silks from many types of arthropods (Warwicker, 1960), and the predominant type is found to be the antiparallel beta-pleated sheet structure. Sheet and chain spacing patterns give another level of classification based on X-ray diffraction patterns; *Araneus diadematus* dragline silk is in Class 5 because its intersheet spacing is large, allowing room for bulkier side chains. Sequencing of beta-pleated crystal types of silks may yield characteristic patterns distinguishable from those of the keratin-like (helical) or collagen-like crystal types. Crystalline regions are so abundant in silks that many appear to form functional crosslinks between chains, in the absence of any other special covalent bonds. In addition, the conformation of a silk protein molecule can change, passing through liquid-crystalline phases even as it is drawn from the spinneret (Kerkam et al, 1991; Work, 1977a). Thus, quantification of molecular alignment through birefringence studies can help determine relationships between crystal alignment and physical properties. The "amorphous" region may even contain certain organized structures, such as helices, which though undetectable by means of birefringence studies could be explored using infrared spectroscopy or circular dichroism.

In order to compare silks, a basis of commonality must be established from which deviations are noted. Despite the wide variation in chemical and physical properties, the fibrous silks seem to share a common structural plan. They are polymer composites; that is, they are made from long chain molecules aggregated together, with some proportion of crystalline inclusions (Gosline, Denny, and DeMont, 1984). The long chains, though cross-linked together for integrity, have some freedom of mobility under certain conditions; therefore some of the "elastic" restoring force of a stretched silk fiber can be entropically driven, as thermoelasticity

experiments demonstrate for frame silk (Gosline, Denny and DeMont, 1984). Such a material is called an elastomer, or rubber. The combination of the amorphous matrix containing crystalline inclusions comprises a sort of filler-reinforced rubber composite. The glue-like gland secretions are different in that they appear to have no stable linkages, and therefore they flow like viscous fluids.

Unlike synthetic rubbers, all rubber-like proteins require polar solvents (for example, water) to allow their polypeptide chains full mobility at room temperature. Without water, there is too much friction for them to act rubbery, so they become more like amorphous glasses, like the stiff and strong frame silk (Gosline, 1980; Gosline, 1987). When frame silk is wetted, it swells anisotropically, contracting lengthwise and expanding in diameter; the process is so dramatic that it has been called "supercontraction" (Work, 1977b). The physical change is accompanied by the change in mechanical properties shown in Figure 1.4, described earlier. That this wet contraction occurs despite a volume increase indicates that the molecules of frame silk are extended and fixed in position during processing, then remobilized in the solvent so that thermal energy enables the rubber-like entropic recoil. Spiral silk also undergoes wet contraction, as mentioned earlier, but spiral silk is especially interesting because it acts like a rubber even at normal, ambient conditions, unlike frame silk and the other biological rubbers that serve internal structural functions and are continuously bathed by body fluids.

Obviously, spiral silk behaves quite differently from frame silk. Yet frame and spiral silks have compositions too similar to expect radically different molecular structures; they both are comprised of nearly half small residues, significant portions of proline, and no sulfur-containing residues (Gosline, DeMont and Denny, 1986). For this reason, some researchers believe that the remarkable properties of spiral strands are due entirely to the glue which coats them. In fact, some researchers believe that spiral silk is drawn from the major ampullate glands (Calvert, 1989), despite much evidence to the contrary. Careful gland dissection and composition analysis have been correlated with observation of the states of gland fullness before and after various spinning tasks, and on the basis of the results, spiral silk was demonstrated to come from the flagelliform gland, not the major ampullate gland (Tillinghast, 1984; Andersen, 1970).

A further argument against the viscid silk's glue being the sole determinant of spiral silk's properties lies with thermodynamics. Consider the silk core, the glue layer, and the atmosphere to be three adjacent compartments (Figure 1.5). Water molecules pass between all three compartments, according to the free energy of each, or its affinity for water. Since the silk fiber is less than three microns in diameter, equilibration occurs in about a tenth of a second (Work, 1985). The argument that the glue layer "protects" the silk from drying out is invalid because an external hydrophilic coating will take water molecules from the core fiber as easily as from the air. The silk can be plasticized only if the fiber compartment itself contains molecules which alter the free energy of that compartment.

If the elastomeric behavior of native spiral silk is not due solely to a coating, then the answer must be sought in the silk fiber's structure and components. In order to determine the causes of the differences between frame and spiral silk, it is important to determine precisely what molecular differences exist; only then can the specific effects of composition, production techniques, or glue coatings be isolated. Such information is of interest to arachnologists, polymer chemists, textile industries, and possibly even military researchers.

This thesis therefore focuses on analyzing the molecular structure of spiral silk. The approach used is based on network models for elastomeric materials. Flory (1953) and others have developed theories of rubber elasticity which can predict the mechanical and optical behavior corresponding to different molecular networks. Conversely, the network of a given material can be deduced from its behavior. Furthermore, deviations from pure rubber-like behavior indicate greater complexity, such as crystalline inclusions. Thus, a better knowledge of the network characteristics of frame and spiral silks will allow other data, like the amino acid sequences which are currently sought by polymer scientists, to be more accurately interpreted. Therefore, the purpose of this thesis is to deduce the network characteristics of spiral silk from its mechanical and optical properties and to develop understanding of why the network of this rubber-like silk may be different from that of frame silk. Compared to frame silk, spiral silk is expected to have a structure which explains its greater extensibility and lower stiffness.

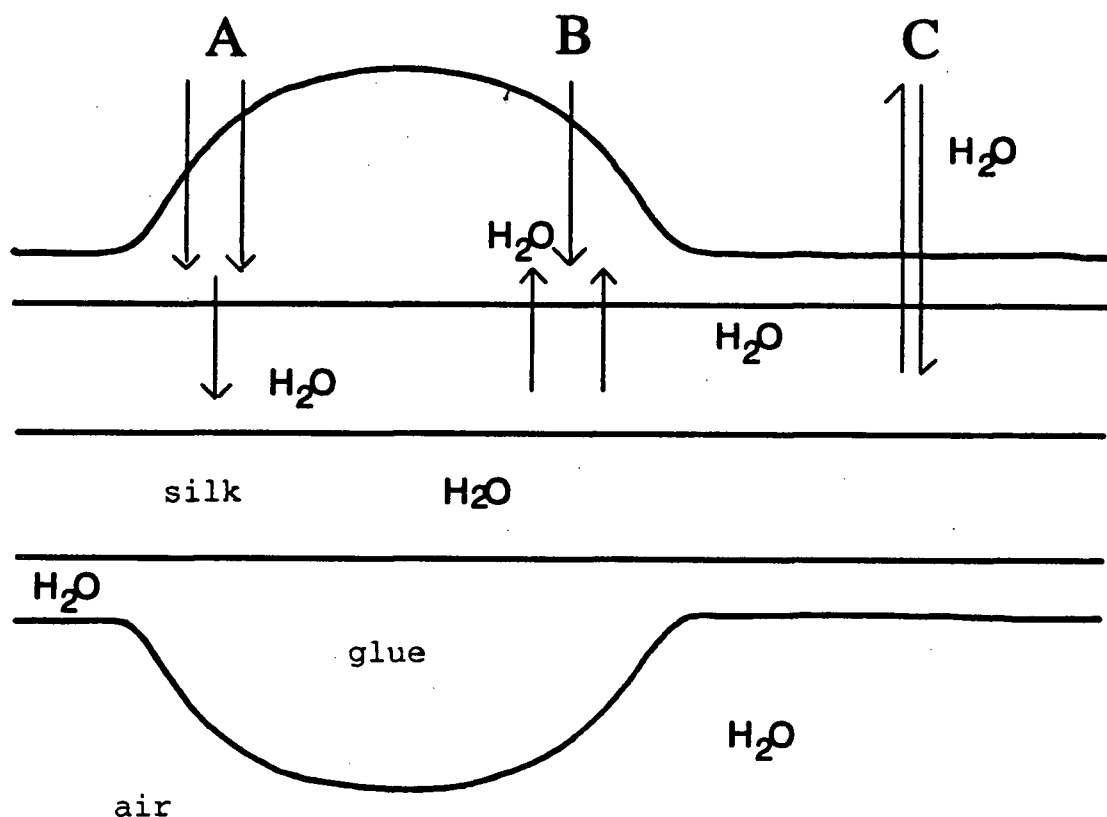


Figure 1.5. Diagram illustrating the movement of water molecules between the three compartments comprising a native spiral silk sample at room conditions of humidity. The diagram shows the spiral core fibers, the viscous glue coating, and the surrounding atmosphere containing water vapor. The water moves freely between the three compartments according to the free energy of each. Condition A illustrates the situation some researchers believe exists, whereby the glue layer hydrates the silk as it absorbs water. However, Condition B shows that if the glue layer absorbs water better than the silk core, water will move out from the fiber as well as from the air, and the silk will be dehydrated. The net result is that Condition C is the most accurate representation, illustrating the fact that the core fibers must ultimately be in equilibrium with the air, regardless of the water content of the glue layer.

CHAPTER II: METHODS

A. GENERAL OVERVIEW

In general, samples were mounted, subjected to a force-extension sequence, then immersed in water and subjected to another force-extension sequence. Finally, an optical analysis was completed. These and other samples were also used to check the uniformity of fiber diameter, fiber cross-section shape, volume change with extension, wet contraction time course, and the nature of spiral silk cross-links. Optical measurements were carried out for dry silk using another set of samples. The amount of information that could be obtained from a individual sample was limited by the incompatibility of certain procedures (for example, water and oil immersion), yet some samples were used for several sorts of data.

Some analyses were performed on entire, double-stranded fibers, while others concerned single, isolated fibers. For clarity, an intact double-stranded fiber, with or without glue, will be referred to as a "bave", and the individual strands comprising the pair as "brins", following terminology adopted for silkmoth threads. "Dry" means fibers are in their native, unwetted state, with the glue layer intact, at laboratory room conditions of temperature and humidity.

B. SAMPLE COLLECTION AND STORAGE

Orb webs of mature female *Araneus diadematus* spiders were obtained in late summer (September-October) from trees and bushes in the Pacific Spirit Park adjoining the University of British Columbia. Females are distinguished from males by their larger size, and they presumably produce larger-diameter silk to support their weight. However, the safety factor is very small when females are very gravid, indicating perhaps a limitation on the largest diameter a spider's valves can produce (if not changes in protein composition due to egg nourishment). Both male and female spiders have distinctive markings. Since spider webs are species-specific, an *A. diadematus* web can usually be distinguished from others by its size, pattern, and decorations; however, since webs were abundant and most were occupied, it was considered worth the extra time to take only webs whose owners had been unambiguously identified as

females of *A. diadematus*. Ideal habitats were fir trees and blackberry bushes, both of which possess branches generously spaced. While a particular site may be "harvested" several times in succession, the first web collected from a spider tends to be the most durable, because the frame is reinforced through multiple use. Since spiders have been known to die after only three consecutive days of entire web removal, at least three pleasant days were allowed to pass before collecting again from a certain local, in order to allow the spiders to replenish protein stores and rebuild the frame securely.

Wooden frames were used for web storage. The frames were two feet square, cut from quarter-inch plywood, with the perimeter one inch wide. Web collection was carried out by taping each web to a frame, severing the mooring lines, and storing the frames in wooden boxes with slots spaced one inch apart. Scotch brand Magic Tape was used on the frames to avoid long-term deterioration or embrittlement. Airborne particles, both animate and inanimate, tend to adhere to spiral glue, so the boxes had been air-blasted and vacuumed to remove sawdust, spray-varnished, and solvent vapors allowed to dissipate. The boxes were kept at room temperature and humidity, so the webs were not unduly exposed to extreme temperatures or ultraviolet light. The date, sample number, habitat, spider color, and general weather observations were noted directly on the tape of each frame using a permanent marker or ballpoint pen. If the spider was still on the web after its mooring lines were detached, she was gently removed and replaced on her branch to rebuild.

Care was taken to avoid deforming the webs, and silk samples were never taken from sections of web which were suspected to be deformed (except for later comparisons requiring potentially crystallized samples). Unusual webs, such as those with large spiral spacing, were also avoided, as such webs may be built by spiders late in the season and therefore may have anomalous compositions and properties due to age, cold or starvation; sometimes the catching spiral may even be glue-deficient.

Samples were removed from a web by placing the legs of a divider against the desired strand and snipping the silk to the outside of each tip with microscissors. The tips of the dividers were lengthened with flat toothpicks, to ensure a rough surface to which the silk would adhere well. Samples were taken at approximately three-quarters of the distance from the hub to the

rim. Samples in this region tended to be long enough for easy handling, yet did not seem to be overly strained. The natural (in-web) length of the web segment was compared with the slack length, to ensure that any overly-strained samples were avoided. (A strand that is held extended for a long time may crystallize; Gosline, DeMont, and Denny, 1986). Slack length was found by decreasing the length of the strand until it sagged briefly. Due to the surface tension of the glue, silk can be "reeled in" by the glue droplets, therefore the slacking process must be performed reasonably quickly (rates of about a half millimeter per second were usually used). If the silk slacks immediately, it may be already at an extension of less than slack; it must be extended a small increment, held at this length for a few minutes to allow glue redistribution, and then the slacking may be attempted again. This process was repeated until results were reproducible.

C. PHYSICAL PARAMETERS

1. Diameter measurements. Diameters of both dry and wet samples were measured, but each sample could only yield one type of data, either dry or wet, but not both. Some wet samples were single-stranded, having been isolated during the mounting process, while others remained in their naturally double-stranded state. All room condition diameters were taken from double-stranded bave, due to the near impossibility of separating the gluey brins.

All diameter measurements were made under a Wild M21 polarizing microscope with either an 80X water immersion lens (wetted samples) or a 100X oil immersion lens (dry samples). The trinocular insert magnification of 1.25X plus ocular magnifications of 15X yielded total magnifications of 1500 and 1875. A Wild 15X Filar eyepiece micrometer, calibrated using a slide etched with both 10- and 100-micron spacings, was used for the initial studies. Later measurements employed a Nikon 10X eyepiece micrometer calibrated using the same slide. The accessory magnification ring of the Nikon, checked before and after each session, was always set on "1". Standard Koehler illumination protocol was followed. Proper condenser focus was especially critical because the small size of the strands, only a few times larger than the wavelength of light, meant the limit of resolution of the light microscope was approached. Details such as edges were liable to be confounded by diffraction and scattering.

Consistency in measurement methods was important, since the sighting filament has a finite width. Readings were taken by moving the filament from the outside of the brin's image until the filament merged with the edge of the brin. This method reduced the amount of variation that occurs when taking diameter measurements at different magnifications. For example, when a 10-micron glass fiber is measured, its apparent size increases as the magnification is increased from 10X to 20X to 40X. The increase is unacceptably high when the reading is taken by moving the filament from the "inside" of the fiber until it merges with the edge, but is within the coefficient of variation when the outside-merge method is applied. Error is smaller when switching between higher magnifications, so difference between the 80X and 100X lenses is negligible.

The orientation of brins relative to the viewer can be deduced from the type of image perceived (see Figure 2.1). If the image appears as three narrow parallel lines equally spaced, the two brins are lying in the horizontal plane. This orientation will be referred to as "Adjacent". If only two lines can be seen, the brins are in a vertical plane, and are called "Stacked". If three lines are seen, but their spacings are not equal, the brins are lying in a plane not exactly horizontal or vertical and are called "Tilted". If fine focus is adjusted, the middle line can be seen to shift closer to one edge and away from the other, thus confirming that the viewer is not simply seeing a thin and a thick strand adjacent to each other. At some points, the transition from one orientation to another can be very sudden, within the distance of a few diameters, and this phenomenon is called a twist. Diameter measurements were not taken from any region showing anomalous orientations, since such a region was likely to be damaged (for example, flattened). Since the thickness of the middle line was no greater than the outer lines in the adjacent orientation, diameters could be taken using the outer lines only, and dividing by two.

2. Uniformity of diameter. Early in the study, it was observed that although the diameter measurements at a particular position on a sample were highly reproducible with little scatter, there was significant statistical variation between measurements at different locations on the same sample. A few samples were therefore measured at frequent intervals along their length, to estimate the extent of the variation. Diameter data incidental to force-extension and

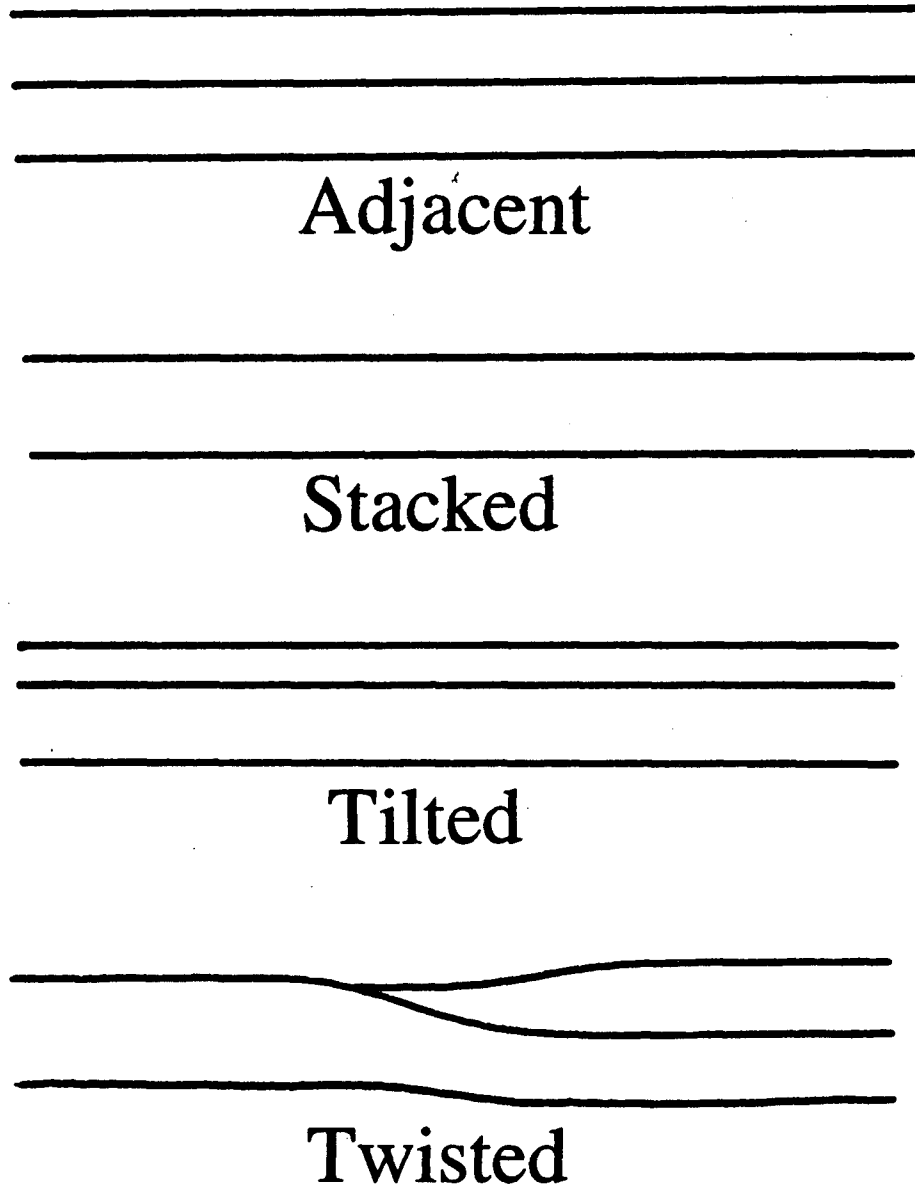


Figure 2.1. Four typical orientations of silk bave as viewed under the microscope, either dry or wetted. Note that the diameter of stacked fibers is greater than the diameter of adjacent fibers, and that there is a measurable difference in the diameters on either side of the twist.

birefringence studies were also analyzed. Means and coefficients of variation were calculated for measurements made at a single location and at multiple locations, with small sample formulae applied where necessary. The same simple statistics were used to compare diameters of fibers at known angles of orientation.

3. Cross-sectional shape analysis. The rotating mount.

The diameter of a fiber can be measured from different angles, and the degree of ellipticity can be estimated, as illustrated in Figure 2.2. A special mount was designed for rotating a sample about its long axis by 180 degrees. Two 27 1/2-Gauge syringe needles were extracted from their cement-and-plastic bases. The tip of each needle was dulled to reduce the risk of injury. Each needle was then bent into a right angle with needle-nose pliers, such that one leg was twice as long as the other. The long shank was lightly greased with Vaseline petroleum jelly and then set on a medium coverslip, perpendicular to the edge, with half the length of the long shank extending past the edge. A drop of Araldite Rapid epoxy was deposited over the part of the shank resting on the coverslip, being careful that the shank did not shift and smear the grease.

Upon hardening, the shaft could be turned easily using the short angle as a lever, since the grease (usually such a problem when glueing!) prevented the epoxy from adhering. One of the coverslips was epoxied to a large slide; the other was placed opposite but given a tiny dab of Silicone vacuum grease on which it could ride. The needles were cleaned free of oil with a sequence of Sparkleen labware detergent, Xylene, and rinsing with distilled water. A silk sample was positioned along the axes of both long shanks, then glued with Araldite Rapid. The sliding coverslip allowed adjustment to wet slack and measurements at any extension.

After sufficient hardening time, the mount was wetted, the length adjusted, and diameter measurements were made at 0, 45, 90, 135, and 180 degrees rotation, where 0 and 180 correspond to the short shank resting on the coverslip, and 90 degrees corresponds to the short shank pointing vertically. The correct angles were determined by holding an index card, with the angles drawn on it, vertical next to the shaft. The needles were rotated simultaneously to discourage twisting of the silk.

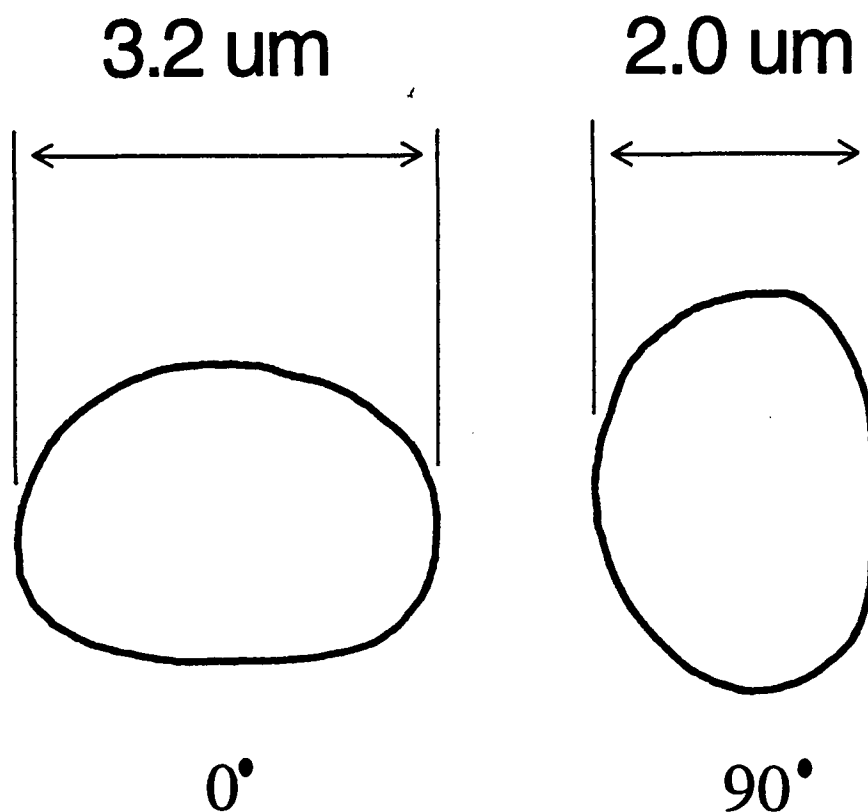


Figure 2.2 Cross-sectional views of a brin being rotated by ninety degrees. Light rays would pass from the bottom to the top of the page. The viewer will perceive the fiber as having a different diameter at each angle of orientation, with the maxima and minima corresponding to the major and minor axes of an ellipse. Note that the edges of the brin at zero degrees will appear sharper than those of the brin at ninety degrees.

Analysis of rotation data: A regression was performed on the diameter data. Each set of five readings was fit to the formula

$$(1) \quad Ax^2 + 2Bxy + y^2 = D,$$

derived from the equation given by Batschelet (1981). The equation obtained was first rearranged for regression use, yielding

$$(2) \quad y^2 = D + Ax^2 + 2Bxy.$$

For regression purposes, y^2 is considered to be dependent, while x^2 and xy are independent variables. Next, diameter data were converted so that measurements of isolated brins at unknown orientations could be used, yielding the following formulae, where d =diameter at a particular rotation-angle of θ :

$$(3) \quad x^2 = (0.5*d)^2 \cos^2\theta$$

$$(4) \quad y^2 = (0.5*d)^2 \sin^2\theta$$

$$(5) \quad xy = (0.5*d \cos \theta)(0.5*d \sin \theta)$$

STATGRAPHICS software performed a multiple regression on each set of five diameter readings, yielding the constant, D , and the coefficients A and $2B$ (x^2 is treated as independent, while both y^2 and xy are considered dependent). Given the above values, the major (a) and minor (b) axes of the elliptical cross-section, plus its area and orientation (angle of tilt, Φ), can be determined using these formulae:

$$(6) \quad R = \sqrt{(A-1)^2 + 4B^2}$$

$$(7) \quad \gamma_1 = (A+1-R)/2D$$

$$(8) \quad \gamma_2 = (A+1+R)/2D$$

$$(9) \quad a = 1/\sqrt{\gamma_1}$$

$$(10) \quad b = 1/\sqrt{\gamma_2}$$

$$(11) \quad \Phi = \tan^{-1}[2B/(A-1-R)]$$

$$(12) \quad \text{Area} = \pi ab$$

In order to simplify calculations of stress and comparisons of samples and webs, two additional terms were introduced. "Ellipticity", E , is defined here as the ratio of the major axis to the minor axis. In cases involving bave at known orientations, the average of "stacked" diameters (d_{st}) is considered to represent the major axis, and the average of "adjacent" diameters (d_{adj}) represents the minor axis, such that

$$(33) \quad E = d_{st}/d_{adj}.$$

"Effective diameter", d_{eff} , is defined as the square root of the major and minor axes multiplied together, such that $d_{\text{eff}} = \sqrt{d_{\text{st}} \times d_{\text{adj}}}$. The effective diameter was used, whenever available, for cross-sectional area and volume calculations. Also, in tables which include values for "average" diameters, the effective diameter is quoted whenever possible.

4. Volume-extension measurements. The volume of a sample is calculated as for a cylinder, where

$$(13) \quad \text{Volume} = \text{Length} \times \pi r^2.$$

Data from several sorts of experiments were used; any involving the gradual stretching of a sample with diameters measured at known intervals of extension were useful. Orientations were not known because isolated brins were used. For this reason, it was not possible to use effective diameters.

D. MECHANICAL STUDIES

1. Models for elastomeric materials. Gaussian rubber network theory. The kinetic theory of rubber elasticity, developed by Flory (1953) and others, is based on a molecular model with two tenets: firstly, rubbers are composed of long-chain molecules which can move about freely, and secondly, the chains are bonded together at enough locations to keep the material from flowing apart, without restricting chain mobility. Thus, a rubber can be described by the packing density of the long molecules and the frequency of the bonding crosslinks.

A "chain" is defined as the portion of a molecule whose ends are defined by two crosslinks. The chains (in this case, long polypeptides) are modelled as many rigid segments joined by flexible hinging joints, like a chain of paperclips. It is assumed that each segment can randomly orient relative to the segments attached to itself, and is kept in continuous motion due to thermal energy.

The Gaussian theories of rubber elasticity are so called because simple predictions of rubber behavior are based on the Gaussian probability distribution of the distance between chain

ends. Thus, if one is given a polymer with chains of length L , and s ideal random segments, Gaussian theory predicts a most-probable distance between chain ends (cross-links, in this case).

If the ends, on average, are closer or further apart than the most probable distance, a force is required to maintain that less-random state, just as energy is required to decrease entropy of any physical system. The force required is dependent only on the density of the chains, as long as the chains are long relative to the distance by which the ends are separated. If there are more chains packed into a given volume of material, the retractive force is greater. The relationship between stress, σ , and extension ratio, λ , is given by this equation:

$$(14) \quad \sigma = NkT(\lambda - \lambda^{-2})$$

The quantity NkT is the shear modulus, G , of the material as it is initially extended. The shear modulus is therefore dependent on the number of chains per unit volume (N), Boltzmann's constant (k), and the temperature in Kelvin (T):

$$(15) \quad G = NkT$$

Non-Gaussian network theory. Experimenters noticed, though, that the Gaussian theory failed when chains were "short"; that is, when the object was stretched such that the distance between chain-ends was close to the chain length. The theory was extended, encompassing these "non-Gaussian" phenomena, by accounting for the extra recoil forces produced when a chain is stretched out to the point where the orientation of each segment begins to be restricted. The non-gaussian theory, as outlined by Treloar (1976), predicts the forces for a stretched network, given two parameters: the average number of random segments between crosslinks (s), and the chain density (N):

$$(16) \quad \sigma = NkT(\lambda - \lambda^{-2}) \{ 1 + (3/25s)(3\lambda^2 + 4/\lambda) + \\ (297/6125s^2)(5\lambda^4 + 8\lambda + 8/\lambda^2) + \\ (12312/2.205 \times 10^6 s^3)(35\lambda^6 + 60\lambda^3 + 72 + 64/\lambda^3) + \\ [126117/693(673750)s^4][630\lambda^8 + 1120\lambda^5 + \\ 1440\lambda^2 + 1536/\lambda + 1280/\lambda^4 + \dots] \}$$

The above equation is not merely a high-order, empirically deduced formula; it is derived from the inverse Langevin probability function governing the chain-end distribution of non-Gaussian

(high-extension) networks. The formula can be arrived at using either mathematical or thermodynamic theories.

Conversely, the theory can be used to analyze a force-extension curve and estimate the network parameters. The latter procedure is the one applied to viscid silk in this study. Each stress-extension data set is fitted to the above formula, using a range of possible segment count values, s . The best fit is determined as the value of s that yields the highest coefficient of determination, R^2 , for a linear regression. Then, the slope of the best-fitting regression yields the modulus, G , of the network.

Researchers realized that for real molecules, not every chemical unit (e.g., amino acid or monomer) has completely free rotation about its neighbor; that is, a single amino acid does not constitute a "random segment". Steric hindrances exist which restrict each chemical unit but, on average, a certain number of these units together can behave as a random segment. The number of amino acids required for a segment of protein to behave as a random segment can be deduced from the known material density (mass per volume, not including water), the known average monomer weight (grams per amino acid), and the predicted chain density, N , taken from the stress-extension curve. The chain density is determined from the shear modulus using Equation 15. Then the mass of the chain between crosslinks can be derived:

$$\text{mass/chain} = (\text{mass/vol})/(\text{chains/vol})$$

$$(17) \quad M_C = \rho_{\text{wet}}/N$$

where M_C = kg per mole of chains, and the density of the wet material is in units of kg/m^3 . Note that the density of the rubbery protein matrix is needed, excluding water and crystalline regions. If V_X is the crystal volume fraction of the dry silk, then the wet matrix volume fraction (V_R) can be determined from the change in volume (ΔV) from dry to wet states:

$$(18) \quad V_R = (1 - V_X)/(\Delta V - V_X).$$

Then the density of the water-swollen rubber is the product of the wet matrix volume fraction and the dry density.

Once the weight of the entire chain between crosslinks is determined, the molecular weight of a random segment is

$$(19) \quad M_S = M_C/s.$$

where s = the number of ideal random segments per chain. Then, since the average amino acid residue weight (M_{aa}) can be calculated from a composition analysis, the number of amino acid residues comprising one random segment is

$$(20) \quad A = M_s/M_{aa}.$$

2. General setup for extension studies. The general experimental setup involved gluing a piece of silk between a transducer and a micrometer, that were in turn affixed to a platter that was mounted on the stage of a compound polarizing microscope (see Figure 2.3). The transducer was a thin glass rod acting as a cantilever beam, with the silk attached to the tip. The beam deflection was monitored by a Video Dimension Analyzer via a camera mounted on the accessory viewport of the microscope. Signals were transmitted to a chart recorder for later analysis. Optical retardation measurements were made by either electronic or manual methods.

3. Platter stage mount. Dry bave samples were mounted on a stage-mountable extension platter (Figure 2.4). This assembly consisted of a 1/10th inch thick plate of aluminum with a viewing hole in the center. Screws with washers large enough to span the location-adjustment slots attached the platter to a microscope stage. A Mitutoya micrometer with a non-rotating shaft, for extension control, was bolted to one edge. A brass ring 7 mm wide and 4 mm thick was fitted to the shaft; it was secured with a brass or nylon set screw. A hole barely larger than an 18 gauge needle was drilled into the rim of the brass ring, parallel with the axis of the shaft and on the side opposite to the set screw. An 18 gauge syringe needle was epoxied into the hole with slow-setting Araldite epoxy. Two successively smaller syringe needles were fitted so as to extend the first, but no epoxy was necessary to hold them, since the fit was so close that friction prevented slippage. The last 2 mm of the tip was bent at a right angle to provide a protrusion about which silk could be wrapped.

Four screws with brass and neoprene washers secured a large (75 x 50 mm) glass slide over the viewhole. It is critical to avoid epoxying the slide to the platter, especially if heat-curing is employed, since aluminum and glass have different coefficients of thermal expansion; any temperature change induces strain in the glass which interferes with birefringence

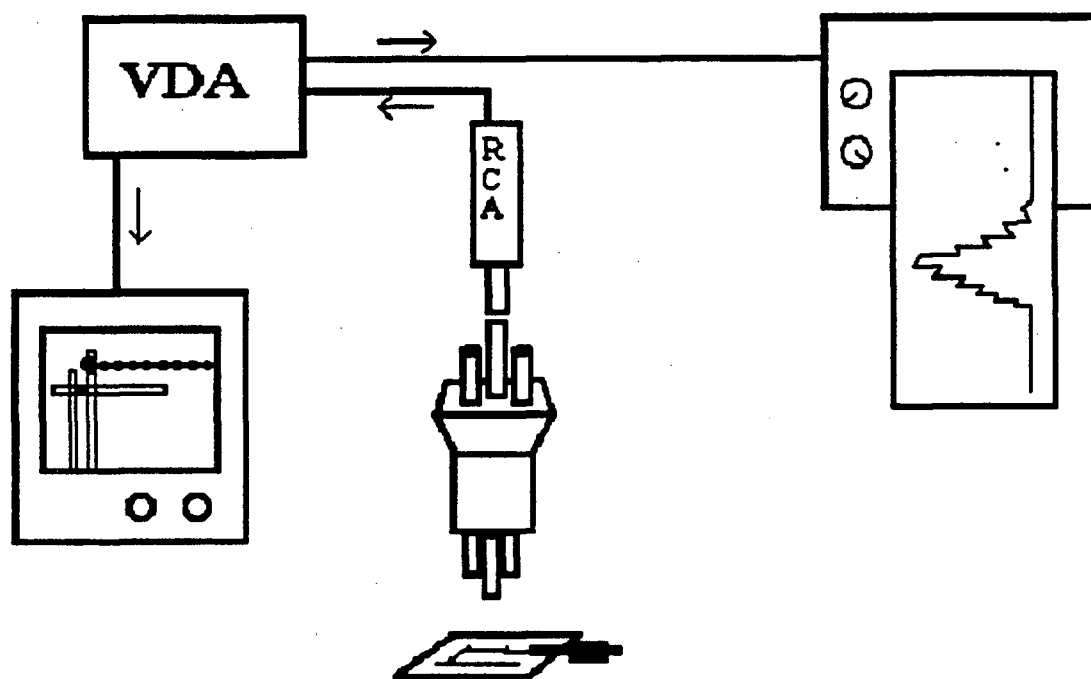


Figure 2.3. Instrumentation setup for mechanical studies. The camera is placed over the accessory trinocular viewport such that the image of the reference and transducer beams is located in the central left region of the monitor, with the electronic voltage "window" positioned across both of them, as close to the silk sample as possible.

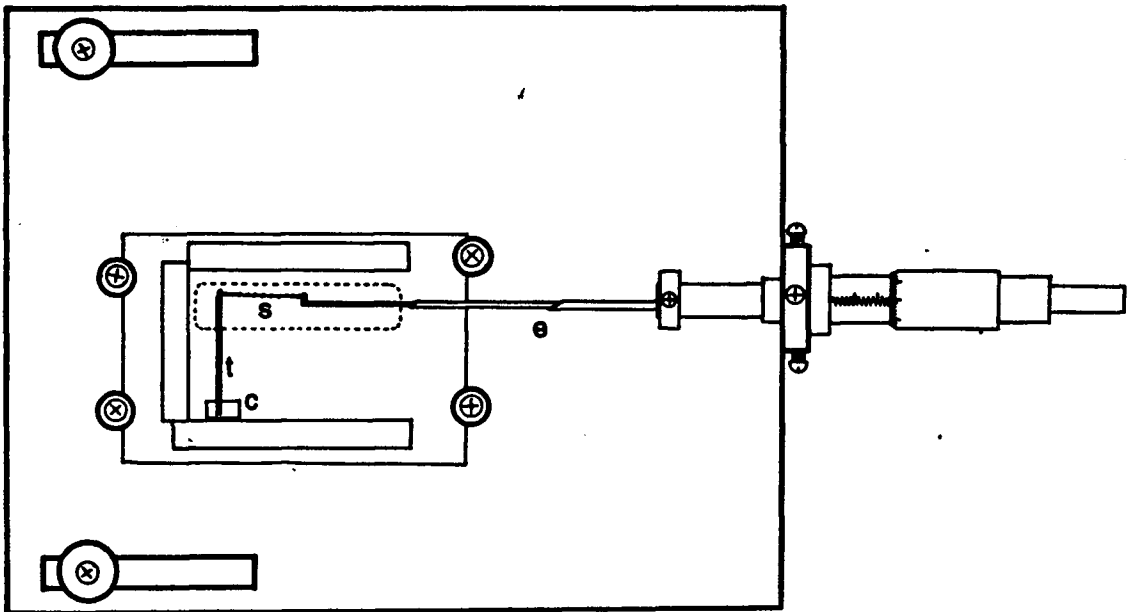


Figure 2.4. Stage platter for mounting silk samples. The silk sample, *s*, is mounted between the transducing beam, *t*, and the micrometer extender, *e*. The beams are mounted on a stack of coverslips, *c*, on a large glass slide which is fastened over a light hole (dashed line).

measurements. On the slide, two adjacent flexible glass cantilever beams are affixed to a platform of two stacked coverslip bits. One of the beams is used as a force transducer and the other as a reference beam from which the deflection is monitored. The beams are pulled from 5mm rods over a gas/oxygen torch. The torch and the oxygen mixture are necessary to produce a hot enough and local enough melting of the glass rod; a standard lab gas burner is acceptable for making fibers over 150 μm in diameter, but fibers under 100 μm diameter are almost impossible to obtain given finite arm length for pull-distance. Successful glass beams were about 15-20 mm long and 65-100 microns in diameter.

Since the beams are later viewed under a compound microscope, depth of field can become critical. It is best that both beams in a transducer-reference set are of similar diameters, else the edges, tangent to the light rays, may focus at different levels. While gluing the beams to their base platform, it is also important to support the free ends of the beams with a stack of coverslips equal in thickness to the platform itself. The beams should not touch each other at any point along their length, and the tips should be no more than two beam-diameters ($\approx 200\mu\text{m}$) apart.

Three to four narrow pieces of glass were glued down to help contain water in the area of the beams and silk sample. Two-part epoxy (either Fast-Weld, Araldite Rapid or Devcon 5-Minute) was used for all glass gluing. A pair of EM forceps whose inside tip surfaces had been thinly coated with silicone sealant (caulk) were useful for manipulating bits of glass and syringe needle.

One end of the silk sample was laid across the tip of the transducing beam, and the other end was laid along the end of a syringe-needle extension of the micrometer. Both ends were then persuaded to detach from the dividers.

4. Glue types and techniques. Methods of gluing the silk to the beam and needle varied. The viscid glue has the potential to form a lubricating layer between the brins and the adhesive, so that poor adhesion might allow the silk to slip from its mount. Thus, progressively more thorough though time-consuming methods were used to ensure that the silk was truly "breaking" due to failure, and not simply slipping out of the adhesive. Initially, the mount was cleaned with

Sparkleen glassware detergent and Araldite Rapid was used, as it was used successfully with frame silk previously. The epoxy was tried on top of the strand, under the strand (i.e., applied to the beam and needle before the silk was laid down), or both below and on top, by far the most effective option. Epoxies and glues were applied with disposable pipettes drawn to a fine tip over a burner.

Later methods involved a two-part polymerizing adhesive called Loctite Depend, which should seal even through oil layers. This glue was tried in case skin oils or other residues were discouraging adhesion. The mount was cleaned thoroughly first with Sparkleen, followed by 96% ethanol to dissolve Depend polymers which are derived from methacrylic acid (Merck Index, 1976), then Xylene, and a final distilled-water rinse.

Depend is not mixed before application: the recommended method for macroscopic applications is to apply Part A to one side, Part B to the other, and press them together. Since hardening occurs in 45 seconds, and the placement of silk strands takes substantially longer than the working time of Depend, an alternative method was adopted. First, the beam and needle were coated with as thin a layer as possible of Part A. Second, the silk was positioned and wrapped around the beam. Third, a thin coating of Part B was applied over Part A. These two layers were allowed an hour to polymerize, then several more alternating layers were applied. Two to three days were allowed for full hardening to proceed, indicated by a clouded appearance, and lastly a "safety layer" of Devcon 5-Minute epoxy was used to coat the surfaces and inhibit water penetration or slippage. Devcon was used because although its water-permeability is somewhat greater than that of Araldite, it is less viscous immediately after mixing and therefore coats the beam tip easily.

For a period of time, Ciba-Geigy Fast-Weld epoxy was tried for certain stress-extension experiments where both dry and wet data were desired from a single sample. Fast-Weld is opaque, and there was a possibility that the pigment fillers might have lent greater stability to the epoxy when wetted. The epoxy was successful for use in dry experiments, but of the three samples attempted, all immediately broke when water was added. It seems that the heat given off by the Fast-Weld curing reaction is significantly higher than that of the other epoxies, and weakens the silk at its junctions with the beam and needle. Araldite Rapid, on the other hand,

has not just a longer pot-life, but a significantly longer curing period once the process begins. Thus heat has a chance to dissipate without harming the silk. The five-minute epoxies lie somewhere between as regards heat generation. The success of Depend may be due in part to its long polymerization time.

The epoxies cured into rigid shells which often could be slipped off the beam after several days of immersion in water. The Depend, on the other hand, seemed much more pliable than epoxies, yet it had the redeeming quality of admirable tenacity. Even after days of immersion, scraping with scalpels could not entirely remove the polymer. Instead, the ethanol rinse was introduced to remove all traces before reusing a mount.

5. Force calculations. To calculate the force causing the bending of the transducer beam, a formula was used that incorporates the known stiffness of glass, the dimensions of the beam, and the observed deflection from the reference:

$$(21) \quad F = 3(D * E * I) / L^3,$$

where D is the observed beam deflection, E is the modulus of the glass used ($6.2 \times 10^{10} \text{ N/m}^2$ (Aaron and Gosline, 1981)), L is the length of the beam from its base to the point of silk attachment, and I is the second moment of inertia for the glass beam, given by

$$(22) \quad I = \pi r^4 / 4.$$

Note that as the silk is extended, it pulls on the beam, therefore the deflection of the beam must be accounted for in calculating the actual length of the silk. The beam deflection must be subtracted from the micrometer reading.

One problem encountered using small-diameter beams was the high incidence of taper. The odds of creating a non-tapered beam were so small that it was necessary to derive a formula for the "effective diameter" of a tapering beam.

The tapered-beam formula. The Moment-Area Integration method is used. This theory states that the bending stiffness of each increment of the beam adds to the net result in proportion to its distance along the beam. In symbolic notation,

$$(23) \quad D = \int_0^L \frac{Mx}{EI} dx.$$

where M is the bending moment, E the modulus, and I the moment of inertia. Note that x is the distance from the tip, not the base, of the beam.

In the case of terminal transverse loading (a load perpendicular to the beam and concentrated at its tip),

$M = Fx$ at any given point along the beam. Conventionally, the origin ($x=0$) is the tip of the beam, so $x=L$ at the base. Since the weight of the beam causes bending orthogonal to both the beam axis and the silk tension, the weight can be ignored. Thus

$$(24) \quad D = \int_0^L \frac{(Fx)x}{EI} dx = \frac{F}{EI} \int_0^L x^2 dx = \frac{F}{EI} \frac{1}{3} x^3 \Big|_0^L = \frac{FL^3}{3EI}$$

The above equation is the standard force-deflection formula for a straight parallel-edged beam. Note that because the beam is parallel, the moment of inertia (the second moment of area, determined by the cross-sectional size and shape) is constant along the length and can be moved outside of the integral. Thus, for a circular beam,

$$(25) \quad I = \frac{\pi}{4} R^4, \quad \text{so } D = \frac{4}{3\pi} \frac{FL^3}{ER^4}, \quad \text{and } F = \frac{3\pi}{4} \frac{DE}{L^3} R^4$$

For a tapered beam, however, the cross-sectional area and therefore the second moment of area varies continuously along the beam's length, and the integral becomes more complex.

If the radius is a linear function of x , then

$I = (\pi/4)(R+px)^4$, where R = tip radius and p = change in radius per unit length, towards the base. Thus

$$(26) \quad D = \int_0^L \frac{F}{E(\pi/4)(R+px)^4} x^2 dx = \frac{4F}{\pi E} \int_0^L \frac{1}{(R+px)^4} x^2 dx.$$

From integral tables,

$$\int \frac{1}{(a+bx)^4} x^2 dx = - \left[\frac{x^2}{b} + \frac{ax}{b^2} + \frac{a^2}{3b^3} \right] + (a+bx)^{-3}$$

and so

$$(27) \quad D = - \frac{4F}{\pi E} \left[\frac{x^2}{p} + \frac{Rx}{p^2} + \frac{R^2}{3p^3} \right] + (R+px)^3 \Big|_0^L$$

This equation reduces to

$$(28) \quad D = \frac{4L^3}{3\pi E} \frac{F}{R(R+pL)^3} \quad \text{or} \quad F = \frac{3\pi}{4} \frac{DE}{L^3} R_{\text{tip}} (R_{\text{base}})^3 .$$

The effective radius is therefore

$$(29) \quad R = 4\sqrt{R_{\text{tip}}(R_{\text{base}})^3} .$$

This means the base radius is most significant. In fact, an error of 33% can be made if the tip radius, the easiest place to measure, of a 2 cm-long beam with 10% taper (10% narrower at base) is taken as the overall radius. Conversely, epoxy at the tip of the beam will have a negligible effect, even if its modulus were comparable to that of glass.

6. Preparation of wet samples. In order to ensure that the silk was fully plasticized, samples were immersed in distilled water throughout the entire course of wet force and birefringence data collection. It is important that no section of the sample be exposed to air at any moment after wetting, however brief, since once the glue is washed off the fiber, its properties change (Gosline et al, 1991). Wetting was carried out in such a way as to discourage the sample from sticking to the slide or floating in the surface tension of the fluid. The method entailed wetting the needle first, so that the droplet of water surrounded it entirely and bulged above it somewhat, and then "feeding" the droplet so that the water front advanced past the tip and along the length of the silk sample to the beam.

This method kept the silk thread perpendicular to the water surface at all times, so that surface tension was unable to stick the silk down or catch it in the interface. When either of these events did occur, it was usually impossible to detach or immerse the silk without damaging it; glue caught between silk and glass proves itself surprisingly resistant to dissolution.

Samples were immersed in early morning. Water causes viscid silk to swell laterally and contract lengthwise, so immediately after wetting the silk was slacked again. The sample was allowed to equilibrate for a few (2-4) hours, until the contraction rate was negligible, or less than about 0.03 mm per half-hour. At this time, a single brin was isolated from the bave. (If a gap

appeared earlier on, the isolation was performed before equilibration was complete). Probes, made from toothpicks with a Size 0 insect pin epoxied to the tip and a Minutae insect pin epoxied to the larger pin, were used to separate strands. Difficult samples sometimes required a pulled glass capillary tube, like those used for nerve electrodes. EM forceps held one brin aside while microscissors were used to clip it as closely as possible to the beam and needle tip. Single brins were first used because diameter measurements seemed to be easier without the complication of twisted and overlapping strands; this was before the ellipticity of fibers was confirmed.

After equilibration, a large coverslip was placed over the beam and strand, and the platter was mounted on the rotating stage of a Wild polarizing microscope. The slot/screw/washer system allows fine positioning, yet the platter can be fixed firmly in place. Smooth movement and no lifting of the platter is ensured by spreading a liberal amount of silicone vacuum grease on the stage.

The sample was examined for defects under low power (10X objective). Generally, any strand which had reached this stage without sticking to slides or breaking during isolation had done so because it was a smooth fiber with no large dirt particles to discourage glue dissolution. If a large particle was detected at an early stage, the mount was discarded because of the high probability of adhesion to the water immersion lens during birefringence measurements.

7. Camera/VDA setup. The tips of the beams were next located under 4X or 10X. The microscope is equipped with a third viewing tube (a trinocular insert), and an RCA closed circuit TV camera (TC-2011/N) with high sensitivity and automatic gain control was attached. The image from the camera was input to the Video Dimension Analyzer (VDA), model 303 (manufactured by Instrumentation for Physiology and Medicine, Inc.). The VDA outputs the image from the camera, as well as a voltage proportional to the spacing between two contrast boundaries. The contrast boundaries are selected by the user by positioning a superimposed electronic window across the desired edges of the image, as illustrated in Figure 2.3. The voltage output was directed to one channel of a Linear two-channel chart recorder for a permanent record.

Two methods were used for calibrating the VDA output. Initially, an etched calibration slide with both 100- and 10-micron increments was used. A more reliable calibration used the beam itself, the diameter of which had been previously measured using an ocular micrometer. This procedure allowed easy calibration at the beginning and end of each experiment, without having to remove the platter or change focus.

The zero offset and calibration of the VDA were found to be extraordinarily stable, both during an experiment and from week to week. The maximum error due to trigger adjustment was less than 1%. The effect of image location relative to the field viewed by the monitor was investigated by making measurements on the etched calibration slide in different field locations. The variation due to image position was about 5% for the entire screen, but readings were confined to a central left region with a variation of only 1%.

Force-extension (F-E) measurements were performed on the same scale as the birefringence measurements. Since the birefringence measurements are time-consuming and should be done on a sample whose birefringence is not changing, both sets of data were collected under pseudo-static conditions; that is, extension was in increments or steps, and the sample was allowed time to equilibrate at each step. The equilibration time necessary ranged from negligible at very low extension to five minutes at the highest extensions. The equilibrated force values were the ones recorded. The silk was extended to 2X or greater wet slack length, then returned to its new slack length. Larger increments were permitted at higher extensions, and fewer data points were taken during recoil, in order to reduce the total time needed for experiments. Good resolution was more critical for the rising curve, as these were the points fitted to the non-Gaussian model. The recoil data will be useful for analysis of hysteresis at a later date.

8. Modifications for dry samples. Extension of dry fibers was carried out in a similar manner, but the silk was mounted higher to decrease the chances of the strands sticking to the slide at slack extensions. The glass reference and transducer beams were mounted on a small piece of slide glass, rather than coverslip bits, and the micrometer's syringe needle extension was slightly bent to raise the tip higher from the slide surface. Samples that were subjected first to dry

extension cycles and then to wet cycles did not usually yield good wet diameter measurements, because the necessary higher-altitude mounting prevented correct condenser focus.

E. WET CONTRACTION

When a sample of spiral silk is wetted, it shortens and increases diameter. Thus, three types of data are relevant to the phenomenon. Firstly, the "Wet Contraction Ratio", given as the wet slack length divided by the dry slack length, $WCR = L_{0,wet}/L_{0,dry}$, was easily calculated for most samples subjected to wetted force-elongation experiments. Secondly, the time-course of the contraction process was followed by recording the wet slack length as soon as possible after wetting and at 15 to 30-second intervals, gradually increasing the interval until one-half to one hour is required to note further change in length. The process was viewed under a dissecting microscope with the strand oriented at approximately right angles to a low-angle light source. "Slack" is determined as the extension just barely required to prevent the sample from crinkling as tension is removed.

F. OPTICAL STUDIES

1. Birefringence theory. Birefringence occurs because the electric and magnetic fields of atoms interfere with the propagation of light waves. If atoms are not randomly arranged in a material, there will be a net effect of their fields on passing rays. Then, the material is perceived as having different refractive indices depending on the relative orientation of the material and the light ray. In the case of a silk fiber with molecules stretched along the axis, the strand will exhibit a lower refractive index (RI) for light whose electric field oscillates parallel to the fiber, and a higher RI for light whose electric field oscillates perpendicular to the fiber, or across the chain molecules. (The relative magnitudes of the RI's can be remembered by thinking of the aligned molecules as letting light slip through faster (lower RI) along the axis.)

If polarized light is passed through the fiber at a 45° angle to it, the electric field of the ray can be resolved into two components: one affected by the axis of the fiber, the other crosswise to it. Due to the difference in refractive index in these two directions, the component

of the ray which is affected by the low refractive index axis will emerge sooner than the other component of the ray, and will be out of phase with it. The net effect is that the angle of the polarized light that emerges appears altered.

Thus, if the source of the polarized light is precisely crossed by another polarizing filter (the analyzer), the isotropic background field will be completely dark, but the birefringent material will change the angle of the polarized light so that the altered component passes through. The optical retardation is calculated from the angle by which the rays have changed, according to the protocol dictated for the specific compensator, and is expressed in nanometers (in other words, one component of the light vector emerges a certain number of nanometers ahead of the other component). The amount of retardation observed increases with the thickness of the object, since a greater thickness allows a greater discrepancy to accumulate before the rays emerge again into isotropic water or air. Thus, retardation (Γ) divided by optical path length (l_{obj}) gives birefringence (β), a measure of the optical anisotropy of the material comprising the object:

$$(30) \quad \beta = \Gamma/l_{obj}$$

The path length used to calculate birefringence varied according to the type of mount being used. Since it is not possible to tell at what orientation an isolated brin is, the diameter measured at the point of the reading was used. Later in the study, when techniques were improved and the silk had been confirmed to be elliptical in cross-section, the path length was used which was appropriate to the perceived orientation of the bave.

2. Rubber photoelasticity theory. Since birefringence is affected by the degree of alignment of molecules, birefringence is expected to change as a material is extended. The change in birefringence can be related to the change in stress. For a Gaussian rubber this factor, the stress-optical coefficient (SO), is given by the slope, $\Delta\beta/\Delta\sigma$ of a birefringence-stress plot. That is, the relationship between stress and birefringence is linear at low extensions. Note that for photoelasticity theory, the force is not normalized by the area at slack length, but instead is

normalized by the area at each successive extension. When stress is calculated in this way, it is called "true stress".

Not surprisingly, the prediction of non-Gaussian network birefringence from extension requires the addition of factors similar to those introduced to describe chain-end distribution.

First, as given by Treloar (1976),

$$(31) \quad p_1 - p_2 = N(\alpha_1 - \alpha_2) \left[\left(\frac{1}{5} \right) (\lambda^2 - \lambda^{-1}) + \right. \\ \left. \left(\frac{1}{150s} \right) (6\lambda^4 + 2\lambda - 8/\lambda^2) + \right. \\ \left. \left(\frac{1}{350s^2} \right) (10\lambda^6 + 6\lambda^3 - 16/\lambda^3) \right].$$

where $\alpha_1 - \alpha_2$ is the polarizability of random segments and

$p_1 - p_2$ is the network polarizability (a subscript of 1 indicates the direction parallel to the axis).

Finally, birefringence β is given by

$$(32) \quad \beta = (p_1 - p_2) [4\pi(n^2 + 2)] / 18n$$

where n is the mean refractive index of the protein.

3. Microscope and sample setup. After three to four wet stress-extension loops, the mechanical properties were usually stable. Then the VDA calibration was re-checked, the VDA equipment was turned off, and retardation measurements were made. The settings for Koehler illumination were first verified; the base mirror, field iris, and condenser diaphragm were set at optimum positions for the sample altitude. Next, the polarizers were crossed to produce maximum field darkness. The crossing was double-checked by confirming that removal of an eyepiece showed the characteristic maltese cross, with arms precisely at right angles. The extinction angle of the silk sample was next determined and that angle (approximately horizontal) marked with the stage click mechanism. To take retardation measurements, the stage was rotated through 45° counter-clockwise and a compensator inserted at 90° to the sample.

A single distinctive location on the fiber was selected (such as near an unusually-shaped particle) and that location was followed throughout the procedure, as the silk was stretched. Rotation could sometimes be detected as the particle's position changed. There are some problems with this method. Since particles are usually highly birefringent or are associated with slight irregularities in the fiber, it is not possible to take readings right next to the particle; then,

the distance from the particle increases by an unknown amount as the sample stretches, so it is difficult to tell whether measurements are really being taken in the same location. Some samples had no good particles, so no location could be tracked with any assurance; otherwise-perfect samples were sometimes discarded for this reason. A single isolated brin guarantees a clear view, but the tilt, or angular twist, cannot be determined. If the entire bave is used, then there is the risk of not getting any view clear enough for retardation readings.

Initially data were collected by eye using a Zeiss $1/30\lambda$, 654 nm Brace-Koehler rotary compensator in a dark room. The Zeiss compensator was used because it permitted very accurate readings at low retardations, and the taking of four minima rather than one allowed stray retardations not due to the silk to cancel each other out. A low-wattage red bulb enabled data to be recorded without saturating the eye's green-light receptors. A half hour was given to help the eyes accommodate before beginning, as otherwise readings were inconsistent. There was a tendency to judge the darkest angle as the point at which the majority of the fiber was as black as possible; instead, it was necessary to focus only on the core, where the greatest pathlength is. Retardations were too small to use monochromatic green light, as the image was then too dim and inconsistent readings resulted, so white light was used. (On occasions when both green and white light could be used, results were not found to differ significantly. In fact, variation was reduced using white light since the critical angles were more easily noted.)

Later data sets were collected using an EG&G Gamma Scientific fiberoptic wand which was inserted in the accessory tube of the microscope. The light was guided to an EMI 9798B photomultiplier tube powered by an ORTEC 164 high-voltage power supply. A supply of 1200-1270 V was found to be optimal for low noise yet adequate amplification. The tube was wrapped in black felt to prevent stray light leakage, then installed in a styrofoam container. A few handfuls of dry ice pellets were placed in the container, separated from the tube by a cardboard barrier to prevent too rapid or uneven a chill rate from damaging the electronic components. Chilling was necessary to reduce the dark current to a level for which the chart recorder could compensate. The output current was converted to voltage for the chart recorder by a voltage divider of 1 M Ω . Since light levels were so low that individual photons could cause

spikes in the current, a 1 μF capacitor was added to the circuit, yielding a time constant of one second to average the output.

The electronic method had the disadvantage of being frustratingly finicky regarding the placement of the optical wand. The fiberoptic light guide was 50 μm in diameter, and with an objective magnification of 80X, the image of a fiber with a diameter of 2 μm is still only 160 μm ; thus, one-third of the width of the brin is sampled, and any minute vibration or slippage shifts the silk fiber and invalidates readings. It is not possible to observe whether the wand is on target during readings because the eyepiece must be covered completely to prevent stray light from entering (especially light reflected from an observer's face!). Therefore, multiple readings must be taken, which takes considerable time and still does not guarantee a single core reading.

Due to the above difficulties, the original method was renewed, but with a modification. Since the main problem with 'by-eye' methods is the variation in human perception caused by factors such as ambient light levels and acclimation, a reference would make the difference between subjective and objective measurements. Thus, the fiberoptic wand was employed as a passive, physical 'black' reference. When the wand is aligned with the central axis of the silk strand, it is surprisingly easy to decide when the axis is darkest by identifying when the boundary between wand tip and fiber core disappears. This improved method is faster, is not nearly as sensitive to ambient light levels, requires less acclimation time before readings, and gives results comparable with the other methods. It is still best, however, to dedicate one eye to taking retardation measurements and the other to viewing manipulations under the brighter light necessary to see the particles that mark locations.

Surprisingly, no mention of this type of dark-reference method was found in any of the literature, perhaps because traditionally birefringence was in the realm of geology, where large mineral samples with high birefringence are the norm. The dark-reference method should be most useful in biological applications where fine fibrous materials are of interest. Since both the eye and electronic methods appeared consistent within the variation present, the data were pooled.

Some samples which survived birefringence measurements were subjected to another F-E loop to verify that the mechanical properties had not changed. The cause of fiber failure was

inevitably destruction while attempting to find a new location on the fiber. Isolated strands tended to be more fragile, perhaps due to previous manipulations.

4. Modifications for dry samples. Birefringence studies at room condition humidity were carried out differently, because of the impossibility of getting close enough to a glue-coated fiber to measure diameter or birefringence without also sticking to it and making further measurements impossible. Birefringence was measured at five to seven extensions for each web studied, from 1.0 to 2.4 in increments of 0.2.

For each extension, a separate spiral sample was taken from the web. For each sample, the slack length was found, the desired extension was attained, and then the bave was laid down on a slide and epoxied to it while the calipers maintained the extension. Next, spun glass rods of around 10 microns in diameter and a couple centimeters in length were laid across the sample and their ends epoxied down at a centimeter or so from the fiber. (Fast-weld was adequate for these purposes.) Care was taken to avoid rolling or moving the spun glass rods, as they could crush and distort the silk. At least three rods were laid across at equal spacings, to prevent any liquid surface tension from causing the coverslip to crush the silk. A coverslip was then trimmed to size and epoxied on top. After a couple hours of curing, a small drop of immersion oil was placed at the edge of the coverslip and allowed to wick under and surround the silk. Retardation was measured that same day at several points on each double-stranded fiber, attempting a good selection of both adjacent and stacked readings whenever possible. A 100X oil immersion lens was used.

CHAPTER III: RESULTS

A. DIAMETER AND CROSS-SECTION DATA

The means and coefficients of variation for the diameter measurements of dry and wetted fibers from several webs are given in Table 3.1. "Single" means that the measurements were taken at one site, while the silk was at a single orientation. "Adj" and "St" refer to measurements taken at the adjacent and stacked orientations, respectively. "All" means the diameters measured at several locations along one sample were pooled, irrespective of fiber orientation. "Intra" refers to the averaging of the effective diameters of all samples from an individual web (that is, the intra-web variation).

Note the small coefficient of variation for multiple measurements at a single site, contrasted with the large coefficient of variation for all measurements pooled from a fiber. Note also the large reduction in coefficients of variation when the tilt, or angular orientation, of the sample is taken into consideration.

During measurement of viscid silk, it was often difficult to focus both edges clearly. However, it was possible to focus on each edge separately. The edge which focussed higher was consistently higher along some interval of the sample, so the phenomenon did not appear to be due to optics or limits of resolution. The qualitative observations and the manner in which variation can be reduced when orientation is considered both provide strong proof of the non-circular cross-section of spiral silk. The data from rotation experiments, listed in Table 3.2, also showed silk fibers to be non-circular in cross-section. Those data are supplemented by the ellipticity data in Table 3.3, derived from diameter measurements along bave samples with definite orientations. The latter data set has a much larger number of samples because the data are pooled from all experiments using bave. From this data, the average ellipticity of spider spiral silk, defined in Equation 33, was calculated to be 1.56.

The irregularity of the rotation data is probably due to the very slight torque on the silk causing less reproducible results, since it was not possible to verify a change in orientation of an isolated fiber. Very few sites were examined, as well. Rotation of the entire bave may enable more accurate readings to be taken, since orientation would be perceptible. Rarely, a bave was

A. Dry brins

Web	Mean diam (microns)	Coefficients of Variation				
		single	adj	st	all	intra
IV	2.46		14%	3%		
VIII	2.21	7%	9%	7%	24%	6%
X	1.85		11%	7%	26%	7%
IX	1.58					10%
XI	3.12					12%
all samples mean stats	2.20 (CoV=28%)	7%	11%	7%	25%	9%

B. Wet brins.

Web	Mean diam (microns)	Coefficients of Variation				
		single	adj	st	all	intra
I	2.8	3%	4%	2%	17%	3%
II	4.71	4%			10%	8%
III	2.3	4%			10%	6%
IV	3.57	6%	14%	16%	26%	19%
V	3.01	15%	6%	1%	20%	9%
VI	1.78	6%			3%	
VIII	2.32	5%			17%	
IX	3.25	5%			27%	5%
X	2.24					
XI	3.32					
all samples mean stats	3.12 (CoV=26%)	4%	8%	6%	19%	8%

Table 3.1. Diameters of spiral samples at slack extension.

Where possible, values are for effective diameters. Some diameters were calculated from data taken at non-slack extensions, using Eqn. 34. "Mean diams" are the averaged diameters from all samples from a web. The other abbreviations are explained in Results, Section 3.A.

Note the large difference between the variation for the means of all samples from all webs, versus the average variation of samples from a single web ("intra" column).

Sample		E	mean
A	location #1	1.34	
	location #2	1.19	1.27
B	extension #1	1.11	
	extension #2	1.33	
	extension #3	1.26	
	extension #4	1.11	
	extension #5	1.60	1.30

Table 3.2. Ellipticity data from two rotated samples. Sample A was maintained at a single extension, but measurements were made at two locations. Sample B was measured at only one location, but at several extensions. Ellipticity (E) was calculated using Equations 1-33, which involve fitting diameter data to the formula for an ellipse.

Web	State	E	CoV
I	Wet	1.46	10%
IV	Dry	1.71	
IV	Wet	1.57	
V	Wet	1.67	
IX	Dry	1.58	7%
X	Dry	1.53	11%
X	Wet	1.41	
XI	Dry	1.59	6%
XI	Wet	1.24	
XII	Dry	1.60	9%
all	Dry	1.58	8%
all	Wet	1.47	11%
all	both	1.56	10%

Table 3.3. Ellipticity data from both wet and dry non-rotated samples. Most of these measurements were obtained during the course of optical studies. Where no coefficient of variation is listed, only one sample from that web was measured. For these samples, ellipticity was calculated from the ratio of the average "stacked" and "adjacent" diameters, according to Equation 33.

rolled along the water-immersion lens as its position was adjusted, and diameter measurements during one of these lucky events clearly confirmed the non-circular cross-section.

B. EXTENSION-VOLUME DATA

Some volume-extension estimates were made using data obtained during the birefringence measurements. Other samples were specifically used to test the relationship, and were mounted and wetted following normal force-extension procedures. Still more data was obtained from the rotation analysis, using data from the experiments that repeated the rotation for different extensions.

Figure 3.1 shows the results of all extension-volume experiments. The data are plotted as the change in volume relative to an initial slack volume of 1.0. There does not appear to be any clear trend among the samples. Note that some of the curves show a continuous trend, while others exhibit distinct discontinuities. The deviations from constant volume that are observed at lower extensions, especially for isolated strands (whose orientations are difficult to determine), are probably due to the fact that samples twist as they are stretched. The twisting can take place gradually or, when the sample is restrained by the proximity of the immersion lens, the torque can be released suddenly. Inevitably, such a quick shift in particle position is accompanied by a significant change in diameter readings, which is notable since single site measurement variation is usually very low. Such abrupt shifts in readings were usually associated with visible changes in particle orientations on isolated fibers, indicating that the fiber had rotated suddenly. In addition, most volume changes occurred in the first 20% of extension and were relatively stable afterwards; if strain-crystallization were causing a volume decrease, it would most likely occur at higher extensions.

It appears that much of the variation of the volume change experiments is due to the earlier completion of that data collection, before sufficient proof for elliptical cross-section had been amassed; more precise data should be possible using entire bave. So far, the general conclusion drawn is that there is no significant change in volume for spiral silk as it is stretched. Given this result, the diameter at any non-slack extension (ext) can be derived by dividing the

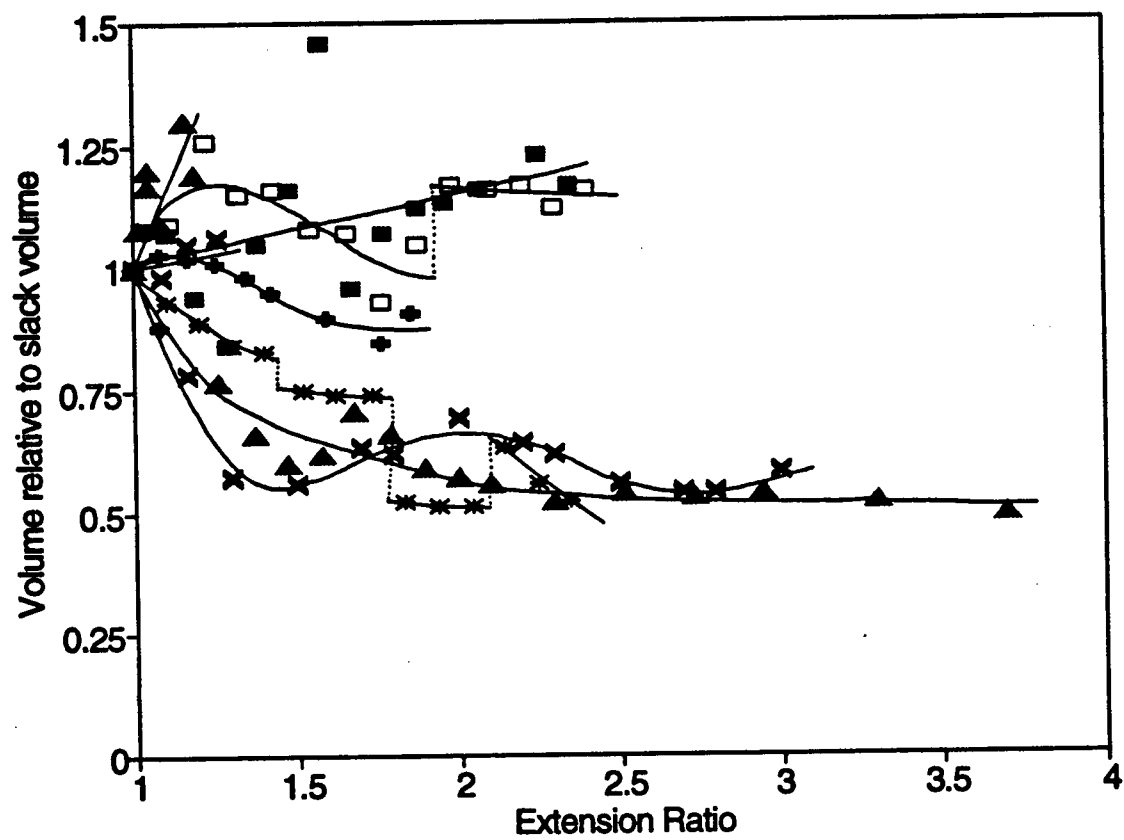


Figure 3.1. Changes in volume (relative to volume at slack extension) for nine extended wet samples.

diameter at slack extension (d_0) by the square root of the extension:

$$(34) \quad d_{\text{ext}} = d_0 / \sqrt{\text{ext.}}$$

Conversely, the diameter at slack can be estimated from that at another extension by multiplying by the same factor. Thus, the assumption of the volume-extension relationship allows fewer diameter readings, since the diameter can be calculated from one set of reliable measurements from each strand.

C. WET CONTRACTION DATA

Table 3.4 gives the contraction ratios of samples from a variety of webs. The table summarizes the means and coefficients of variation from several webs used. Spiral silk contracts to 0.63 times its dry slack length when it is wetted, which is not significantly different than frame silk. The wet contraction experiments provide more evidence that silk samples from a given web are more similar than from different webs. The average coefficient of variation for contraction ratios of individual webs (9%) is less than the coefficient of variation of the pooled data (24%).

A typical time-course for wet contraction is plotted in Figure 3.2. Note the two linear regions that are evident when the time axis is logarithmic. The plot shows a rapid decrease in length immediately upon wetting, then the rate soon settles to a much lower one, as the slope of the plot shows. The transition between the phases (the point of inflection of the plot) occurs between 200 and 400 seconds after wetting. The silk does not appear to ever completely stop contracting. The fact that the second phase has no perceptible end indicates that eventually the silk could entirely dissolve. In the short term, however, that can be ignored; spiral silk shows no perceptible change in behavior even after immersion for at least five days. The mount would likely fail first, given the non-negligible water-permeability of epoxies when applied in minute quantities.

There are no obvious correlations between contraction ratio and any other physical property; of course, this may simply be due to the small total sample size and the inability to perform all the different experiments on a single sample.

Web	WCR	CoV
II	0.68	3%
IV	0.69	4%
V	0.84	9%
VII	0.40	6%
VIII	0.43	11%
IX	0.72	21%
X	0.62	
XI	0.65	19%
XII	0.70	
all	0.64	24%
unknown	0.60	21%

Table 3.4. Wet contraction ratios (WCR), calculated as the ratio of wet slack length divided by dry slack length.

The coefficient of variation indicates variation between samples from one web, except where "all" refers to all samples whose webs of origin were known, and where "unknown" refers to results from twelve additional samples whose webs were unknown.

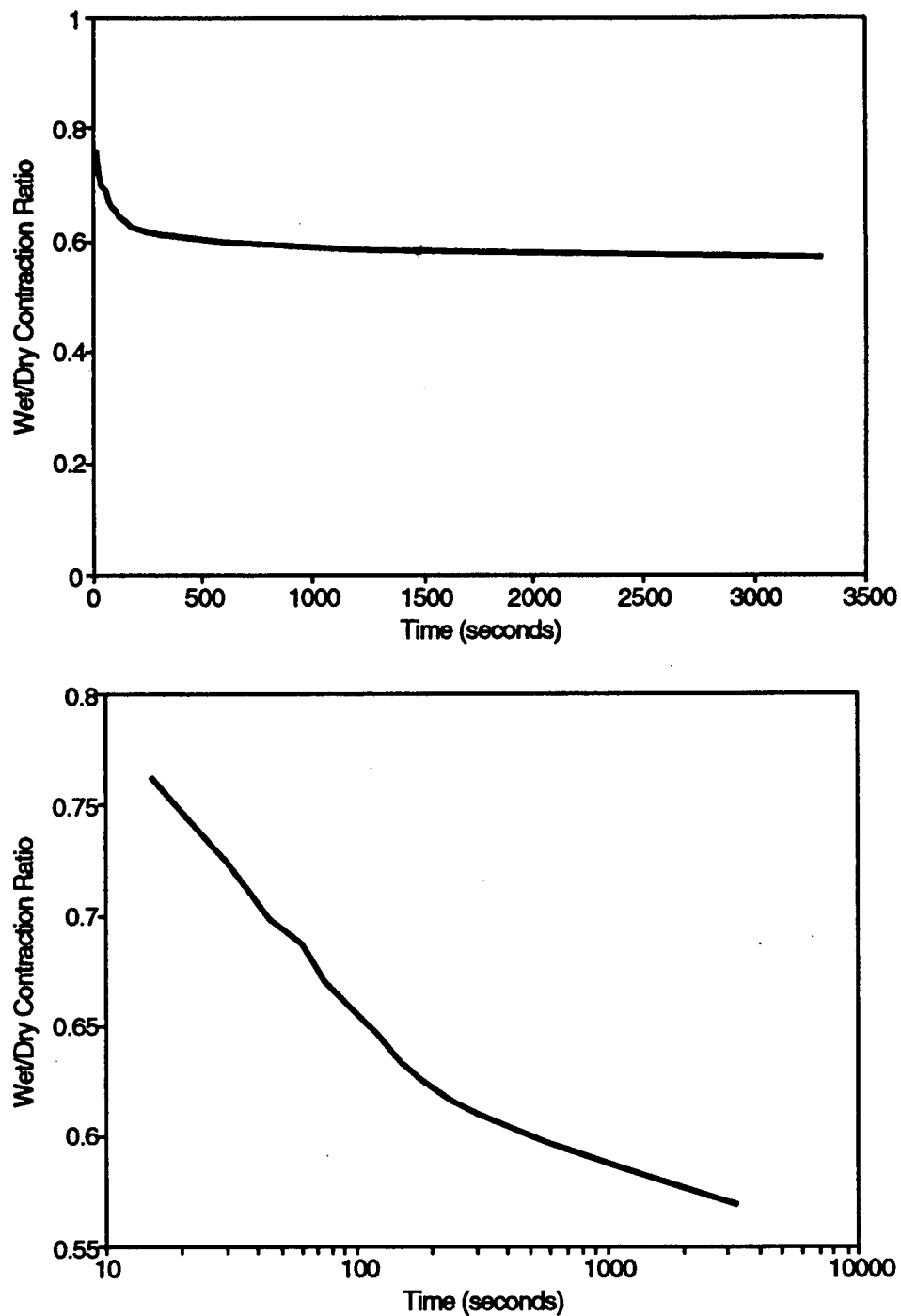


Figure 3.2. Wet contraction time-courses. The upper plot illustrates the sudden initial phase, contrasted with the later slow phase. The lower plot, with a log time-scale, shows the linear relationship in each phase, and the transition at around 200 seconds.

D. MECHANICAL RESULTS

1. Force-extension data. The raw data obtained from the glass transducing beams is in the form of a deflection which is proportional to force (see Equation 21). Since force calculations require no confounding factors involving silk diameter measurements, and VDA recalibration was performed before wet recordings, force data are much more accurate than dry-wet stress estimations can be; therefore it is useful to analyze the results from some samples which provided both dry and wet data.

Notice the consistent results yielded on successive cycles of a single sample, either wet or dry, during one day, as shown in Figure 3.3. There are slight changes in slack length and initial slope, but the curves are almost identical. The results for a wetted sample which was cycled a few times almost every day, to extensions over 2.0, for eleven days also shows no significant trend, aside from a slight increase in stiffness between the first and second days (Figure 3.4). The slack length increase observable for both dry and wet samples is mostly reversible, if enough time is allowed for the silk to recover after retraction. Such recoverable changes are usually caused by viscoelastic inter-chain frictional forces. A very fast cycle reduces the time available for chains to rearrange themselves and results in higher forces, since the sample does not "relax".

One interesting effect of wetting, which is at first counterintuitive, is that the *force* exerted by wetted strands is often significantly higher than the force at the same length when the sample was dry. This result, however, was not guaranteed; in fact, three types of plots were observed while comparing dry and wet force-extension data from several samples. In some cases, the force of the wetted fiber was much lower than the dry fiber; in others, the force was unchanged or even greater. Figure 3.5 shows typical results of each type. Obviously, it was of interest to determine why certain samples exhibited behavior of type A and other samples behavior of type C.

Due to their especially large ranges, two variables in particular were promising candidates with which to attempt correlations. First, when the force data were converted to stresses, the dry samples were found to range in initial stiffness (E_i) from 0.5 to 3.9 MN/m², an

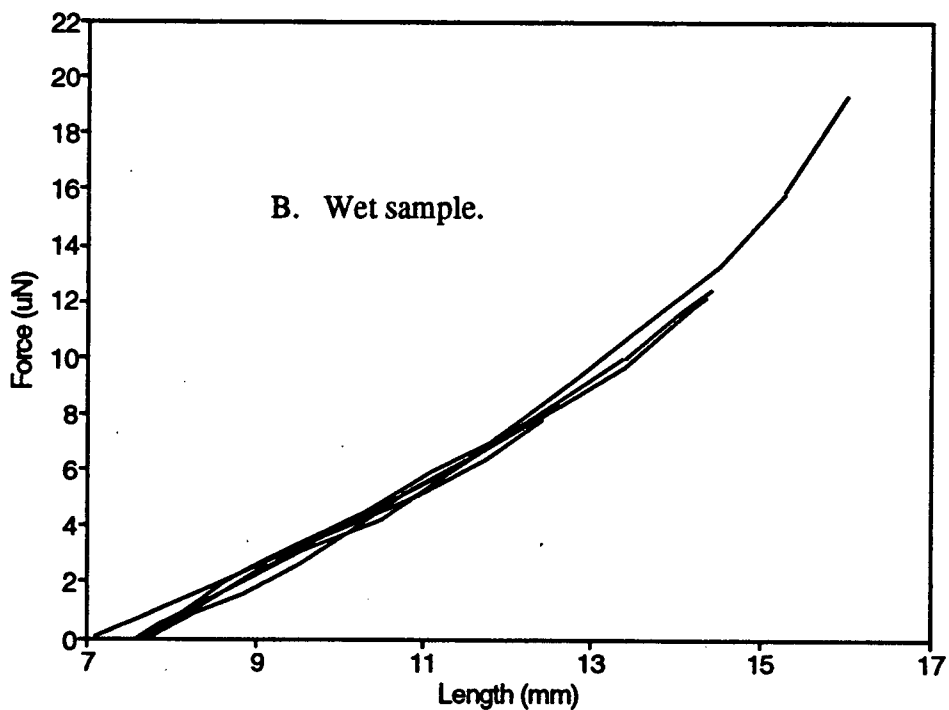
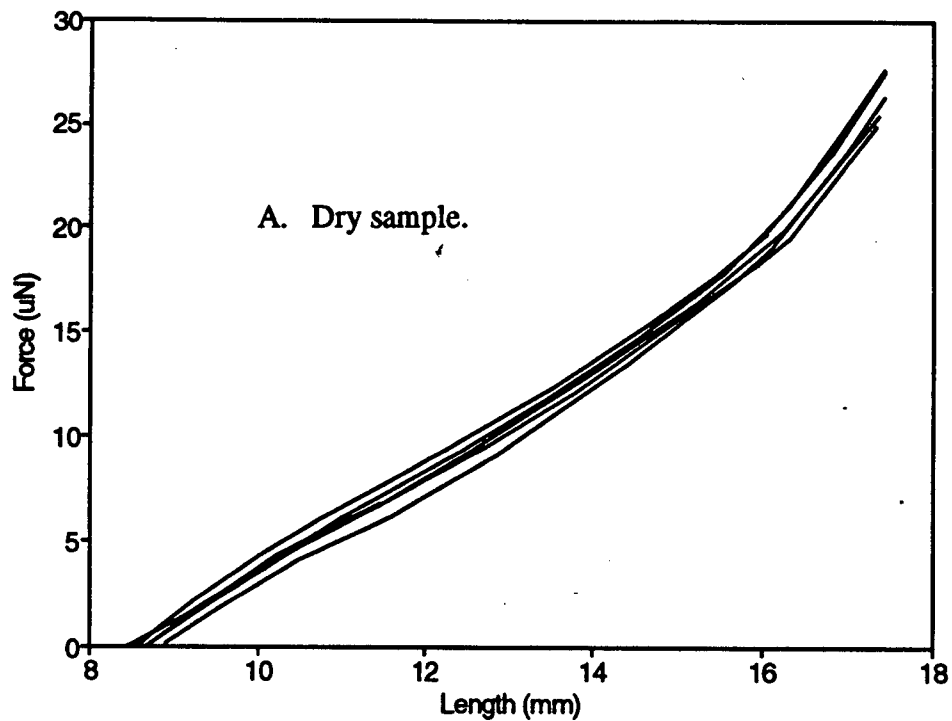


Figure 3.3. Successive length-force cycles, illustrating the preconditioning process for a sample first dry, then wetted.

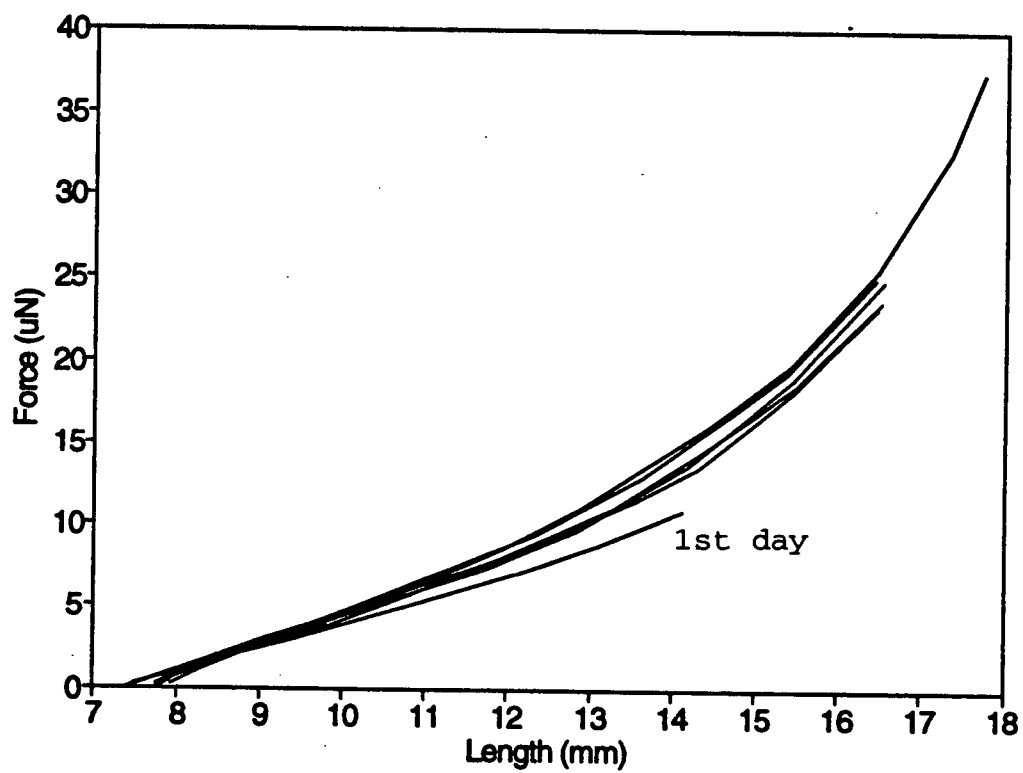
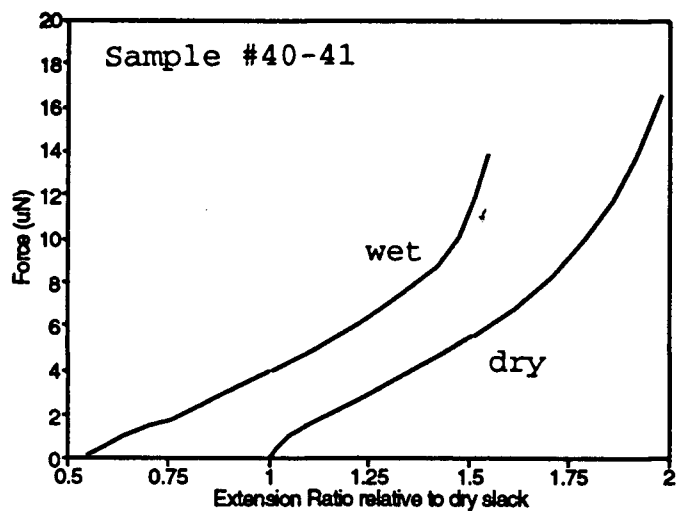
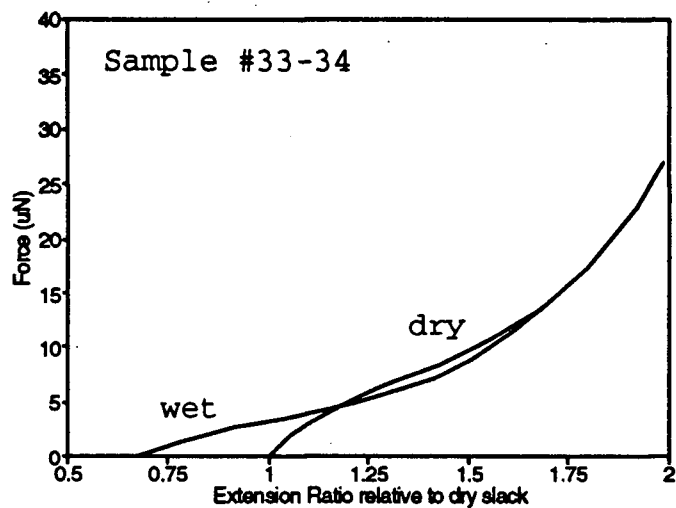


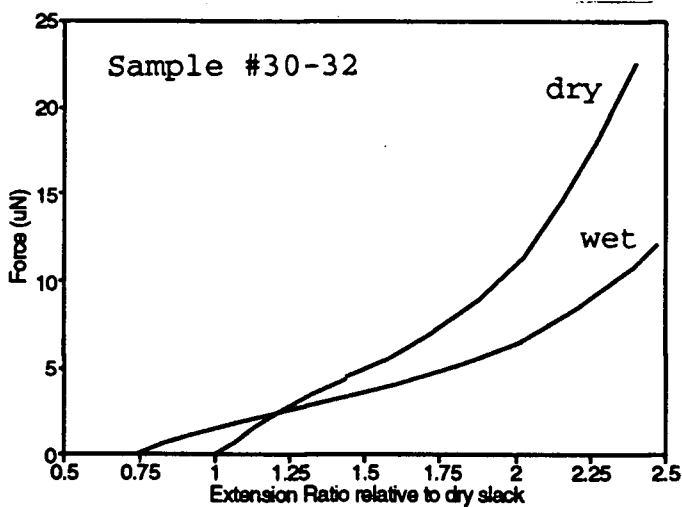
Figure 3.4. Length-Force cycles, repeated over eleven days, showing the excellent stability of a wetted sample.



A



B



C

Figure 3.5. Examples of the three types of behavior that are possible when a sample is wetted. For any given extension, the forces may increase (Plot A), remain stable (Plot B), or decrease (Plot C). Note that the samples in Plot C are extended further than those in Plots A and B.

eight-fold difference. In order to carry out any analysis, a method of quantifying behavior types A, B, and C had to be established. The parameter chosen was the energy required to extend the sample a given distance from its slack length; in this case, a length unit increase of 0.5 was chosen, as all the curves remained linear below this extension. The work for each sample was calculated separately for dry (W_{dry}) and wet (W_{wet}) states, then both dry and wet data sets were plotted together against the initial stiffness of the dry sample, E_i , in Figure 3.6. The two data sets, W_{dry} and W_{wet} , were each subjected to a linear regression (dashed lines), yielding a slope of 0.83 for the dry samples and 0.37 for the wet samples. Both coefficients of determination, R^2 , were about 0.80, and a statistical F-test clearly indicates that the slopes are different ($p < 0.01$) (Sokal and Rohlf, 1973).

Second, the wet contraction ratio (WCR) can vary by two-fold, from 0.4 to 0.84; as wet contraction of a polymer depends on the state of its molecular network, WCR also held promise for being a good candidate for correlation with the three types of force behavior. However, when the Work Ratio, $W_{\text{wet}}/W_{\text{dry}}$, is plotted against the WCR, there is no significant correlation. Thus, the force behavior only correlated with the first variable, the initial stiffness of the dry sample, E_i . Figure 3.6 illustrates that the significantly different slopes for W_{dry} and W_{wet} imply that the stiffer dry samples show the greatest reduction in work of extension when wetted.

Recall that a significant source of uncertainty in such dry-wet comparisons is the estimation of stresses. If the diameters in the dry state were known precisely, there would be negligible deviation from the linear relationship between the work of extension in the dry state, W_{dry} , and the initial stiffness, E_i , of the same sample. However, since only the wet diameter can be directly recorded from a dry-wet sample, the dry diameter must be estimated from the average web diameter. In addition, few dry-wet samples could be measured even in the wet state, since the apparatus for the dry cycles required the sample to be mounted at a higher level. Therefore the estimate of the initial stiffness of the dry sample, which may predict its relative wet behavior, is subject to inaccuracy.

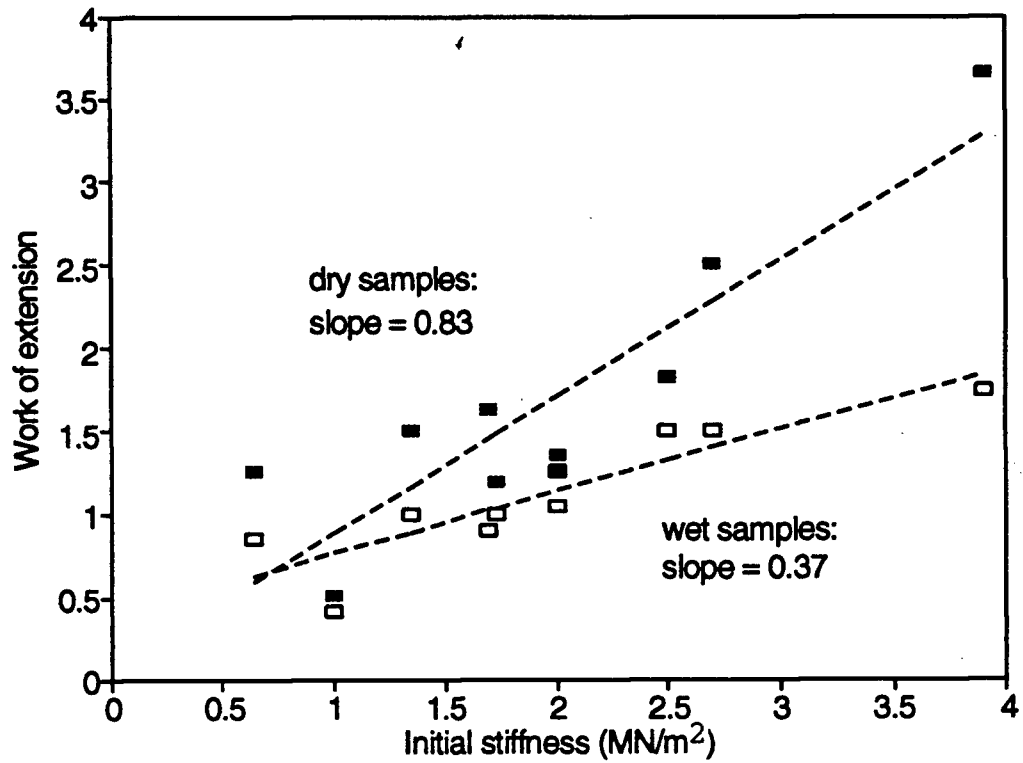


Figure 3.6. Work required to stretch a sample by one-half unit of length, plotted against the initial stiffness of the sample in the dry state. Data for dry samples are plotted with closed squares; data for wet samples are plotted with open squares.

2. Stress-extension data: Non-Gaussian curve fits. Network parameters are derived from stress-extension data by using non-Gaussian curve fits. Figure 3.7 shows two curves from typical dry and wet stress-extension experiments using one sample. Dry and wet stress-extension curves had similar shapes: the typical non-Gaussian curve consisting of a slightly stiff initial portion which gently shoulders into a linear region and thence into a "J curve" of increasing stiffness to the breaking point. The last point on each curve is not the breaking point, since fibers were retained for later optical study. Note that when a force-extension dry-wet plot (refer again to Figure 3.5) is converted to a stress-extension dry-wet plot, the stress data for the wetted sample show a decrease in magnitude relative the dry state, even when the sample was one which maintained high force levels; this is because swelling increases the cross-sectional area over which the force acts, thereby lowering stress.

Because both "dry" and wet curves demonstrated rubber-like behavior, it was deemed reasonable to estimate network parameters for both; the decision was supported by the excellent fits for the regressions. This qualitative judgement should later be supported by thermoelasticity experiments like those performed on wet frame silk, which unequivocally demonstrate the entropic origin of the elastic force (Gosline, Denny, and DeMont, 1984).

Table 3.5 gives results of network parameter determinations for the samples that were extended far enough to justify fitting their data to theoretical non-Gaussian curves. Means and variations of the network parameters are also listed. As mentioned above, the stress-extension curves of both dry and wet silk were well-behaved. Two of the non-gaussian fits were, however, not quite as good as the others, with Coefficients of Determination, $R^2=.97$ and $.98$, compared to $.999$ for most (see Figure 3.8). Note the larger deviations clustered about the lower extensions. The irregular curves were produced by samples which had high initial stress-relaxations in the dry state, causing the initial portion of the curves to be flatter than expected. The high hysteresis made it very difficult to determine the exact slack length, so the initial extension of some of these samples was presumably due to viscous glue forces.

It was necessary to ensure that the curve-fitting routine was not sensitive to the anomalous data. The determination of segment count, s , is based on changes in the inflection of the curve, and fortunately, s is not appreciably altered by the irregular data. Segment counts

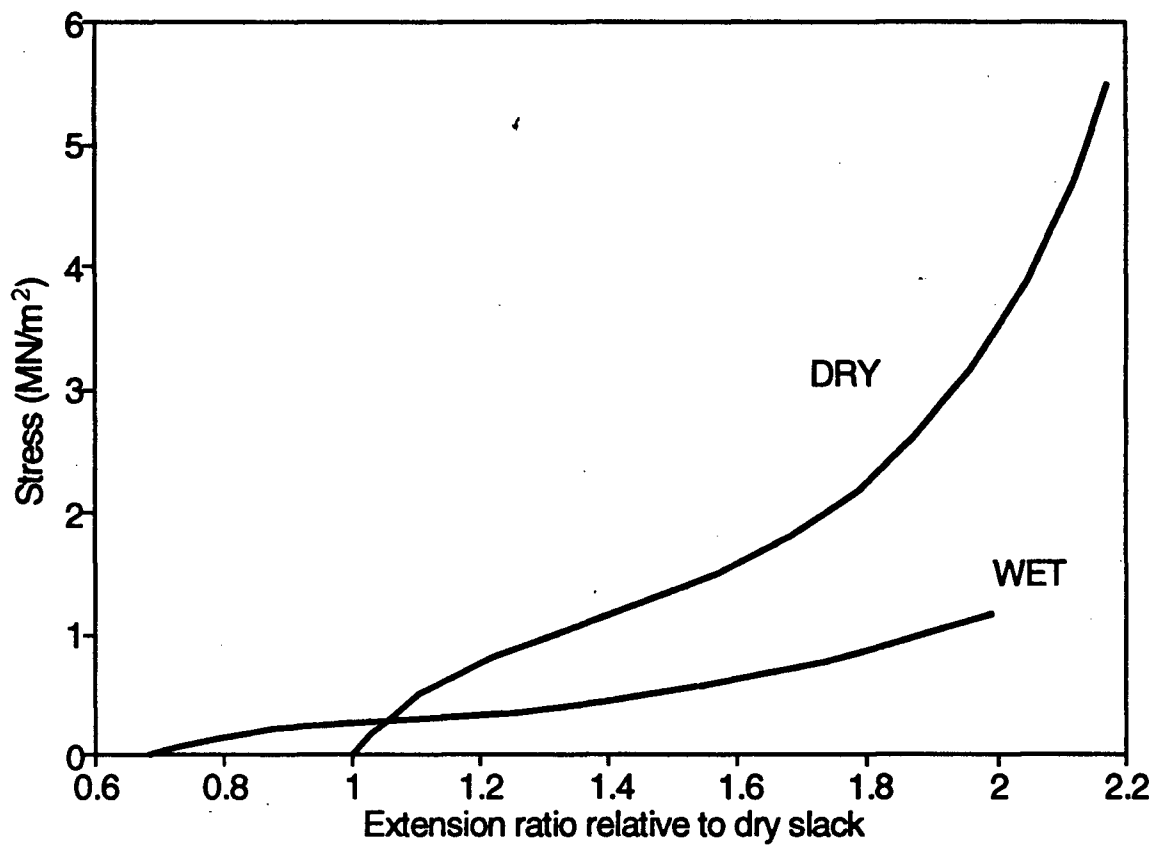


Figure 3.7. Typical dry and wet stress-extension curves for a sample.

Web	Data set	dry samples		wet samples	
		s	G	s	G
IV	#1			7	0.61
	#3			6	0.69
	#30,#32	5.5	1.1	13.5	0.20
	#33,#34	3.5	1.5	6	0.29
IX	#21,#22	3.4	0.83	3.2	0.16
	#23,#24	3	0.40	5.25	0.21
X	#27	8.5	0.64		
	#35,#36	5	0.41	9.5	0.14
XI	#25	1.8	0.58		
	#28,#29	8	0.82	8	0.24
	#40,#41	5	0.60	8	0.13
	#42,#43	3	0.67	4.75	0.52
	#44,#45	3.2	0.49	8	0.37
XII	#26	8.5	0.35		
	#38,#39	5.5	0.26		
mean		4.77	0.67	6.63	0.32
CoV		45%	47%	42%	55%

Table 3.5. Non-Gaussian curve fits for conditioned samples. The segment count (s) and shear modulus (G, in MN/m²) is given for each wet or dry data set. Where two data sets are listed in the same row, the sets are from the same sample (first dry, then wetted).

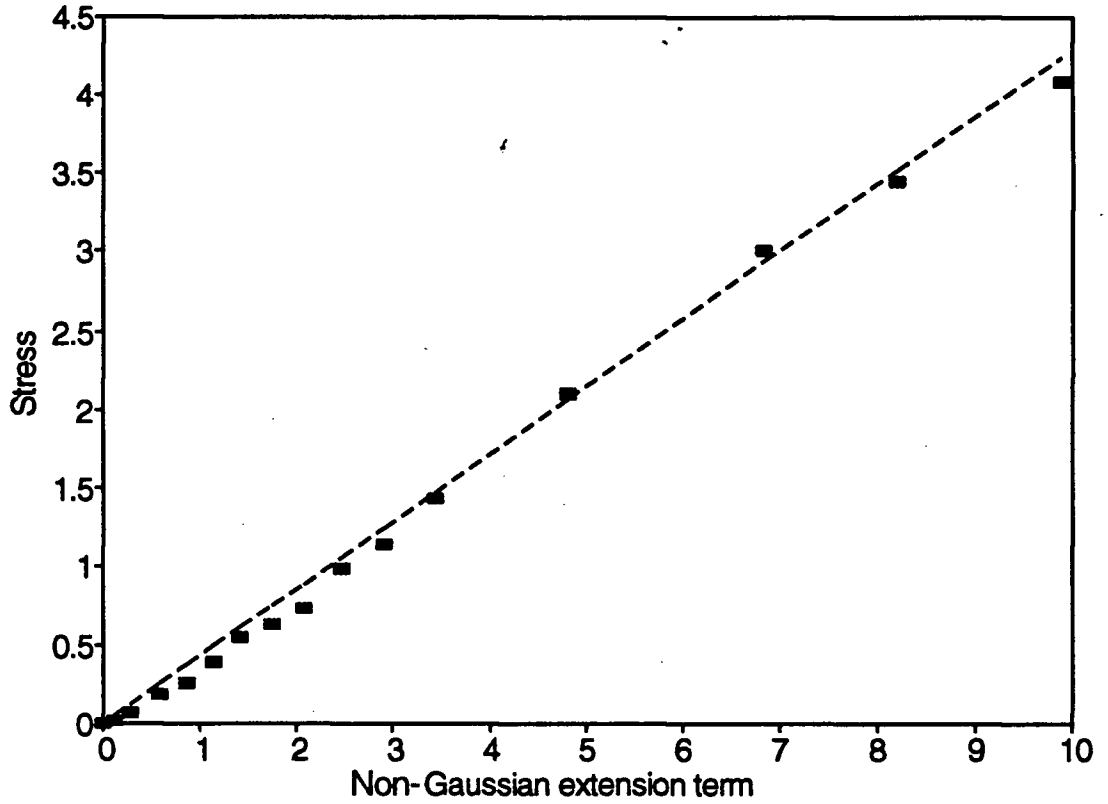


Figure 3.8. Plot of the regression for a stress-extension curve with a relatively low coefficient of determination ($R = 0.997$). Note the consistent deviations at low extensions.

were recalculated for the two irregular curves, assuming initial slacks at lengths past the flat part of the curve, and changes in results were less than one-half segment. Changes in shear modulus were less than 5%. The insensitivity was due to those particular samples being long enough that changes of a few tenths of a millimeter were negligible.

Table 3.6 lists the network parameters for several cycles of a single sample. Note that the differences in network parameters from cycle to cycle on a single day are fractional. The table shows that even when the rate of extension of a conditioned sample is drastically varied over many cycles and eleven days, the change in segment count is less than one segment. Shear modulus is affected to a greater degree, changing by as much as twofold in a wet sample, with most change occurring between the first and second days. Therefore it was important to compare network parameters only of pseudo-static F-E data from the first day of immersion.

The results of the conditioned non-Gaussian curve fits for multiple samples (Table 3.5) were much more variable than expected. Note that some spiral silk samples had segment counts, s , as low as 1.8 when dry, and as low as 3.2 wet, while other samples were extraordinarily stretchy and had segment numbers as high as 8.5 when dry and 13.5 when wetted. Note also that the lowest segment count for spiral silk, which was close to the mean of 2 for wet frame silk, was given by dry spiral silk; the lowest count for wet silk was 3.2. Figure 3.9 shows stress-extension curves which illustrate the observed range of properties.

The variability of chain counts for samples from individual webs was surprising, given the relative consistency of other intra-web parameters. There was no obvious correlation between dry s and wet s , either. Samples #23, #33, and #44, with low dry counts, yielded higher wet counts, while Samples #21 and #42, also with low dry counts, retained low counts when wetted. In a similarly confusing manner, Sample #28, with a moderately high dry s value, retained that same count when wetted, while three others increased s in varying degrees. Of the four samples with highest shear modulus, G , Samples #21 and #28 maintained s when wetted, while Samples #30 and #33 increased s .

In no case did the segment count decrease significantly when wetted. The one sample, #21, which seems to show a fractional decrease in s , will be explained in the discussion. The shear modulus, G , decreased in all cases, in keeping with the dilution of the amorphous network

Data set	Cycle	Speed	s	G
#21	1	Slow	3.4	0.83
	2	Fast	3.2	0.77
	3	Fast	3.4	0.75
	4	Fast	3.2	0.75
	5	Fast	3.25	0.74
	6	Slow	2.9	0.69
#22	1	Slow	3.2	0.16
	4	Fast	3.5	0.24
	12	Fast	3.8	0.31
	16	Slow	3.2	0.24
	20	Fast	2.9	0.24
	21	Slow	3.3	0.27
	28	Fast	2.8	0.27
	29	Slow	3.3	0.32
	37	Slow	3.0	0.28
	40	Fast	2.9	0.26
41	Slow	2.9	0.25	

Table 3.6. Typical non-Gaussian curve fits for a single sample. Data set #21 is for the dry state, and data set #22 for the wet state. The effects of preconditioning and changes of extension rate are shown.

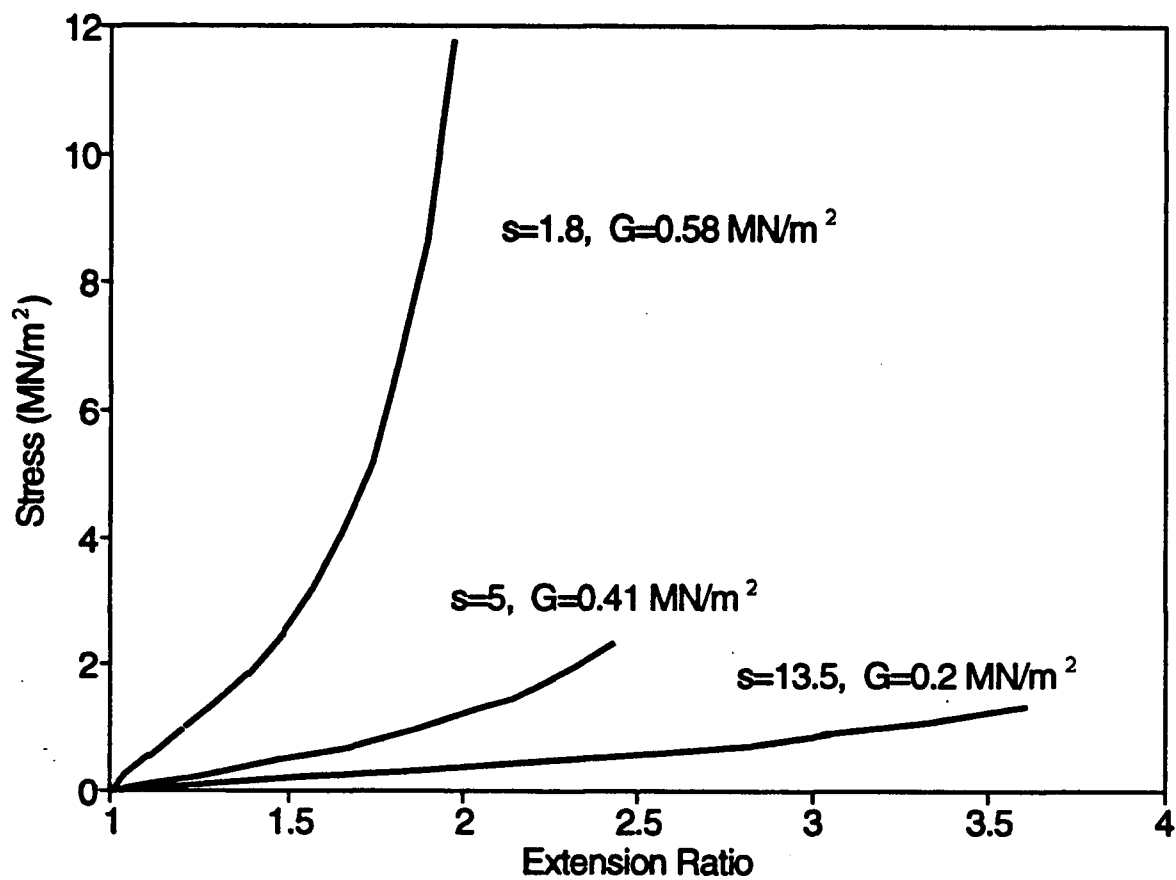


Figure 3.9. Three examples of the range of mechanical properties observed, with the corresponding network parameters indicated.

and thus the chain density decrease. Sample #30-32, whose shear modulus decreased most upon wetting, was also the fiber which increased most in segment count. Surprisingly, that fiber had a relatively high contraction ratio; that is, it did not contract very much, nor was its wet diameter exceptionally large. It would have been more consistent for the fiber with the greatest network change to also show the greatest change in physical parameters, and *vice versa*.

Note that the two network parameters, G and s , are sensitive to different variables. The modulus, G , is sensitive to errors in diameter estimation, because it depends on the increase in force per area of the silk. The segment count, s , on the other hand, is entirely independent of stiffness and stresses. Instead, errors in extension estimates, which change the shape of the force-extension relationship, also affect the segment count. In fact, a change (decrease) of 2 mm (33%) in the slack extension of sample #25 would increase the segment count to 3.5 from 1.8. A 20% increase in slack extension for sample #28 would change the segment count to 6 from 8. Such errors are marginally possible for dry silk if the slack length is determined "by eye" on dividers, but they are highly unlikely for mounted silk being monitored by the VDA, since multiple determinations of slack generally show no more than a couple tenths of a millimeter variation. Determinations based on glue-droplet separation, viewed under the dissecting microscope, were also reproducible and agreed well with VDA determinations.

In the case of wet silk, such errors in slack length determination are simply not possible. Slack wet length is exceedingly easy to verify, both by force detection and visual judgement; error is negligible due to the absence of the confounding glue. Yet wet spiral silk samples show as much variation in the network parameters s and G as dry samples, leading to the conclusion that the variation in dry silk is no doubt also real.

Yet despite the large variations of 40-50% in the network parameters, a trend is evident: the network model with the lowest segment count, $s=1.8$, was a dry sample; the network model with the highest $s=13.5$ was a wet sample; and the model for the average dry sample had a lower $s=4.77$ and a higher shear modulus $G=.67 \text{ MN/m}^2$, compared with the model for the average wet sample with $s=6.6$ and $G=0.32 \text{ MN/m}^2$. The general conclusion is that dry samples have lower segment counts and higher chain densities than wet samples.

3. Calculation of network chain parameters. Calculation of A, the number of amino acids required to act as an ideal random segment, requires estimates of dry crystal volume fraction V_X , wet/dry volume ratio ΔV , dry network density, and average residue weight M_{aa} , in addition to the estimates of shear modulus, G, and segment count, s. The network analyses summarized above provided a range of values for s and G. In the calculations that follow, the models with average dry $s=4.77$, average wet $s=6.6$, highest $s=13.5$, and lowest $s=1.8$, were the four models chosen for further sensitivity analysis.

Some of the values of the other physical parameters are uncertain, therefore calculations were carried out assuming a range of values for those variables. A range of 5-25% was used for dry crystal volume fraction; 1200-1460 kg/m³ for dry density; 1.0 to 1.3 for wet/dry volume ratio of dry spiral; 1.6 to 2.0 for wet/dry volume change of wet spiral; and 84-90 g per mole of average amino acid residue mass. Reasons for the choice of particular ranges are explained in the discussion. Results are summarized in Table 3.7 and Table 3.8 A-D. Table 3.7 shows the general format in a manageable size. Each table lists first, at the top, the network parameters, s and G, of the model being analyzed. Next, the physical parameters are listed: wet/dry volume ratio ΔV , dry crystal volume fraction V_X , dry density ρ_{dry} , and average residue mass M_{aa} . The wet rubbery network volume fraction V_R is then calculated from Equation 18 using ΔV and V_X , and the wet density ρ_{wet} is calculated as the product of ρ_{dry} and V_R . The mass per mole of chains M_C is calculated from Equations 15 and 17, using ρ_{wet} and G; then the number of amino acid residues comprising each chain between crosslinks is calculated from M_C and M_{aa} . Finally, the number of residues per random segment, A, is calculated from Equation 19 and Equation 20. The intermediate results are listed so that the changes in the estimates of A are more meaningful, as the effects of certain suppositions on specific physical parameters may be more clearly followed.

Table 3.7 holds all parameters constant except the network parameters, s and G. A hypothetical network with $s=5$ and $G=0.5$ MN/m² is assumed in the first column; the second and third columns independently decrease first s and then G by twenty percent. It is clear that the number of residues per segment, A, is increased as s decreases, since the number of residues comprising a chain remains constant, while the number of random segments has been lowered.

	vary s		vary G
s	5	4	5
G	0.50	0.50	0.40
ΔV	1	1	1
V_x	0.05	0.05	0.05
ρ_{dry}	1330	1330	1330
M_{aa}	84	84	84
V_r	1.00	1.00	1.00
ρ_{wet}	1330	1330	1330
M_C	6.5	6.5	8.1
aa/chain	77	77	96
A	15.4	19.3	19.3

Table 3.7. Sensitivity analysis for the calculation of network chain parameters. A hypothetical dry network with $s=5$ and $G=0.5 \text{ MN/m}^2$ is assumed, and the network parameters are independently varied by 20%.

See Results, Section III.D.3, for a detailed explanation.

There is also an increase in A when G is decreased, though for a different reason. A lower G implies a smaller number of chains for a given volume of material, meaning the mass of each chain must be higher. Therefore the number of residues comprising a chain is higher while the segment count has been held constant.

How do we distinguish reasonable models from unreasonable ones? The number of residues per random segment, A , is the key parameter to observe. As will be explained in the discussion, previous studies have determined A for several amorphous protein elastomers. The number of residues per random segment falls between 7 and 14 for these materials. Thus, if the value of A in the last row of a table falls in this range, the model is considered to be a reasonable one, conforming with known materials. If the value of A is less than 7 or greater than 14, the model is not reasonable. Thus, Table 3.7 shows that a network with $s=5$ and $G=0.5 \text{ MN/m}^2$ is actually not compatible with the assumed characteristics of normal, amorphous protein elastomers, and that assuming even lower values of s and G makes the model even less appropriate.

Each of Tables 3.8 A-D makes use of the non-Gaussian curve fits of the spiral silk force-extension data and holds a particular pair of network parameters, s and G , constant (for example, Table 3.8-A assumes the model representing the average dry spiral sample with $s=4.8$ and $G=0.67 \text{ MN/m}^2$). The upper section of each table is arranged in three pairs of columns, all of which assume the theoretical value for the dry network density ($\rho_{\text{dry}}=1330 \text{ kg/m}^3$). The first column pair assumes the lowest values for the crystal volume fraction, V_X , and the average amino acid residue mass, M_{aa} ; the second column pair assumes a high V_X but continues to hold M_{aa} low; and the third column pair assumes high values for both V_X and M_{aa} . Within each column pair, only the wet/dry volume ratio, ΔV , is varied. If the model under consideration is for a dry sample, ΔV varies between 1 and 1.3, as in Table A; if the model is for a wet sample, ΔV is 1.6 or 2.

What are some general trends that can be observed? The first pair of columns in Table 3.8-A shows that increasing ΔV decreases estimates of A , since any ΔV greater than 1.0 means the network is partially hydrated and necessitates a calculation of the rubber network volume fraction V_r . Increasing the crystal fraction V_X (the next two columns) has no effect on dry

Table 3.8. The following tables show sensitivity analyses for the calculation of network chain parameters. Each table assumes a different network model based on mechanical studies of spiral silk samples. Both average and exceptional samples are represented.

Physical models assuming a dry network density $\rho_{dry}=1330 \text{ kg/m}^3$. Wet/dry volume ratio ΔV varies within each column pair.

	low V_x and low M_{aa}		high V_x and low M_{aa}		high V_x and high M_{aa}	
S	4.77	4.77	4.77	4.77	4.77	4.77
G	0.67	0.67	0.67	0.67	0.67	0.67
ΔV	1	1.3	1	1.3	1	1.3
V_x	0.05	0.05	0.25	0.25	0.25	0.25
ρ_{dry}	1330	1330	1330	1330	1330	1330
M_{aa}	84	84	84	84	90	90
V_r	1.00	0.76	1.00	0.71	1.00	0.71
ρ_{wet}	1330	1011	1330	950	1330	950
M_C	4.8	3.7	4.8	3.5	4.8	3.5
aa/chain	58	44	58	41	54	38
A	12.1	9.2	12.1	8.6	11.3	8.0

Within each of the following column pairs, the dry network density ρ_{dry} is varied 10% below and above the theoretical value.

	low V_x and M_{aa}				high V_x and M_{aa}			
	low ΔV		high ΔV		low ΔV		high ΔV	
S	4.77	4.77	4.77	4.77	4.77	4.77	4.77	4.77
G	0.67	0.67	0.67	0.67	0.67	0.67	0.67	0.67
ΔV	1	1	1.3	1.3	1	1	1.3	1.3
V_x	0.05	0.05	0.05	0.05	0.25	0.25	0.25	0.25
ρ_{dry}	1200	1460	1200	1460	1200	1460	1200	1460
M_{aa}	84	84	84	84	90	90	90	90
V_r	1.00	1.00	0.76	0.76	1.00	1.00	0.71	0.71
ρ_{wet}	1200	1460	912	1110	1200	1460	857	1043
M_C	4.4	5.3	3.3	4.0	4.4	5.3	3.1	3.8
aa/chain	52	63	39	48	48	59	35	42
A	10.9	13.2	8.3	10.1	10.2	12.4	7.3	8.8

Table 3.8-A. Sensitivity analysis for a network model representing an average dry sample ($s=4.8$).

Physical models assuming a dry network density $\rho_{dry}=1330 \text{ kg/m}^3$. Wet/dry volume ratio ΔV varies within each column pair.

	low V_x and low M_{aa}		high V_x and low M_{aa}		high V_x and high M_{aa}	
S	6.6	6.6	6.6	6.6	6.6	6.6
G	0.32	0.32	0.32	0.32	0.32	0.32
ΔV	1.6	2	1.6	2	1.6	2
V_x	0.05	0.05	0.25	0.25	0.25	0.25
ρ_{dry}	1330	1330	1330	1330	1330	1330
M_{aa}	84	84	84	84	90	90
V_r	0.61	0.49	0.56	0.43	0.56	0.43
ρ_{wet}	815	648	739	570	739	570
M_c	6.2	4.9	5.6	4.3	5.6	4.3
aa/chain	74	59	67	52	62	48
A	11.2	8.9	10.1	7.8	9.5	7.3

Within each of the following column pairs, the dry network density ρ_{dry} is varied 10% below and above the theoretical value.

	low V_x and M_{aa}				high V_x and M_{aa}			
	low ΔV		high ΔV		low ΔV		high ΔV	
S	6.6	6.6	6.6	6.6	6.6	6.6	6.6	6.6
G	0.32	0.32	0.32	0.32	0.32	0.32	0.32	0.32
ΔV	1.6	1.6	2	2	1.6	1.6	2	2
V_x	0.05	0.05	0.05	0.05	0.25	0.25	0.25	0.25
ρ_{dry}	1200	1460	1200	1460	1200	1460	1200	1460
M_{aa}	84	84	84	84	90	90	90	90
V_r	0.61	0.61	0.49	0.49	0.56	0.56	0.43	0.43
ρ_{wet}	735	895	585	711	667	811	514	626
M_c	5.6	6.8	4.4	5.4	5.1	6.2	3.9	4.8
aa/chain	67	81	53	64	56	69	43	53
A	10.1	12.3	8.0	9.8	8.5	10.4	6.6	8.0

Table 3.8-B. Sensitivity analysis for a network model representing an average wet sample ($s=6.6$).

Physical models assuming a dry network density $\rho_{dry}=1330 \text{ kg/m}^3$. Wet/dry volume ratio ΔV varies within each column pair.

	low V_x and low M_{aa}		high V_x and low M_{aa}		high V_x and high M_{aa}	
s	13.5	13.5	13.5	13.5	13.5	13.5
G	0.20	0.20	0.20	0.20	0.20	0.20
ΔV	1.6	2	1.6	2	1.6	2
V_x	0.05	0.05	0.25	0.25	0.25	0.25
ρ_{dry}	1330	1330	1330	1330	1330	1330
M_{aa}	84	84	84	84	90	90
V_r	0.61	0.49	0.56	0.43	0.56	0.43
ρ_{wet}	815	648	739	570	739	570
M_c	9.9	7.9	9.0	6.9	9.0	6.9
aa/chain	118	94	107	83	100	77
A	8.8	7.0	7.9	6.1	7.4	5.7

Within each of the following column pairs, the dry network density ρ_{dry} is varied 10% below and above the theoretical value.

	low V_x and M_{aa}				high V_x and M_{aa}			
	low ΔV		high ΔV		low ΔV		high ΔV	
s	13.5	13.5	13.5	13.5	13.5	13.5	13.5	13.5
G	0.20	0.20	0.20	0.20	0.20	0.20	0.20	0.20
ΔV	1.6	1.6	2	2	1.6	1.6	2	2
V_x	0.05	0.05	0.05	0.05	0.25	0.25	0.25	0.25
ρ_{dry}	1200	1460	1200	1460	1200	1460	1200	1460
M_{aa}	84	84	84	84	90	90	90	90
V_r	0.61	0.61	0.49	0.49	0.56	0.56	0.43	0.43
ρ_{wet}	735	895	585	711	667	811	514	626
M_c	9.0	10.9	7.1	8.7	8.1	9.9	6.3	7.6
aa/chain	107	130	85	103	90	110	70	85
A	7.9	9.6	6.3	7.6	6.7	8.1	5.2	6.3

Table 3.8-C. Sensitivity analysis for a network model representing an exceptional wet sample ($s=13.5$).

Physical models assuming a dry network density $\rho_{dry}=1330 \text{ kg/m}^3$. Wet/dry volume ratio ΔV varies within each column pair.

	low V_x and low M_{aa}		high V_x and low M_{aa}		high V_x and high M_{aa}	
s	1.8	1.8	1.8	1.8	1.8	1.8
G	0.58	0.58	0.58	0.58	0.58	0.58
ΔV	1	1.3	1	1.3	1	1.3
V_x	0.05	0.05	0.25	0.25	0.25	0.25
ρ_{dry}	1330	1330	1330	1330	1330	1330
M_{aa}	84	84	84	84	90	90
V_r	1.00	0.76	1.00	0.71	1.00	0.71
ρ_{wet}	1330	1011	1330	950	1330	950
M_c	5.6	4.2	5.6	4.0	5.6	4.0
aa/chain	66	51	66	47	62	44
A	36.9	28.1	36.9	26.4	34.5	24.6

Within each of the following column pairs, the dry network density ρ_{dry} is varied 10% below and above the theoretical value.

	low V_x and M_{aa}				high V_x and M_{aa}			
	low ΔV		high ΔV		low ΔV		high ΔV	
s	1.8	1.8	1.8	1.8	1.8	1.8	1.8	1.8
G	0.58	0.58	0.58	0.58	0.58	0.58	0.58	0.58
ΔV	1	1	1.3	1.3	1	1	1.3	1.3
V_x	0.05	0.05	0.05	0.05	0.25	0.25	0.25	0.25
ρ_{dry}	1200	1460	1200	1460	1200	1460	1200	1460
M_{aa}	84	84	84	84	90	90	90	90
V_r	1.00	1.00	0.76	0.76	1.00	1.00	0.71	0.71
ρ_{wet}	1200	1460	912	1110	1200	1460	857	1043
M_c	5.0	6.1	3.8	4.7	5.0	6.1	3.6	4.4
aa/chain	60	73	46	55	56	68	40	49
A	33.3	40.5	25.3	30.8	31.1	37.8	22.2	27.0

Table 3.8-D. Sensitivity analysis for a network model representing an exceptional dry sample ($s=1.8$).

networks ($\Delta V=1$), but decreases estimates of A for hydrated networks ($\Delta V>1$), because when protein is occupying crystalline regions, it is unable to swell when wetted, and so the remaining protein is diluted more for a given overall ΔV . Note the changes in wet rubber network volume fraction, V_R , and density, ρ_{wet} . The third column pair shows that an increase in average residue mass, M_{aa} , decreases the number of amino acid residues, A, comprising a chain of a given mass.

The lower half of each table next shows the effect of changing the dry density. The left two column pairs assume low V_X and M_{aa} , while the right two pairs assume high values for those parameters. Each column pair holds ΔV constant and shows the effect of low and high estimates of dry density ($\rho_{dry}=1200$ or 1460 kg/m^3). It is clear that decreasing dry density causes the number of residues per chain, A, to decrease as well, since the chain mass is proportional to the network density.

Now, with an understanding of the general table format, the overall results of the four models can be reviewed. First, the models for the average dry and wet samples in Tables 3.8-A and 3.8-B yield estimates of A ranging from 6.6 to 12.4, while the model for the exceptional wet sample, in Table 3.8-C, yields slightly lower values ranging from 5.2 to 9.6. As explained earlier, these final values for the key parameter, A, mostly falling in the target range of 7-14, imply that the spiral silk samples are behaving much like other protein elastomers. On the other hand, the dry sample with the lowest extensibility, modelled in Table 3.8-D, appears to require as much as four times as many residues per random segment as the other samples; the key parameter, A, approaches 40, as opposed to 7-14. This large discrepancy indicates a violation of the assumptions for the model.

In summary, the estimations of the chain parameters yielded values for the key parameter, A (the number of residues comprising a random segment), ranging from just over 5 to almost 38. The lowest estimates of A are given by network models with a large number of random segments between crosslinks (s), high shear modulus (G), high wet/dry volume ratio (ΔV), high dry crystal volume fraction (V_X), low dry density (ρ_{dry}), high amino acid residue mass (M_{aa}); and *vice versa*.

4. Test for covalent bonds. In order to determine whether the crosslinks bounding each chain were comprised of covalent bonds or non-covalent interactions, one sample was prepared as for a force-extension sequence, extended to about 2.5 times slack length, then wetted and subjected to another extension up to about 3.4 times wet slack length. The sample was then held at an extension ratio of 1.75 and allowed to equilibrate. Finally, a few drops of water were withdrawn from the chamber and replaced with 6M guanidine hydrochloride solution, which disrupts weak intermolecular forces.

The sample used for this test behaved typically during both dry extension and wet extension. When GuHCl was added, the force of the silk bending the beam rapidly and steadily decreased, the whole process taking a little less than a minute (see Figure 3.10). The silk did not seem to snap until the force was very low.

The rapid reduction in force of stretched spiral silk in 6M GuHCl indicates that the majority of crosslinks are non-covalent. That is, they are probably provided by a mix of beta-pleated-sheet crystals and entanglements, with negligible contributions from sulhydryl, lysine, tyrosine, or other bonds. If there are any other exotic linkages, they must not be present in great enough proportions to affect the mechanical properties.

It is difficult to tell what concentration of GuHCl the silk was subjected to; while the drops added could have mixed with the water and produced a homogeneous, lower concentration, it is also likely that the amount added could have swirled in the chamber in such a way as to rapidly expose the fiber to the full 6 M concentration.

The epoxy used in this experiment was Araldite rapid, not a protein-based glue, therefore no effect of GuHCl on the holding capacity was expected. Qualitative examination of the epoxy revealed no atypical properties under the dissecting microscope; the epoxy was no softer than when wetted in distilled water, was no easier to remove from the beam or needle, and retained its smooth surface, in keeping with its rating as a chemical- and acid-resistant material. Since this was one of the last experiments carried out, gluing methods were well-tested and highly successful at this stage. Therefore it is unlikely that the silk slipped off the beam. During the initial cycles, the silk had been purposely extended farther than the GuHCl extension, so that any potential slippage would have been detected at those higher forces if it were to happen at all.

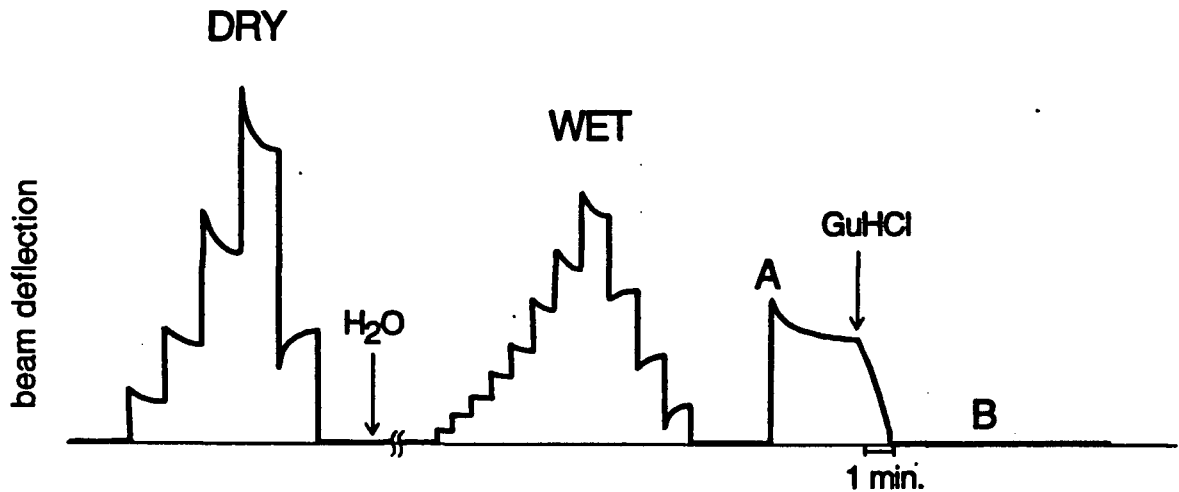


Figure 3.10. Chart record for the GuHCl test for covalent bonds. The sample was first cycled in the dry state, then wetted and cycled once more. Next, it was stretched to an extension ratio of 1.75 and the beam deflection allowed to equilibrate (A). A solution of guanidine hydrochloride was then introduced. Note the steady decrease in force immediately following "GuHCl". Finally, the micrometer was returned to the position corresponding to the previous wet slack length, and another cycle of the sample was attempted (B). Note the absence of any beam deflection during this last phase.

The time-course of the force reduction was also not typical of situations in which slippage was known to happen: rather than being a sudden brief release of tension followed by temporary stability or a complete drop to zero, the reduction was smooth and much slower than the instantaneous drops observed during slippage. There was no evidence of one strand breaking before the other, either. Since the sample was double-stranded, it also would have been less likely to be defective, since handling was minimized by avoiding the isolation process.

E. OPTICAL DATA

Calculations of birefringence for isolated wet brins were restricted to average diameter measurements, due to the lack of information on fiber orientation. Dry sample data sets using bave were not restricted in this way, and for several data sets calculation of birefringence was performed two ways. First, the average diameter for the slack brins, taken under 100X oil immersion, was used to calculate path lengths. Diameters at extensions greater than 1.0 were estimated assuming constant volume of the fibers. This method assumed a circular cross-section. Second, an elliptical cross-section was assumed and path lengths were assigned based on the orientation of the brin-pair at the location of the retardation measurement. The means and coefficients of variation for each method are listed in Table 3.9.

The data provide additional support for the elliptical cross-section of spiral silk fibers, since variation in birefringence values is halved when an elliptical shape is assumed. If the cross-section were actually circular, the elliptical assumption would have resulted in greater variation, since a large pathlength is used in calculations where the measured "diameter" is small, and *vice versa*.

One sample from each of two webs exhibited anomalous birefringences. The values for these samples were not included in the regressions for stress-optical coefficient estimation, as they were obviously outliers (both being three times the magnitude typical for the extension), and two other samples were instead selected to repeat those readings, using identical methods. Both duplicates gave reasonable results. It is, however, important to note the existence of

	Sample a			Sample b		
	Γ	β_c	β_e	Γ	β_c	β_e
Adj	6.65	3.15	2.39	3.28	1.55	1.18
	7	3.32	2.52	3.28	1.55	1.18
St	7	1.66	2.05	4.45	1.05	1.30
	8.1	1.92	2.38	4.74	1.12	1.39
	8.1	1.92	2.38	5.03	1.19	1.48
mean		2.39	2.34		1.30	1.31
CoV		32%	7%		17%	9%

	Sample c			Sample d		
	Γ	β_c	β_e	Γ	β_c	β_e
Adj	5.32	2.52	1.91	2.1	1.00	0.76
	5.6	2.65	2.01	2.2	1.04	0.79
	5.88	2.79	2.12	2.1	1.00	0.76
St	8.34	1.98	2.45	2.7	0.64	0.79
				3	0.71	0.88
				2.4	0.57	0.70
				2.7	0.64	0.79
				3	0.71	0.88
				2.8	0.66	0.82
			2.3	0.55	0.67	
mean		2.48	2.12		0.75	0.78
CoV		12%	9%		24%	8%

Table 3.9. Typical calculations of birefringence, β , using assumptions of circular (β_c) and elliptical (β_e) cross-section. For each sample, the retardation, Γ , was measured at a few locations for each of the indicated orientations. All of the samples were from one web, so the web's average effective diameter of 2.11 μm was used for the pathlength for the circular assumption. For the assumption of ellipticity, a "stacked" diameter of 2.78 μm and an "adjacent" diameter of 1.71 μm were used.

Note the lower coefficients of variation that result when an elliptical cross-section is assumed.

anomalous samples because all of the analysis of spiral silk indicates a high degree of variability which is supported by those two remarkably high-birefringence samples.

Other rubber-like materials can swell in oils. In order to ensure that anomalous results were not caused by the effects of oil, two control experiments were designed. On one sample, the retardation was read at a specific location both before and after oil immersion, in order to ensure that the silk was not altered by the oil. The two independent sets of measurements after oil immersion exactly matched the set of readings taken before oil immersion. Also, while it is not possible to obtain exact diameter readings before the silk is immersed, due to the confounding effects of the irregular glue coating, it is still possible to bracket the probable diameter using reproducible measurements at low and high focus. This method was followed to ensure that diameters were not drastically changing upon oil immersion. When this procedure was carried out for a fine glass fiber, the measurement at low focus gave 4.2 μm and at high focus gave 15 μm , with an average of 9.6 μm . Then, the measurement made under oil (which is precise) gave 10.7 μm , thereby confirming that the bracketing principle is useful. When the same procedure was carried out for a silk sample, the measurement at low focus was 1.5 μm and at high focus was 6 μm , with an bracketed average of 3.75 μm . Then, the measurement taken for the oil-immersed fiber was 3.3 μm , which is not drastically different from the bracketed average and certainly does not imply swelling.

1. Residual birefringence. Residual birefringence was similar for dry and wet silk samples (1.4×10^{-3} and 1.5×10^{-3} , respectively) and statistically indistinguishable; the close similarity was found despite the variations in residual birefringences, which were 30% for dry webs and over 60% for all wet samples, as shown in Table 3.10. The difference in variation is no doubt an artifact of the experimental methods, since the data for the residual birefringence of each dry web were derived from linear regressions of birefringence data taken from several samples, each at a different extension; thus, the intercepts of the regressions were averaged to obtain the mean residual birefringence for all webs. Despite the variations, however, the important facts to note are, firstly, that a significant birefringence did exist even at slack extensions and, secondly, that the birefringence was present in both dry and wet samples.

A. Results for dry webs. Stresses were estimated from the average network parameters of each web.

Web	β_{res}	SO (m^2/N)
IX	0.00134	0.55E-09
X	0.00174	2.04E-09
XI	0.00171	2.77E-09
XII	0.0008	2.1E-09
mean	0.0014	1.86E-09
CoV	27%	44%

B. Results for wet samples. Stresses for each sample were obtained directly from mechanical studies of that sample. In all cases, standard errors were an order of magnitude smaller than the means.

Web Sample	β_{res}	SO (m^2/N)
II #13	0.00136	1.53E-09
IV #1	0.00136	1.67E-09
#2	0.000033	2.31E-09
#3	0.00174	1.67E-09
#4	0.00137	1.20E-09
VIII #6	0.00334	3.54E-09
IX #7	0.00103	3.46E-09
mean	0.00146	2.2E-09
CoV	63%	40%

Table 3.10. Residual birefringences (β_{res}) and stress-optical coefficients (SO) for dry and wet samples.

2. Stress-optical coefficients. Since photoelasticity theory uses true stress for calculations, the areas of fibers at non-slack extensions were estimated based on the assumption that spiral silk remains at a constant volume while stretched. This method was used both for bave (using the effective diameter at slack extension) and for isolated brins with unknown orientations. For such a brin, the average volume of the fiber was calculated based on diameter measurements at as many extensions as possible, and the diameter at slack was calculated from the average volume. For both bave and brins, the diameters at all other extensions were calculated using Equation 34.

The wet and dry stress-optical coefficients for each web studied are listed in Table 3.10, with the residual birefringences. The average coefficient is significantly higher than would be usual for a wholly amorphous rubber like elastin, which exhibits a coefficient of 1.0×10^{-9} (Aaron and Gosline, 1981). Since the typical composition and non-negligible residual birefringence imply that the high stress-optical coefficient is due to crystals, and not to a unique, high-polarizability chemical structure, it was not feasible to use the observed coefficient in calculations for the amorphous matrix; instead, the theoretical stress-optical coefficient of elastin was used to calculate the birefringence that would be expected if the silk were wholly amorphous. The birefringence in excess of the expected amount must be due to crystals.

3. Predicted Birefringence. Figure 3.11 is a plot of the birefringences predicted for wholly amorphous networks, based on Equation 31. Predictions were made for the average dry and wet networks and the two most exceptional networks noted. Note that birefringence smoothly increases as strain aligns the matrix molecules. In order to assess the sensitivity to errors in the estimate of the polarizability of spiral silk's protein chains, Figure 3.12 plots predicted birefringence curves for a network with $G=0.6 \text{ MN/m}^2$ and $s=6$, assuming stress-optical coefficients 10% lower and higher than the theoretical value. Note that the predictions are not very sensitive to changes in the coefficient, since the middle curve is closely bracketed; therefore even if the true stress-optical coefficient of spiral silk amorphous regions is slightly different than the theoretical value, the predictions to follow will not be greatly affected.

Figure 3.13 includes plots of the actual birefringence of samples #1 and #3, wetted, after subtraction of the residual birefringence. These particular samples, both from the same web,

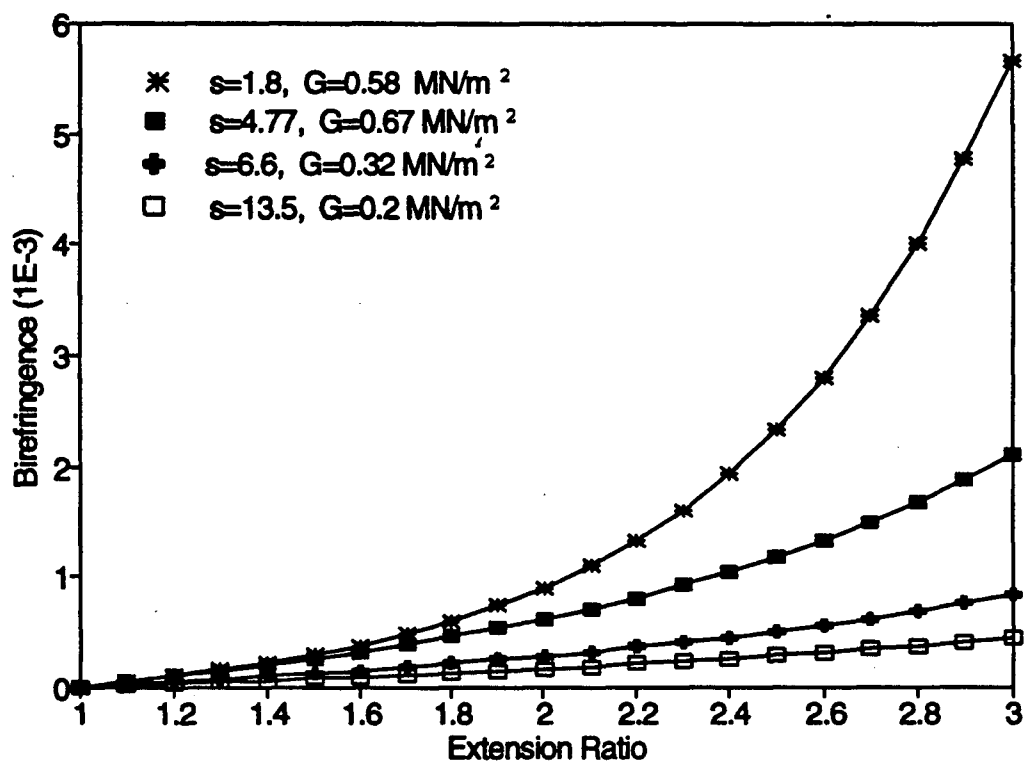


Figure 3.11. Predicted birefringence curves for rubber networks with parameters s and G corresponding to an exceptionally stiff dry sample ($s=1.8$), an average dry sample ($s=4.77$), an average wet sample ($s=6.6$), and an exceptionally stretchy wet sample ($s=13.5$).

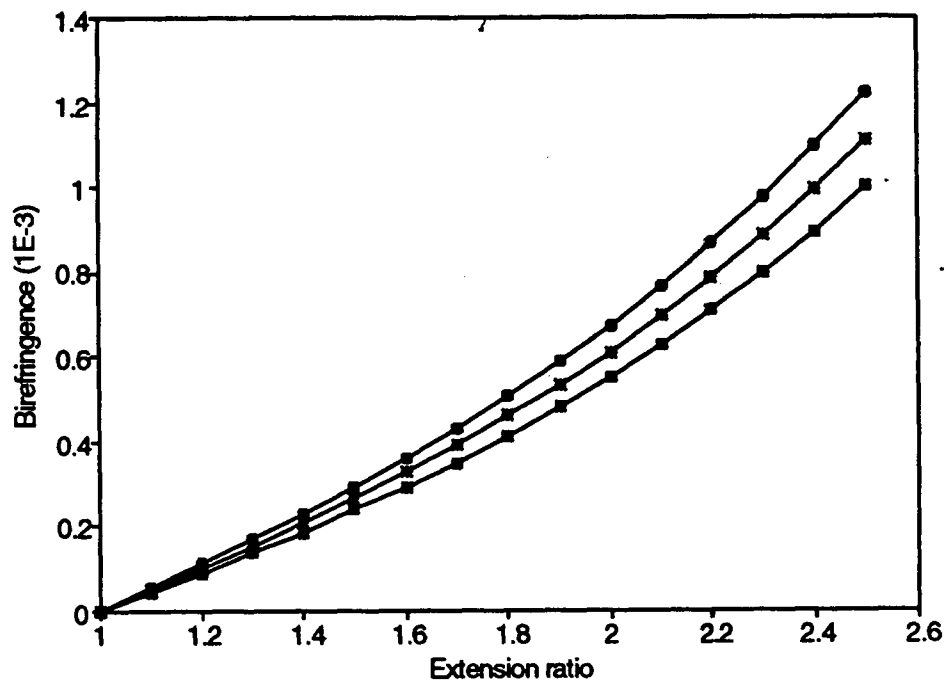


Figure 3.12. Birefringence predicted for a rubber network with $s=6$ and $G=0.69 \text{ MN/m}^2$, showing the variation when stress-optical coefficients 10% below and above the theoretical value are assumed.

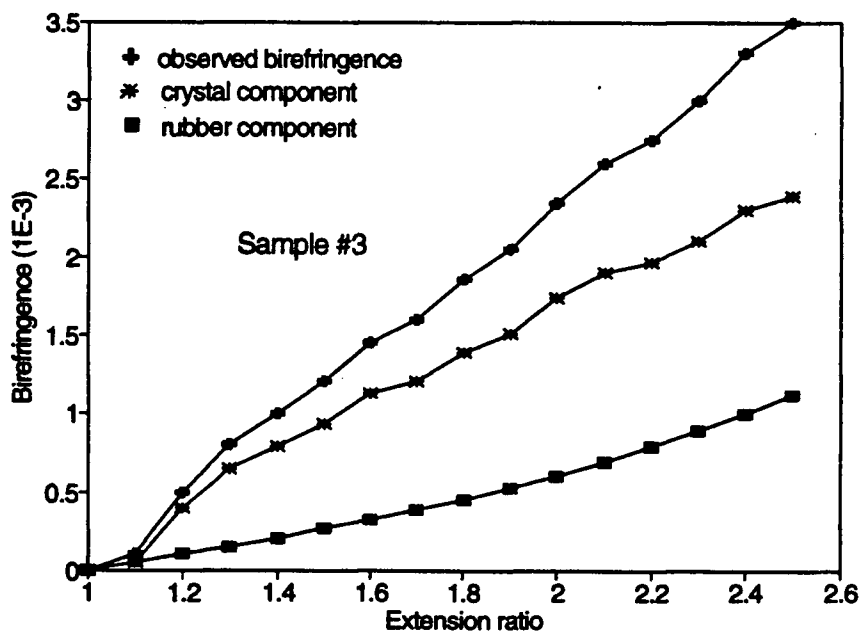
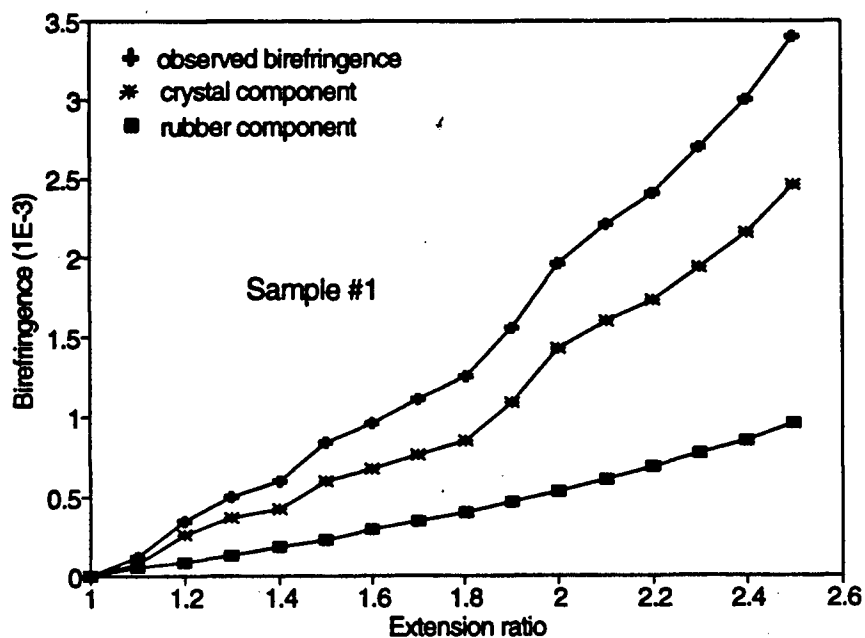


Figure 3.13. Observed extension-birefringence curves for two samples. For each sample, the component of birefringence due to the amorphous matrix was predicted based on network parameters, and the component of birefringence due to crystals was calculated as the difference between the observed and predicted values.

exhibited typical mechanical behavior, having network parameters close to the average wet values. The predicted birefringences due to the amorphous networks alone are the lower curves. The difference between the curves, plotted as the middle curves, are the components of the observed birefringence which must be due to crystal alignment, after subtracting the residual birefringence.

Note that the crystal component of the birefringence increases more quickly per extension increment than the amorphous component. The greater slope is logical since a segment containing crystal is composed of many doubled-back, tightly aligned, folded chains, compared to a single random rubbery chain. With crystals of higher polarizability, the resultant slope will naturally be higher. Without estimates of crystal size or volume, however, it is difficult to make more elaborate conclusions; it must be sufficient to state that spiral silk behaves in accordance with a rubbery material containing crystalline inclusions.

CHAPTER IV: DISCUSSION

A. PHYSICAL PARAMETERS

1. Diameter and cross-section. The first set of experiments concerning physical parameters of spiral silk yielded three useful conclusions. Firstly, spiral silk is not circularly cylindrical as previously assumed; secondly, spiral silk is, at least roughly, a constant-volume system; and thirdly, parameters are more uniform and consistent for a single web than between webs, and even more uniform within a single strand.

The first conclusion, that spiral silk is non-circular in cross-section, is helpful in several respects. One assumption that has been used by virtually all spider silk researchers is that the brins are circularly cylindrical. Many natural fibers, however, are known to be non-circular; in fact, cross-sectional shape is an identifying feature of wools, silks, and vegetable fibers (Preston, 1953, Heyn, 1954). Among the silks, *Bombyx mori* produces paired fibers of hemicircular to triangular section (Iizuka, 1965a), and wild Tussah silks are brownish and flattened or ribbonlike (Heyn, 1954).

Cross-sectional shape is important when stresses are being calculated, because the calculation of stress is dependent on cross-sectional area, which varies as the square of a linear dimension. If the brin is, for example, elliptical in cross-section, one needs to know both minor and major diameters to correctly calculate area. Birefringence is dependent on the first power of diameter since retardation is divided by path length. If the brin is elliptical, the light may be retarded across the major axis while the diameter was being measured across the minor axis, or vice versa.

Obviously, greater accuracy and precision can be expected for any calculation involving diameters. Also, less time need be spent measuring diameters, since a single strand is now known to be fairly regular in dimensions, and thus only a few readings need be taken: a few each of stacked and adjacent orientations. The danger of using entirely randomly-selected locations, or isolated brins, for measurements can now be avoided. The average of the stacked diameters must be weighted equally with the average of the adjacent diameters, even if only four readings contributed to the former and forty to the latter. In addition, even if the entire length of a fiber is

at one orientation, with no twists allowing another angle of tilt to be viewed, the diameter at the other orientation can at least be approximated based on the average ellipticity of the web. In this way, gross over- or under-estimates can be avoided, especially during birefringence calculations which depend on the dimension perpendicular to the measurement. Samples for which preparation consumes a good deal of time can be used, which otherwise might have been discarded.

If part of the reason for the non-circular cross-section is that the edges of the fibers adhere to each other as they are drawn from the spinneret, resulting in a shape more hemispherical than perfectly elliptical, then perhaps the silk of the inner adjacent edges is different than the silk adjacent to the glue layer, that may be applied a moment later. Such a discrepancy, even if slight, could result in the coiling that is observed when one fiber of an immersed double strand is broken and separated from the other.

The rotation method used in this study can only indicate whether fibers are noncircular, not what shape they are. One method of determining cross-section shapes is to bundle fibers together (sometimes also embedding them) and then shave off slices with some variety of microtome (Heyn, 1954). This method is used for reasonably robust fibers: vegetable fibers, wool, and heavier silkworm silks which are easily collected in great quantity. For viscid silk, which is wet, elastomeric, difficult to handle, very slender, and which is available in only short sections, this method would be awkward, though it has been done for some spider dragline silks which are available in large quantity and were packed with larger fibers to facilitate sectioning (Zemlin, 1968). Electron microscopic analysis might provide an easier way to tell whether the spiral shape is hemispherical, triangular, or other.

The reduction in birefringence variance seen in Table 3.9 was presented in defense of the elliptical assumption. Of course, the higher birefringence for adjacent fibers, which look narrower, could theoretically be due to narrow fibers having a higher degree of crystallinity. In fact, the small diameter/high crystallinity relationship has been shown to hold for silkworm silk (Iizuka 1965a), and polymer manufacturers use the principle as well. That possibility was rejected in this situation for several reasons. For one, rarely was a stacked narrow fiber or a wide adjacent fiber observed (in fact, only when silk was obviously separated or damaged). Also, the

observations permitted by negligible depth of field, which imply "tilted" non-circular fibers, can not simply be discarded, nor can the evidence from the "rolled" fiber.

2. Constant volume. The assurance that spiral silk is a constant-volume system would also be a time-saver, when combined with knowledge of bave orientations, since reliable diameter readings at any moderate extension can then be used to estimate the diameter at any other extension. Problems due to vibrations at low extensions, or low precision at high extensions when the silk has decreased in diameter, are then more easily circumvented. Several possible explanations were given for the ambiguity of the volume changes of stretched spiral silk samples, and the assumption of constant volume was defended by the lack of consistent, concrete evidence for either increase or decrease in volume. An additional assurance that the assumption is valid is found in the fact that rubber-like materials in general behave as constant volume systems when stretched to moderate extensions. Since samples were not unduly strained and all stress-extension curves conformed closely to the non-Gaussian predictions, it is most likely that spiral silk possesses a typical rubber-like random network and deforms at constant volume.

3. Wet contraction. Certain network characteristics can be inferred from the time-course of the wet contraction of spiral silk. The two-phase time courses imply that the wet contraction of silk involves two mechanisms. The first rapid contraction is probably due to the water quickly penetrating the accessible amorphous regions of the rubbery matrix. Because silk is drawn out under tension as it is first produced, some of the molecular chains are held in an aligned conformation as the silk quickly dries at normal humidity. When water penetrates those regions, the chains are plasticized and the material is freed to swell laterally and contract lengthwise to a state of greater entropy. The second phase of gradual contraction may be due to small crystals being gradually dissolved, or entanglements gradually unravelling.

B. MECHANICAL PROPERTIES

1. Force-extension behavior. The first issue to be addressed when one is studying mechanical properties of most biological tissues is the question of preconditioning. When a material is cycled repeatedly, even at a fixed rate and maximum extension, its behavior on each successive cycle changes; the changes become slighter with each cycle, until there is no perceptible change between cycles. When the material has attained the latter state, it is said to be preconditioned. The reason preconditioning is important is because it is often the only way to get reproducible results, since otherwise the results of the initial cycles may be highly dependent on the object's history.

For some materials, preconditioning is absolutely essential, yet other materials prove to be more consistent in their behavior. Since the results of repeated force-extension cycles of spiral samples during a single day are so similar, it can be seen that preconditioning is not a critical factor with this material. Thus, the data for curve fitting could even have been taken from the first cycle with little difference in results.

There is nevertheless a perceptible change in the behavior of a wet sample (#22) between the first and second days. The stiffness is seen to increase, as Figure 3.4 illustrates and the change in shear modulus, G , indicates in Table 3.6. These phenomena could be due to a small amount of strain crystallization, as protein chains are aligned and regions of small amino acid residues are brought closer together. There does not, however, appear to be much of a decrease in segment count that is expected with such a crosslink-forming phenomenon; Table 3.6 shows that the segment counts on the first and third days are identical, despite the increase in shear modulus. If the increased stiffness was due to an increase in crystal filler particle size, rather than an increase in particle number, then the results might be explained as the nucleating effects of existing crystal crosslinks.

Sample #21, whose segment count actually decreased upon wetting (Table 3.5), was pointed out in the Results. The decrease was unexpected because an increase in segment count would seem to indicate increased crystallization, whereas water penetrating a protein would be expected to discourage crystallization. Admittedly, if the first cycle of dry fiber #21 is compared

with the first cycle wetted, the network segment count appears to have decreased. However, after repeated cycles in the dry state, preconditioning caused the dry segment count to decrease to 2.9. After wetting, the segment count was 3.2. While the latter value is indeed less than that of the first dry cycle, it is also greater than the final dry cycle before wetting; thus, even if there is a slight amount of crystallization possible during repeated cycles, crystallization does not appear to be increased by wetting.

The changes in force-extension behavior that are observed when a dry sample is wetted (Figures 3.5 and 3.6) provide further insights into the effects of hydration on the silk network structure. First of all, the general increase in force at any given length was noted for Sample #40-41 (curve set A). Notice in particular that the shapes of the dry and wet curves are virtually identical; they simply begin at different lengths. This implies that the energy or work required to pull the sample a certain distance (the area under the force-extension curve) is similar regardless of the sample's state; thus, the number of network chains providing recoil forces must not have changed much upon wetting.

The above behavior can be contrasted with the results shown for Sample #30-32 (curve set C). The decrease in the force exerted by the wetted sample is clearly seen, as the curve for the wet data undercuts the curve for the dry data. Obviously, less energy is required to pull the wet sample a given distance; furthermore, the segment count has more than doubled upon wetting, increasing from 5.5 to 13.5 (see Table 3.5). This combination of events implies that network chains and crosslinks were both significantly reduced by the hydration process; that is, crystals must have been dissolved. A close look at Figure 3.6 confirms that, in fact, all the values of W_{wet} were less than their respective values of W_{dry} .

Surprisingly, the samples with the highest initial stiffnesses, E_i , showed the largest relative reductions in the work parameter. This result was unexpected because higher stiffness in dry samples was understood to indicate higher crystallinity, and a higher crystallinity might be expected to cause greater network stability. The discrepancy between expectations and observations may be due to the presence of two types of crystalline regions which are affected by production methods to different degrees. For example, the amount of permanent, stable, beta-pleated sheet crystals in spiral silk may be determined primarily by predefined factors such as

the sequence of the polypeptides comprising the fibroin, or the amount of plasticizing agent present, with only small increases in crystal filler particles possible when the progenitive fluid is subjected to greater strain during the drawing-out of the silk. At the same time, it is conceivable that production methods may affect glassy, semi-stable regions to a greater degree; thus, the stiffest samples would have a greater proportion of their stiffness due to water-labile structures.

In summary, wetting allows entropy-driven retraction to overcome previously restricted, glassy or crystalline regions, permitting the lateral swelling and lengthwise wet contraction typically observed. In some cases, the crystalline structures appear barely affected by hydration. However, other samples show that crystal crosslinks are, at times, penetrated by water and dissolved; furthermore, there is no evidence of any *increase* in crystallinity in any sample.

2. Network chain parameters. As described in the Results, the network parameters, s and G , derived from the force-extension data, were assumed to model the amorphous network with no other assumptions (such as crystalline filler particles) necessary. The network parameters were then used to calculate the key chain parameter, A (the number of amino acid residues comprising a random segment). A sensitivity analysis tested the effects of varying physical parameters whose values for spiral silk are not definitely known; now, the reasons for the selection of certain value ranges and the results of those models will be explained in more detail.

The first physical parameter varied was wet/dry volume ratio, ΔV , in Table 3.8-A. The wet/dry volume change choices of 1.0 and 1.6 relied on the assumption that spiral silk is essentially dry at room conditions. This could be inaccurate, as even some stiff, non-rubbery dragline silks of other orb weavers contain some moisture, and possibly as much as 15% when forcibly silked (Tillinghast, Chase and Townley, 1984). Yet web scaffolding (frame silk), appears to be quite dry; perhaps its function requires more rigid, controlled properties for proper vibration transmission. It is believed that control of hydration may be effected via changes in water extraction by the exceedingly long ducts, since potassium is associated with web fibers (Tillinghast, Chase and Townley, 1984).

If spiral silk is not fully dehydrated at room conditions, then what is an appropriate hydration level to assume for the upper bound of ΔV , without having to painstakingly measure

the water content of microgram quantities of a material covered with tenacious glue that was itself likely to confound the values obtained? First of all, analysis of data from Work (1977b) indicates that the average wet/dry volume ratio for frame silk is 2.0, whereas spiral silk shows an average volume ratio of 1.6 going from room condition to fully hydrated. Secondly, spiral silk could theoretically be capable of swelling to the same degree as frame silk, since they are proteins with similar compositions (Gosline, DeMont and Denny, 1986); thus, a maximum $\Delta V=2.0$ was chosen for the hydration level of wetted spiral silk. Thirdly, if this upper bound is assumed, yet the observed increase in volume when actual samples are wetted is only 1.6, the discrepancy could be due to spiral silk already having 1.3 times the volume it would if it were entirely dehydrated. Thus, a maximum $\Delta V=1.3$ was assumed for native spiral silk.

The next parameter varied was the dry crystal volume fraction, V_X . Frame silk has been estimated to contain 20-40% crystal volume fraction based on comparisons with the even more highly crystalline silk of *Bombyx mori* (Iizuka, 1965a), and 25% based on chain parameter analysis. Therefore, a range of 5-25% seemed appropriate for the extreme limits of the sensitivity analysis for spiral silk's chain parameters. A larger volume fraction is highly unlikely, since higher volume fractions of filler particles prevent a rubber-composite from being analyzed as a wholly amorphous material. For example, when frame silk is analyzed, it is necessary to adjust the extension ratios of the stress-extension curves to account for the true strain in the amorphous chains being much larger than the macroscopic strain of the object (the principles will be explained later). Yet, the majority of spiral silk samples require no such elaboration of the elastomer model; therefore the crystal volume fraction must be lower. Note that the calculation of wet rubber matrix density, ρ_{wet} , assumes that the crystals of dry silk do not dissolve when wetted. X-ray diffraction studies of Fornes, Work and Morosoff (1983) proved that this supposition holds true for frame silk. Since some portion of the crystals in spiral silk appear to be water-labile (see Figure 3.6), the actual crystal volume fraction of wet silk will likely be lower than the values based purely on the dilution of the dry sample; thus, $V_X=25\%$ is even more assuredly an upper bound.

Next, the average mass of the amino acid residues comprising amorphous chains was varied. There are several values that could have been used for M_{aa} . The "average" protein (for

example, an enzyme) has amino acid residues averaging 110 g/mol (not including the water of hydrolysis), which is lower than the average weight, 120 g/mol, of all 20 amino acids (if present in equal proportions). It is clear, however, that the average molecular weight (MW) of an amino acid in silk protein is less than the average enzyme, since silks have particularly large proportions of small amino acids. As described in the Introduction, both frame and spiral silk contain about 50% glycine, alanine, and serine.

Thus, spiral silk is estimated to have an average residue weight of 84 g/mol; yet the value of 84 g/mol is obviously biased by the small residues. What is really needed to calculate the average number of residues per random segment is the average MW of a residue in the mobile chains. Judging from the Gly-Ala ratio of 2:1 in many β -pleated sheet structures, including silkworm, it might be reasonable to exclude these two residues, in those proportions, from the average. A portion of *N. clavipes* dragline protein also shows a high proportion of Glycine and Alanine, but in a different pattern (Xu and Lewis, 1990); these regions of the polypeptide are not known for certain to contribute to the crystalline regions. Furthermore, the intersheet spacing of *A. diadematus* implies that larger residues are present (Warwicker, 1960). Thus, if it is assumed that the fraction of small residues that must be eliminated is the fraction tied up in crosslinks, this will be an upper limit. Given that the dry crystal volume fraction is V_X , and the proportion of small amino acids in the total silk protein is V_S , the proportion of small residues that was excluded from averaging was $V_e = V_X/V_S$. This formula yielded the value of 90 g/mol when a high $V_X=25\%$ is assumed, and it is obviously an upper bound.

Finally, the value for the dry network density was varied. The dry density of elastin, the protein rubber most thoroughly studied, has been determined to be 1330 kg/m³ (Aaron and Gosline, 1981). This was used as the median value. One researcher obtained a value of 1347 kg/m³ for frame silk (Work, 1976); the possibility of spiral silk having a higher or lower density was allowed by assuming values approximately 10% higher and lower, (1460 kg/m³ and 1200 kg/m³, respectively).

3. Validity of the network models. As stated earlier, the network models chosen for sensitivity analysis were the two models representing an average dry and an average wet sample, plus the two models representing the samples with lowest and highest segment counts. In the results, the comment was made that Tables 3.8-A, B and C (the average dry and both wet networks) yielded estimates of A which were reasonable for elastomeric proteins. This comment was based on the fact that the number of amino acids per random segment, A , has been estimated for several swollen protein rubbers, and found to fall within a range of 7-14 residues. Actually, most rubber-like proteins seem to tend toward the lower end of the range, with only Octopus Arterial Elastomer (OAE) showing the exceptionally high values of $A=12-14$ residues per segment (Shadwick and Gosline, 1985). Since spiral silk has a composition and average amino acid residue mass more similar to elastin and resilin, it is more likely that the reasonable range for the A of spiral silk is 7-10 residues per segment. Models which yield estimates of A outside this range presumably violate one or more of the assumed physical parameters.

A closer look at the tables, using the stricter guidelines of 7-10 residues, can help narrow down the physical models to the most-likely possibilities. For example, there are eight models in Table 3.8A (for the average dry sample) which yield values for A that exceed 10, and seven of the eight models propose an entirely anhydrous network for samples in the native state. This result clearly provides support for the idea that spiral silk is partially hydrated at room conditions. Proceeding to Table 3.8-B (for the average wet sample), there are five models which yield $A > 10$. All five of these models propose a wet/dry volume change $\Delta V = 1.6$, which again assumes that spiral silk is totally dry in its native state. Conversely, all of the models which assume that spiral silk is capable of swelling to the same degree as frame silk ($\Delta V = 2$) yield reasonable values for A , which is in accordance with the hypothesis that the average dry sample is partially hydrated.

Analysis of the models for the exceptional wet sample (Table 3.8-C) requires a slightly different approach; there are no overestimates of the number of residues per segment, A , but there are several low values. In fact, six models yield values of A less than 7. Five of these models assume a high crystal volume fraction V_X and/or a high M_{aa} , thus implying that this

stretchy, low-stiffness sample is best modelled with a low degree of crystallinity, exactly as one expects.

The model departing most drastically from the expected estimates of the number of residues per segment, A , is the exceptional dry, low- s sample in Table 3.8-D. None of the estimates for the number of residues per segment, A , are even close to the theoretical values; all are too high to be reasonable. Yet, note that even this table is somewhat logical, since values of high crystal volume fraction, V_x , and high average residue mass, M_{aa} , do reduce the estimates. Perhaps the "unreasonable" values are due to an unusual phenomenon such as a drop of dew having washed the plasticizers from this segment, causing an abnormally high crystal volume fraction. In this case, the assumption that the sample was a wholly amorphous rubber would be violated; the material would instead be considered a filled rubber, like frame silk, and it would be necessary to correct the apparent extension to get a value for the true, amplified extension of the chains. The latter possibility will be investigated as part of the comparison of frame and spiral silks, later in this discussion.

Thus, the sensitivity analysis was helpful in that it provided further support for two notions. First, that spiral silk can be generally approximated as a wholly amorphous elastomer; and second, that spiral silk is partially hydrated in its native state at room conditions. Thus, the network model for the average dry spiral silk sample (with a segment count, $s=4.77$ and a shear modulus, $G=0.67$ MN/m²), the model for the average wet sample, ($s=6.6$, $G=0.32$ MN/m²), and the model for the exceptional wet sample ($s=13.5$, $G=0.2$ MN/m²), are in agreement with other protein elastomer models, without assuming extra effects due to filler particles. Furthermore, despite the large variations observed, the overall results of the network analyses were intuitively satisfying. A dry sample exhibited the lowest s , and a wet sample the highest; also, the average for the dry networks yielded a lower s and higher G than the average for the wet networks.

C. OPTICAL ANALYSIS

The non-negligible residual birefringence of spiral silk supports the view that there are crystalline regions in spiral silk, even at slack extension and when wetted. The majority of crystals appear to be stable in water, as there is no significant decrease in residual birefringence when silk is wetted. Part of the birefringence of wet fibers could no doubt be due to "form" or "edge" birefringence, where birefringence is induced by the difference in refractive indices of an object and the medium in which it rests. In fact, even a wet fiber of low birefringence could often be detected by its brighter edges, so it was important to take readings at the core of the fiber. However, the magnitude of form birefringence of elastin was found to be an order of magnitude lower than the average residual birefringence observed for spiral silk (Aaron and Gosline, 1980), and a few birefringence readings taken for spiral silk samples were actually even lower than the form birefringence of elastin, so the effects of form birefringence did not seem to distort readings. Form birefringence was consistently negligible for dry samples, since they were immersed in oil with a refractive index very close to the spiral silk's RI, making detection of edges difficult.

The high value for the stress-optical coefficient, and the comparisons of predicted birefringence versus actual birefringence curves, likewise indicate the presence of crystals, as explained in the Results. It is highly improbable that such a high stress-optical coefficient could be due to a difference in the polarizability of the amorphous chains; the optical characteristics of protein chains do not vary much, based on studies of other biological rubbers (Gosline, 1987), and spiral silk does not have an anomalous composition. More support for the presence of crystallites was provided by the test for covalent linkages. Since dissolution in guanidine hydrochloride indicated the absence of any functional covalent crosslinking mechanisms, secondary bonds must provide the means by which the rubber-like network chains are held together; crystalline protein conformations are formed by the cooperative effect of just such weak molecular interactions.

D. A MODEL FOR SPIDER SPIRAL SILK

In summary, wet spiral silk was found to have a segment count, $s=6.6$, slightly greater than dry spiral silk with $s=4.8$. Given the current data, this difference is not statistically significant; if it is later shown to be real, it would indicate some dissolution of crystals, thereby making longer chains available to the rubber-like matrix. The wet shear modulus, $G=0.32$ MN/m², is half that of dry spiral silk at 0.67 MN/m². These values are again not statistically different, yet the difference is logical considering the dilution of the network which occurs upon wetting. Other physical parameters are difficult to determine accurately, but it is not unlikely that spiral silk is capable of a wet/dry volume ratio of 2, and is partially swollen at room conditions. Crosslinking of the rubber-like network is via secondary bonds only, and the residual birefringence of $1.43 \cdot 10^{-3}$ and high stress-optical coefficient of $2 \cdot 10^{-9}$ m²/N indicate that both dry and wet spiral silk contain crystalline regions which could accomplish the task. The average sample of dry or wet spiral silk can be modelled as a wholly rubber-like network, but exceptional pieces of dry silk appear to violate this assumption and require the effects of filler particles to be included in any reasonable model.

E. COMPARISON OF FRAME AND SPIRAL SILK MODELS

1. Network parameters and strain amplification. The network model of frame silk stipulates a segment count of 2, similar to the exceptional dry spiral sample, but with a higher matrix shear modulus $G=0.8$ MN/m² (Gosline et al, 1991). It should be noted, however, that the model for frame silk must be arrived at somewhat differently than the model for spiral silk. The difference in analysis procedures is due to the high degree of crystallinity of frame silk. If frame silk is assumed to be a wholly rubber-like material, estimates of the number of residues per random segment are ridiculously high, even in the hundreds and thousands (Gosline et al, 1988). The huge numbers are due to the fact that frame silk is not simply a rubber, but a rubber-composite reinforced with crystallite filler particles. The large volume of particles makes the material behave more stiffly. The stiffness is due to the fact that for a given amount of protein, a significant volume of the material is taken up in crystals, leaving a relatively small amount

actually capable of acting rubbery. Thus, the actual extension of a chain between crystal crosslinks can be much larger than the extension which is observed for the whole sample. In addition, the increase in stiffness is enhanced by the inhibition of polymer flow around the particles, and depends on their shape.

The apparent extension of the sample can be adjusted by a "strain amplification" factor to arrive at a guess for the effective extension of the amorphous network chains. (Note that the value of $G=0.8 \text{ MN/m}^2$ which is then quoted for frame silk is the shear modulus of the rubbery matrix alone.) Reasonable values for the number of residues per segment are given by a strain amplification factor of about 2 for frame silk. Differently-shaped crystals increase stiffness to varying degrees, but the exact size and aspect ratio of frame silk crystals are not known, so the crystals of frame silk were assumed to have an aspect ratio similar to those of silkworm silk, which have a length:width ratio of about 5:1. From the strain amplification and crystal aspect ratio, the crystal volume fraction of dry silk was estimated to be 25% (Gosline et al, 1988).

When the exceptional dry spiral sample is dealt with as a composite material instead of a wholly amorphous elastomer, much more reasonable models are calculated. Furthermore, the non-Gaussian curve fits yield higher values for the Coefficient of Determination, with R^2 increasing from 0.9984 for no strain amplification to 0.9996 for strain amplifications from 1.75-2.25. As Table 4.1 shows, when a strain amplification of 2-2.25 is assumed, many estimates of the number of residues comprising a random segment (A) fall in the reasonable range of 7-10 residues; compare these new values with those of Table 3.8-D. (The models which assume a high wet/dry volume ratio, ΔV , are reasonable at even lower strain amplifications, but it is questionable whether the high level of swelling should be assumed under these conditions).

Thus, the crystal volume fraction of this exceptional spiral sample appears at least to match, if not exceed, the crystal volume fraction of frame silk. (As a side note, it is appropriate here to recall the two spiral samples that exhibited anomalously high birefringence.) At the same time, remember that a strain-amplified model proposes a higher segment count, s , than a non-composite model; in effect, the burden of explaining high stiffness is deflected from the network chains to the filler particles. In the case of this dry spiral sample, there is an increase from the original estimated $s=1.8$, to a value of $s=4.2$ to 6.2 . Thus, even if the spiral sample has a degree

A. A dry fiber ($\Delta V = 1$) is assumed, with low V_x .

F	1.0	1.25	1.5	1.75	2.0	2.25
s	1.8	2.5	3.2	4.2	5	6.2
G	0.58	0.76	0.77	0.87	0.81	0.85
ΔV	1	1	1	1	1	1
V_x	0.05	0.05	0.05	0.05	0.05	0.05
ρ_{dry}	1330	1330	1330	1330	1330	1330
M_{aa}	84	84	84	84	84	84
V_r	1.00	1.00	1.00	1.00	1.00	1.00
ρ_{wet}	1330	1330	1330	1330	1330	1330
M_c	5.6	4.3	4.2	3.7	4.0	3.8
aa/chain	66	51	50	44	48	45
A	36.9	20.4	15.6	10.6	9.5	7.3

B. A partially-hydrated sample is assumed ($\Delta V = 1.3$), with a low crystal volume fraction.

F	1.0	1.25	1.5	1.75	2.0	2.25
s	1.8	2.5	3.2	4.2	5	6.2
G	0.58	0.76	0.77	0.87	0.81	0.85
ΔV	1.3	1.3	1.3	1.3	1.3	1.3
V_x	0.05	0.05	0.05	0.05	0.05	0.05
ρ_{dry}	1330	1330	1330	1330	1330	1330
M_{aa}	84	84	84	84	84	84
V_r	0.76	0.76	0.76	0.76	0.76	0.76
ρ_{wet}	1011	1011	1011	1011	1011	1011
M_c	4.2	3.3	3.2	2.8	3.0	2.9
aa/chain	51	39	38	34	36	34
A	28.1	15.5	11.9	8.0	7.2	5.6

Table 4.1. Calculations of the chain parameters for Sample #25. The strain amplification factor, F, is varied from 1.0 to 2.25. See Discussion, Section IV.E.1.

F	1.0	1.25	1.5	1.75	2.0	2.25
s	1.8	2.5	3.2	4.2	5	6.2
G	0.58	0.76	0.77	0.87	0.81	0.85
ΔV	1.3	1.3	1.3	1.3	1.3	1.3
V_x	0.25	0.25	0.25	0.25	0.25	0.25
ρ_{dry}	1330	1330	1330	1330	1330	1330
M_{aa}	84	84	84	84	84	84
V_r	0.71	0.71	0.71	0.71	0.71	0.71
ρ_{wet}	950	950	950	950	950	950
M_c	4.0	3.1	3.0	2.7	2.9	2.7
aa/chain	47	36	36	32	34	32
A	26.4	14.6	11.2	7.5	6.8	5.2

Table 4.1-C. Calculation of chain parameters for Sample #25 (continued). A partially-hydrated sample is assumed ($\Delta V = 1.3$), with a high crystal volume fraction.

of crystallinity similar to or exceeding frame silk, the chains between the crystal crosslinks are longer.

As a final note of caution when evaluating results from non-Gaussian curve fits, it is important to note that the models and mathematics were developed for application to networks with a segment count, s , greater than 10. As most of the results for frame and spiral silk are well below that threshold, the physical interpretation of the models is in error by an indefinite amount; however, relative standings will of course remain valid for comparative purposes.

2. Birefringence and crystallites. Up to this point, only mechanical parameters of the two silks have been compared. How do optical properties compare? The average residual birefringences of elastin (a wholly amorphous protein rubber), spiral silk, and frame silk, are listed in Table 4.2 with a few other parameters for comparison. Note that the values for spiral silk are between the other two materials. The value for spiral silk being lower than that of frame silk indicates that crystals are likely to be fewer and/or smaller, therefore the dry volume fraction of crystals in spiral silk is probably less than 20%. The lower residual birefringence also could be due to whatever crystals are present being more randomly oriented. If spiral silk crystals have a low aspect ratio, it would be possible for a higher proportion to be present before the effects of strain amplification would be felt. On the other hand, recall that the birefringence of the low- s dry sample was not determined; it may have been close to that of frame silk, like the two anomalous samples mentioned previously.

The orb weaver *Argiope aurantia* has silk compositions remarkably similar to *Araneus diadematus*. The spiral silk of *A. aurantia* shows relatively low resistance to protease digestion, compared with frame silk (Kavanagh and Tillinghast, 1979), suggesting that the amorphous chains of spiral silks are more accessible, perhaps because the crystalline regions are smaller than those of frame silk. Yet, crystals are obviously present in an amount large enough both to cause a non-negligible birefringence at slack extension, even wet; and also to stably crosslink the material, since covalent bonds were proven to play a negligible part in this role.

In keeping with its higher birefringence and crosslink density, frame silk is known to maintain force when wetted, as illustrated by Figure 1.4 in the Introduction, giving support to the

	ELASTIN	DRY SPIRAL	WET FRAME
E_{ini} (MN/m ²)	1.2	2.0	10
G (MN/m ²)	0.4	0.7	0.8
λ_{break}	2-3	3	2
s	10	5	2
β_{res} (10 ⁻³)	0	1.4	4

Table 4.2. A comparison of the approximate values of some physical parameters of three rubber-like proteins. The initial stiffness, E_{ini} , the shear modulus, G , the breaking extension, λ_{break} , the number of random segments between crosslinks, s , and the residual birefringence, β_{res} , are all listed. Note that the values for elastin are for hydrated samples, the values for spiral silk are for room condition samples, and the values for frame silk are for wetted samples.

notion that stiffer samples of spiral silk may likewise maintain force after wetting. Other clues to relationships between the silks' properties may be given when the wet contraction time-course of frame silk has been measured. If it is two-phase like that of spiral silk, perhaps comparative network stability or crystal characteristics could be inferred. For example, the second phase of frame silk's contraction could be predicted to have a lower slope if the crystals of frame silk are larger and more stable. The first phase, on the other hand, may be faster, since there is no glue to penetrate, and dragline is more hydrophilic than spiral silk, as explained below.

3. Wet/dry volume ratios. While comparing the physical behavior and parameters of frame and spiral silks, it is worthwhile examining the possible values of the wet/dry volume ratio once again. Analysis of data from Work (1977b) indicates that the average wet/dry volume ratio for frame silk is 2.0, whereas spiral silk shows an average of 1.6. It is actually not possible to tell whether these values are significantly different, for several reasons. Part of the difficulty lies in the form of the data. Both values are calculated from average diameters from many samples. In the case of Work's value for frame silk, the data does not even distinguish silk from different spiders; he did not appear to be interested in volume changes of individual samples. Since it is not possible to pair specific dry diameters with specific wet diameters, it is not possible to tell the amount of variation in volume change. While the amount of variation may be indirectly guessed based on variations in wet contraction ratios and diameters, and thus could be as low as 15%, it could also be as high as 50% in a worst-case scenario.

Despite this uncertainty, several observations can be made. The change in volume calculated for one of the spiral webs is equal to the average calculated from Work's data. Yet, if the average of all four spiral webs is taken, that value is somewhat lower due to all of the other webs exhibiting ratios lower than 2.0. Based on that tendency, however weakly supported by such a small sample size, it is *possible* that spiral silk does not swell as much as frame silk. Until such a time that a more accurate and precise value is obtained, it is worthwhile to consider whether it is logical for spiral to swell differently than frame; in other words, if it does swell less, what does that tell us about its molecular network?

How similar are the two silk compositions? There is a parameter called the Hydrophobic Index which is a measure of the relative portions of hydrophobic and charged residues in a protein. It has been used to assess the potential of certain rubber-like proteins to increase swelling with decreasing temperature, thus retaining their rubberiness despite the tendency of amorphous materials to become glassy when chilled (Chalmers & Gosline, 1991; Gosline & French, 1979). This temperature-swelling compensation is caused by the peculiar temperature-dependent interactions of water and hydrophobic amino acids. Since silk is a protein rubber which is used in constantly changing temperatures, it is possible that some silks could take advantage of the same temperature-swelling compensation to maintain properties reliably. A hydrophobic silk would, however, more easily dehydrate and turn glassy under average conditions of humidity. Then again, silks are known to contain many non-protein molecules which are hydrophilic, and could keep the matrix water-swollen; some silks might be able to afford being somewhat hydrophobic.

In order to begin exploring some of the above possibilities, calculations of hydrophobic indices (HI's) were carried out for a few silks (Sage and Gray, 1981).

4. Hydrophobic Index. Average Hydrophobicity is a measure of protein non-polarity. It represents the free energy change that would be measured if all the constituent amino acids were transferred from a non-polar solvent (e.g, ethanol) into water. The quantity is weighted according to the proportions of amino acids present in the protein. The hydrophobicity of each amino acid has been separately determined; it is assumed that they act the same when strung together, once the effects of the amino and carboxyl groups are subtracted. Thus,

$$(34) \quad H_{avg} = \Sigma(\Delta F_{ti} \times N_i),$$

where ΔF_{ti} is the standard free energy for the transfer of one mole of species i from nonpolar solvent to water, and N_i is the mole fraction (residues per 1000 residues in the protein).

Fractional Charge is defined as the sum of the numbers of Lysine, Arginine, Aspartic acid, Glutamic acid, and Histidine residues per 1000 amino acid residues. The Hydrophobic Index is thus defined by the Average Hydrophobicity (H_{avg}) per fractional charge (F_x):

$$(33) \quad HI = H_{avg}/F_x$$

The amino acid compositions of the silks were taken from several sources to ensure that the most complete and reliable assays were used for each. In particular, the values for the spiral silk were taken from Andersen (1970), as his analyses were performed on gland material, thereby avoiding any problems associated with removing the proteinacious glue. He also provides an analysis of frame silk, thus allowing direct comparison of the two without confounding factors.

All of the available amino acid analyses for spider silks showed no tryptophan. If the lack of tryptophan were due to analysis methods, which tend to break down the delicate ring structure during acid hydrolysis, then the HIs could be seriously in error due to that amino acid having the highest hydrophobicity. However, even analysis methods which used basic hydrolytic procedures to preserve a greater proportion of tryptophan showed no evidence of the residue in several types of silks from several species of spiders, including *A. aurantia* (Tillinghast, 1984); *A. diadematus* (Andersen, 1970); and the genus *Nephila* (Xu and Lewis, 1990; Lombardi and Kaplan, 1990); thus, it is reasonable to assume that the probability of encountering significant amounts of tryptophan in *A. diadematus* spiral silk is low. The proportion of tryptophan in *Bombyx mori* silk is also very small. Since most silks are somewhat similar in composition, being uniformly low in sulfur-containing residues and histidine, it is probable that there is no significant contribution from tryptophan in the other silks.

Resultant values for silks are compared with hydrophobicities of pig, bovine, and salmonid elastins in Table 4.3. The average protein, such as an enzyme, has an HI of about 2-3. A hydrophobic protein rubber, such as elastin, can have an HI of over 30. Note that the silks listed have HI's ranging from 2.75-10.47, with the highest being significantly higher than the average protein. Spiral and silkworm silk are in the range of shark and salmonid elastins, but none of the silks listed approached the range of the elastins of the mammals and birds.

The drag and cocoon silks of *N. clavipes* have the lowest HI of those calculated (in fact, they are lower than the HI of the glue of *A. diadematus*). *Araneus* drag/frame silk has a somewhat higher HI, while silkworm cocoon silk and *Araneus* spiral silk have the highest - both around 10. Thus we see that the Araneid spider's spiral fibroin is different enough to have twice the hydrophobic index of its frame silk, which would mean that if all other factors were equal,

Species:	Araneus diadematus ¹			Nephila clavipes ²		Bombyx mori ³
Silks:	drag	spiral	glue	drag	cocoon	cocoon
H_{avg}	137.4	87.4	321.4	198	207	52
F_c	749	915	1043	574	569	488
HI	5.45	10.47	3.24	2.90	2.75	9.38

Elastins:	Cow ⁴	Salmon ⁵	Shark ⁶
H_{avg}	35	94	111
F_c	1046	820	1120
HI	30	9	10

Table 4.3. Hydrophobic Indices of some silks and elastins.

- 1) Andersen, 1970
- 2) Lucas & Rudall, 1968
- 3) Lombardi & Kaplan, 1990
- 4) Chalmers, 1989
- 5) Sage and Gray, 1979
- 6) Sage and Gray, 1981

the spiral silk should absorb less water at the same room conditions of humidity and temperature. In that case, however, spiral silk would be in an even glassier state than frame silk. It certainly would not behave like an elastomer under those conditions. Since native spiral silk demonstrates rubber-like behavior under conditions which leave frame silk stiff and relatively inextensible, it is clear that some other factor is nullifying the dehydrating effect of its greater hydrophobicity. If spiral silk contains plasticizers in its rubber matrix, whether from the glue or the gland, these solvents or solutes would render the protein HI meaningless as a predictor of rubber elasticity, and it would not be unreasonable to assume the room condition hydration level of 1.3.

5. Potential for Plasticizers. The question then arises of what evidence has been found for the existence of hydrophilic molecules and plasticizers. As stated in the introduction, there is ample evidence for many types of non-proteinacious molecules in fibroins, including ions, carbohydrates, and amines, several of which are known to have hygroscopic properties (Tillinghast et al, 1987; Sinohara and Tillinghast, 1984). Researchers have only begun to identify and classify them. Further support for the presence of plasticizers, and not just water molecules, is given by data presented by Vollrath and Edmonds (1989), though they use their data to defend different arguments. They compare the mechanical behavior of frame silk with spiral silk which was dried over P_2O_5 . If the difference in properties between frame and spiral were due only to water, then drying out coated spiral over P_2O_5 should cause it to behave like frame silk. However, even after generously accounting for differences in diameter, dried-out spiral silk still behaves far more linearly and less stiffly than the frame silk at room conditions of 50% humidity. Plasticizers, plus differences in crosslinking and chain density, should help to explain the difference.

Note, also, that the viscid aggregate gland glue itself is not immune to the effects of humidity. On muggy days, experiments were not carried out due to the fluidity of the glue preventing slack length determinations: the silk was "reeled in" by the glue droplets too quickly. On very dry days (usually during winter), the glue was highly viscous, appeared darker yellow-gold than usual, and stuck with greater tenacity to objects such as spun fiberglass strands, insect

pins, or forceps. It was then possible to pull out a "strand" of glue 2-3 mm long, and more time had to be permitted for force to equilibrate at very low extensions.

When samples are wetted, the glue becomes transparent but does not appear to be wholly washed away, as particles have a tendency to remain enmeshed in an invisible boundary layer as much as 40-50 μm thick. When the silk is later dried by evaporation, moisture remains on the slide close to the fiber, as if the glue were merely distributed thinly in the vicinity, yet not evenly across the entire available surface of the slide. Despite traces of the glue's presence, such evaporated samples behave in a brittle manner, as if no longer plasticized at all.

6. Washed spiral samples. The fact that wetted and dried spiral does not return to its rubbery state (Gosline et al, 1991) supports the theory that the extra factor which presumably plasticizes spiral silk is not one of the glycoproteins, since those are tightly associated with fibroin and are not washed off (Tillinghast, 1984). Since both frame and spiral silks demonstrate similar tendencies to crystallize (Gosline et al, 1991), the difference is probably due to either an extra glandular factor or to production methods, such as increasing shear rate or draw ratio to make stiffer silk. If the factor is in the glue itself and acts by penetrating the core fiber, then an experiment involving the placement of spiral glue directly covering the major ampullate (dragline) glands while forcibly silking a spider should reveal that dragline silk behaves more like spiral silk when glue-coated during production. Alternately, if glue-covered dragline silk retains its normal behavior, then it is reasonable to conclude that the aggregate gland glue and its components do not themselves penetrate the fiber and instead serve a purely capture-enhancing function. In this case, it is possible that plasticizing factors are produced in the flagelliform glands, which synthesize the spiral silk fibroin. If this is true, the same plasticizing factors are probably absent or produced in lower quantities in the large ampullate glands, which synthesize frame silk.

F. WHY IS SPIRAL SILK VARIABLE?

At first, it may seem that knowledge pertaining to the uniformity of silk samples is useful only with respect to time that can be saved during experimental procedures. At the same time, however, the fact that there is a certain degree of NON-uniformity within webs raises some interesting questions.

Variation does not seem to be due to compositional variability, since other spider silks have been shown to be remarkably constant both among spiders of the same species, and among samples from a single spider (Lombardi and Kaplan, 1990). (That conclusion does not, however, rule out the possibility of local composition variation, even within a single segment.)

The magnitude of the variation in spiral silk contraction is greater than the variation that has been observed for dragline silk. According to Work (1981), the coefficient of variation for samples of dragline taken from many spiders is 13.6%, compared with 25% for spiral (the means are not significantly different). There may be subtle differences in production techniques, such as draw rate, water extraction, or distal valve control, that result in greater variation in the spiral silk (Tillinghast, Chase, and Townley, 1984; Kovoov and Zylberberg, 1980).

Unfortunately, it has not yet been possible to convince a spider to produce spiral silk in a continuous strand, apart from her web. Instead, even the slightest disruption causes her to immediately cease spiral production and resume dragline production. For this reason, researchers are restricted to short spiral samples with varied histories, which may be the sole source of variation.

Human engineers design and manufacture materials to meet certain specifications, so that performance is predictable. High-performance materials are subject to the strictest quality control, since structures which are optimized for both high performance and low weight have little leeway for error. A spider's web is a high-performance, low-weight structure that is absolutely essential for the animal's survival. Thus, one must ask whether there is a functional significance to the variations observed, and the spider is controlling variation, or whether the variation is incidental and merely within ranges of strength, stiffness, and performance which are

acceptable given a less-controllable environment of wind-blown branches, fickle weather, and high prey variety.

Variation in performance relative to sample position in the orb has not been studied; instead, the samples were almost all taken from the same relative distance from the hub, to eliminate that source of variation if it existed at all. If such a study is made, it could be difficult to tell whether variation is actually "controlled" by the spider, or is simply an irrelevant side-effect of gland secretion or construction methods (e.g., valve diameter, water extraction, draw ratio, lay-down extension, and weather).

The variations would have to be proven to affect capture success, web weight, construction time, or some other parameter related to survival. It may be that spiral silk can simply afford to be less stable, since it is removed daily. Furthermore, the performance of individual strands may be relatively unimportant, since any sort of single glue-coated strand can catch a gnat, while it is the average performance of many neighboring strands that is important when a yellow-jacket wasp impacts the orb. If a single fiber is stiffer than the others, it would initially bear the majority of the load, and therefore would be forced to stretch until the majority of force was carried by many additional fibers.

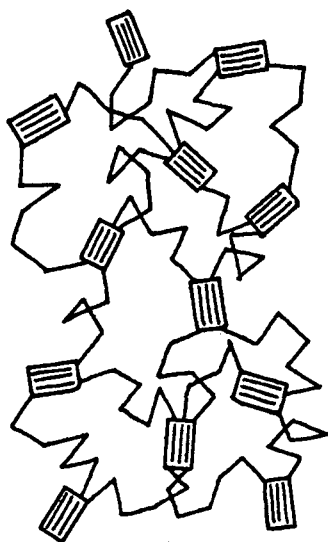
Of course, these arguments are all null and void if the observed variations are seen only in webs which have been stored for some time. Future studies using fresh silk from laboratory-raised spiders, under controlled conditions of temperature and humidity, should reveal further insights into the modulation of the properties of silks.

CHAPTER V. CONCLUSIONS

In summary, two general goals were met by this research. First, a few previously unknown parameters were determined. Spiral silk fibers were found to be non-circular in cross-section, with an ellipticity of about 1.5, allowing future researchers to calculate stresses and birefringences more accurately. The degree of lengthwise contraction when spiral samples were wetted was found to be about the same as for frame silk (the ratio of wet to dry slack lengths was around 0.6); the discovery of a two-phase contraction process may lead to further investigation into the cause of each phase. The increase in volume of spiral silk when wetted was found to be less than the volume change of frame silk. While not statistically significant due to shortcomings of methods and a small sample size, the data may imply that room-condition spiral silk is already partially plasticized. Results from the sensitivity analysis of network chain parameter calculations support this conclusion. Results for volume changes of wetted, stretched samples were less conclusive, as there was no consistent or significant evidence for either a decrease or increase in volume; but until more precise data are obtained, it seems acceptable to assume a constant-volume system.

Second, the mechanical and optical analyses provided coherent evidence that the molecular arrangements of spiral and frame silk are different. Based on the network parameter estimates, spiral silk was shown to have longer and fewer chains between crosslinks, since spiral silk has a lower stiffness and higher extensibility than wet frame silk. In addition, the guanidine hydrochloride test provides insight into the nature of the network crosslinks, confirming hypotheses that they are provided by non-covalent interactions (probably crystalline, beta-pleated sheet structures). The high stress-optical coefficient further indicates the presence of crystalline regions. The lower residual birefringence of spiral silk implies that it contains fewer, smaller, or more randomly-oriented crystals than frame silk, and the higher segment counts of spiral silk further imply that there must be fewer crystals acting as functional crosslinks. Especially significant is the fact that the network analyses of spiral silk can usually be performed under the assumption that the material is a wholly amorphous rubber, while network analyses of

Spiral



Frame

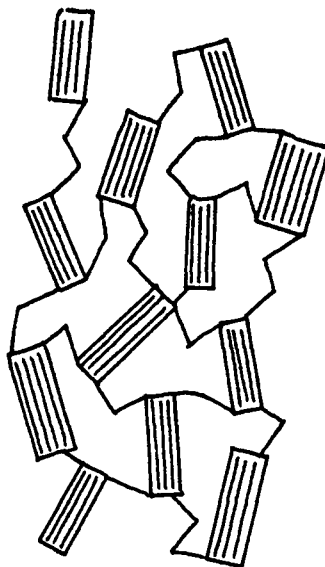


Figure 5.1. Pictorial representations of the molecular structures of frame and spiral silks. The spiral silk diagram shows fewer and smaller crystals which are more randomly oriented and have longer chains between crosslinks.

frame silk require a more complex model which includes the effects of high proportions of crystal filler particles.

Thus, a pictorial comparison of wet frame silk and the average spiral silk might look like Figure 5.1. Note the longer chains and smaller, more randomly-oriented crystals pictured for spiral silk. Finally, the high variability of spiral silk must be noted; individual samples are clearly capable of network characteristics and performance deviating widely from the average, raising questions about the stability and/or safety factors of such a high-performance biopolymer.

REFERENCES

- Aaron, B.B. and Gosline, J.M. (1980). Optical properties of single elastin fibers indicate random protein conformation. *Nature*, 287(5785):865-867.
- Aaron, B.B. and Gosline, J.M. (1981). Elastin as a random-network elastomer: a mechanical and optical analysis of single elastin fibers. *Biopolymers*, 20:1247-1260.
- Andersen, S.O. (1970). Amino acid compositions of spider silks, *Comp. Biochem. Physiol*, 35:705-711.
- Batschelet, E. (1981). *Circular Statistics in Biology*. New York: Academic Press.
- Calvert, P. (1989). Spinning ties that bind. *Nature*, 340:266.
- Chalmers, G.W.G. and Gosline, J.M. (1991). The role of hydrophobic interactions in the temperature-dependent swelling of vertebrate elastins. Submitted to *Biopolymers*.
- Denny, M. (1976). The physical properties of spider's silk and their role in the design of orb-webs. *J. Exp. Biol*, 65:483-506.
- Denny, M. (1980). Silks - their properties and functions. In: *The Mechanical Properties of Biological Materials*, J.F.V. Vincent and J.D. Currey (eds), 247-272.
- Dreesbach, K., Uhlenbruck, G. and Tillinghast, E.K. (1983). Carbohydrates of the trypsin soluble fraction of the orb web of *Argiope trifasciata*. *Insect Biochem*, 13(6):627-631.
- Flory, P.J. (1953). *Principles of Polymer Chemistry*. London: Cornell University Press.
- Fornes, R.E., Work, R.W., and Morosoff, N. (1983). Molecular orientation of spider silks in the natural and supercontracted states. *Journal of Polymer Science: Polymer Physics*, 21:1163-1172.
- Gage, L.P. and Manning, R.F. (1980). Internal structure of the silk fibroin gene of *Bombyx mori*. *J. of Biol. Chem*, 255(19):9444-9457.
- Gosline, J.M. and French, C.J. (1979). Dynamic mechanical properties of elastin. *Biopolymers*, 18:2091-2103.

- Gosline, J.M. (1980). Elastic properties of rubber-like protein and highly-extensible tissues. In: Mechanical Properties of Biological Materials, J.F.V. Vincent and J.D. Currey (eds), 331-357. Cambridge: Cambridge University Press.
- Gosline, J.M. (1987). Structure and mechanical properties of rubberlike proteins in animals. Rubber Chem. and Techn., 60(3):417-438.
- Gosline, J.M., DeMont, M.E. and Denny, M.W. (1986). The structure and properties of spider silk. Endeavor, 10(1):37-43.
- Gosline, J.M., Denny, M.W., and DeMont, M.E. (1984). Spider silk as rubber. Nature, 309(5968):551-552.
- Gosline, J.M., Nichols, C.C., Guerette, P., Cheng, A. and Katz, S. (1991). The macromolecular design of spider's silks. In: Design and Processing of Materials by Biomimicking, M. Sarikayi and I. Aksay (eds). In press.
- Gosline, J.M., Shadwick, E.S., DeMont, M.E. and Denny, M.W. (1988). Non-Gaussian elastic properties in biopolymer networks. In: Biological and synthetic polymer networks, O. Kramer (ed), 57-77.
- Heyn, A.N.J. (1954). Fiber Microscopy: A textbook and laboratory manual. New York: Interscience Publishers, Inc.
- Iizuka, E. (1965a). Degree of crystallinity and modulus relationships of silk thread from cocoons of *Bombyx mori* L. and other moths. Biorheology, 3:1-8.
- Iizuka, E. (1965b). Mechanism of fiber formation by the silkworm, *Bombyx mori* L. Biorheology 3:141-152.
- Iizuka, E. (1968). Species specificity of the conformation of silk fibroin in solution. Biochim. Biophys. Acta, 160:454-463.
- Jessop, H.T. and Harris, F.C. (1949). Photoelasticity: Principles and Methods. New York: Dover Publications.
- Kavanagh, E.J. and Tillinghast, E.K. (1979). Fibrous and adhesive components of the orb webs of *Araneus trifolium* and *Argiope trifasciata*. J. Morphology, 160:17-32.

- Kerkam, K., Viney, C., Kaplan, D. and Lombardi, S. (1991). Liquid crystallinity of natural silk secretions. *Nature*, 349:596-598.
- Kovoor, J. and Peters, H.M. (1988). The spinning apparatus of *Polonecia producta* (Araneae, Uloboridae): Structure and histochemistry. *Zoomorphology*, 108:47-59.
- Kovoor, J. and Zylberberg, L. (1979). Ultrastructure of the excretory duct of aggregate and flagelliform glands in *Araneus diadematus* Clerck (Araneae, Araneidae). *Zoomorphologie*, 92:217-239.
- Kovoor, J. and Zylberberg, L. (1980). Fine structural aspects of silk secretion in a spider (*Araneus diadematus*). I. Elaboration in the pyriform glands. *Tissue and Cell*, 12(3):547-556.
- Kovoor, J. and Zylberberg, L. (1982). Fine structural aspects of silk secretion in a spider. II. Conduction in the pyriform glands. *Tissue and Cell*, 14(3):519-530.
- Lombardi, S.J. and Kaplan, D.L. (1991). Amino acid composition of major ampullate silk (dragline) of *Nephila clavipes*. *J. Arachnol*, 18(3):297-306.
- Lucas, F. (1964). Spiders and their silks. *Discovery*, 25:20-26.
- Lucas, F. and Rudall, K.M. (1968). Extracellular fibrous proteins: the silks. In: *Comprehensive Biochemistry*, Vol 26B, M. Florkin and E.H. Stotz (eds), 475-558. Amsterdam: Elsevier Publishing Company.
- Lucas, F., Shaw, J.T.B., and Smith, S.G. (1960). Comparative studies of fibroins. I. The amino acid composition of various fibroins and its significance in relation to their crystal structure and taxonomy. *J. Mol. Biol*, 2:330-349.
- Masters, W.M. (1984). Vibrations in the orbwebs of *Nuctenea sclopetaria* (Araneidae). I. Transmission through the web. II. Prey and wind signals and the spider's response threshold. *Behav. Ecol. Sociobiol*, 15:207-223.
- The Merck Index (1976). An encyclopedia of chemicals and dyes, 9th edition, M. Windholz (ed), entry 5796. Rahway, New Jersey: Merck and Company, Inc.

- Nakajima, B., Hirata, K., Nishi, N., and Noguchi, J. (1981). Silk fibroin model, poly(L-alanyl-glycyl-L-alanyl-glycyl-L-alanyl-glycyl-L-seryl-glycine). *Int. J. Biol. Macromol.*, 3:46-52.
- Palmer, J. (1985). The silk and silk production of the funnel-web Mygalomorph spider *Euagrus* (Araneae, Dipluridae). *J. of Morphology*, 186:195-207.
- Palmer, J., Coyle, F.A. and Harrison, F.W. (1982). Structure and cytochemistry of the silk glands of the Mygalomorph spider *Antrodiaetus unicolor* (Araneae, Antrodiaetidae). *J. of Morphology*, 174:369-274.
- Peakall, D.B. (1964). Composition, function, and glandular origin of the silk fibroins of the spider *Araneus diadematus* Cl. *J. Exp. Zool.*, 156:345-352.
- Preston, J.M., ed. (1953). *Fibre Science*. Manchester: The Textile Institute.
- Sage, H. and Gray, W.R. (1981). Studies on the evolution of elastin - III. The ancestral protein. *Comp. Biochem. Physiol.*, 68B:473-480.
- Sasaki, T. and Noda, H. (1973). Studies on silk fibroin of *Bombyx mori* directly extracted from the silk gland. I. Molecular weight determinations in guanidine hydrochloride or urea solutions. II. Effect of reduction of disulfide bonds and subunit structure. *Biochim. Biophys. Acta*, 310:76-103.
- Shadwick, R.E. and Gosline, J.M. (1985). Physical and chemical properties of rubber-like elastic fibres from the octopus aorta. *J. Exp. Biol.*, 114:239-257.
- Shadwick, R.E. and Gosline, J.M. (1985). Mechanical properties of the octopus aorta. *J. Exp. Biol.*, 114:259-284.
- Shimura, K. (1983). The physiology and biology of spinning in *Bombyx mori*. *Experientia*, 39(5):441-550.
- Shimura, K., Kikuchi, A., Katagata, Y., and Ohotomo, K. (1982). The occurrence of small component proteins in the cocoon fibroin of *Bombyx mori*. *J. of Sericultural Science of Japan*, 51(1):20-26.

- Sinohara, H. and Tillinghast, E.K. (1984). Carbohydrates associated with the orb web protein of *Argiope aurantia*. *Biochemistry International*, 9(3):315-317.
- Sokal, R.R. and Rohlf, F.J. (1973). *Introduction to Biostatistics*, 244-251. San Francisco: Freeman and Company.
- Tillinghast, E.K. (1984). The chemical fractionation of the orb web of *Argiope* spiders. *Insect Biochem*, 14(1):115-120.
- Tillinghast, E.K., Chase, S.F. and Townley, M.A. (1984). Water extraction by the major ampullate duct during silk formation in the spider, *Argiope aurantia* Lucas. *J. Insect Physiol*, 30(7):591-596.
- Tillinghast, E.K., Huxtable, R.J., Watson, W.H., and Townley, M.A. (1987). Evidence for the presence of gabamide on the web of orb weaving spiders. *Comp. Biochem. Physiol*, 88B(2):457-460.
- Tokutake, S. (1980). Isolation of the smallest component of silk protein. *Biochem. J*, 187:413-417.
- Treloar, L.R.G. (1976). *The physics of rubber elasticity*, 3rd edition. Oxford: Clarendon Press.
- Vollrath, F. and Edmonds, D. (1989). Modulation of the mechanical properties of spider silk by coating with water. *Nature*, 340:305-307.
- Vrahopoulou-Gilbert, E., and McHugh, A.J. (1984). Thermodynamics of flow-induced phase separation in polymers. *Macromolecules*, 17:2657-2663.
- Warwicker, J.O. (1960). Comparative studies of fibroins. II. The crystal structures of various fibroins. *J. Mol. Biol*, 2:350-362.
- Work, R.W. (1976). The force-elongation behavior of web fibers and silks forcibly obtained from orb-web-spinning spiders. *Textile Research Journal*, 46:485-492.
- Work, R.W. (1977a). Mechanisms of major ampullate silk fiber formation by orb-web-spinning spiders. *Trans. Amer. Micros. Soc*, 96(2):170-189.

- Work, R.W. (1977b). Dimensions, birefringences, and force-elongation behavior of major and minor ampullate silk fibers from orb-web-spinning spiders - the effect of wetting on these properties. *Textile Research Journal*, 47:650-662.
- Work, R.W. (1981). A comparative study of the supercontraction of major ampullate fibers of orb-web-building spiders (Araneae). *J. Arachnol*, 9:299-308.
- Work, R.W. (1985). Viscoelastic behavior and wet supercontraction of major ampullate silk fibres of certain orb-web building spiders (Araneae).
- Xu, M. and Lewis, R.V. (1990). Structure of a protein superfiber: spider dragline silk. *Proc. Natl. Acad. Sci. USA (Biochemistry)*, 87:7120-7124.
- Zemlin, J.C. (1968). A study of the mechanical behavior of spider silks. Technical Report 69-29-CM, US Army Natick Laboratory, Natick, Massachusetts.